

A review of photovoltaic performance of organic/inorganic solar cells for future renewable and sustainable energy technologies

J. Ajayan ^{a, **}, D. Nirmal ^{b,*}, P. Mohankumar ^c, M. Saravanan ^a, M. Jagadesh ^a, L. Arivazhagan ^b

^a Department of Electronics and Communication Engineering, SNS College of Technology, Coimbatore, Tamilnadu, India

^b Department of Electronics and Communication Engineering, Karunya Institute of Technology and Sciences, Coimbatore, Tamilnadu, India

^c Department of Mechatronics Engineering, SNS College of Technology, Coimbatore, Tamilnadu, India

ARTICLE INFO

Keywords:

Air-mass 1.5 global solar spectrum (AM1.5)
Multiple quantum wells (MQW)
Open-circuit voltage (V_{OC})
Perovskites
Short-circuit current density (J_{SC})

ABSTRACT

Solar cells are emerging as serious contenders to rival leading energy sources to generate electricity for environment friendly renewable and sustainable energy technologies. Earth is receiving an incredible amount of solar energy which can be converted into electricity by means of high-performance solar cells for meeting the future global energy needs. This article reviews the rapid progress in the developments of inorganic and organic solar cells (SCs) such as silicon SCs, perovskite SCs, III-V SCs, quantum dot SCs, dye sensitized SCs, flexible SCs, thin film SCs and tandem SCs. This article highlights the factors influencing the photovoltaic (PV) performance of SCs such as solar cell architectures, photovoltaic materials, photo-electrode materials, operational and thermal stability challenges, recombination losses, thermal and chemical treatments, trap defects, hole transport materials and optical irradiation. This paper also point out the reliability issues and challenges in the commercialization of SCs. Solar cells are emerging as a promising solution for power generating windows, power saving display systems, self-powered flexible and wearable electronic devices, building integrated photovoltaics, charging of e-vehicles, space craft and satellite applications and solar lighting.

1. Introduction

The demand for energy is growing globally, but the primary energy sources like fossil fuels are gradually depleting. Fossil fuels also affect the air quality and public health by emitting green house gases like CO_2 and other air pollutants. Based on the current economic growth figures, the world needs energy of 28 TW in 2050 and 46 TW in 2100. A significant amount of this energy should be generated by environment friendly renewable energy sources. Therefore, it is high time to explore new energy sources for future renewable and sustainable energy technologies. Solar cells have been considered as the most promising solutions for meeting the global energy needs because solar energy is the safest, clean and abundant energy source for future renewable and sustainable energy technologies. IBSC (Intermediate band solar cells) have emerged as an attractive choice for improving the energy conversion efficiency of single gap solar cells. Techniques like quantum dot (QD) nanostructures and highly mismatched semiconductor alloys can be used for improving the energy conversion efficiency of IBSCs [1]. Back junction back contacted (BJBC) solar cells are also gaining attention because of their

* Corresponding author.

** Corresponding author.

E-mail addresses: email2ajayan@gmail.com (J. Ajayan), dnirmalphd@gmail.com (D. Nirmal).



outstanding energy conversion efficiencies which arises from the absence of optical shading and reduction of recombination losses with the use of carrier selective junctions [2]. Full area rear Al-alloyed BSF (back surface field) and PERC (passivated emitter and rear cell) are the two popular designs used for industrial mass production of c-Si (crystalline-silicon) solar cells. PERC design is gaining popularity over the years for the mass production of solar cells having power conversion efficiency (PCE) over 25% [3–5]. a-Si:H (amorphous hydrogenated silicon) and mc-Si (micro-crystalline silicon) materials can be used for developing Silicon (Si) SCs. The advantage of incorporating hydrogen in mc-Si and a-Si materials is that it can significantly improve the minority charge transport through the grained Si material and reduces the recombination at the grain boundary. Compared with a-Si:H material, mc-Si:H material is highly stable against optically induced degradation [6]. Because of the increasing environmental concerns on materials for photovoltaics, photovoltaic researchers are looking towards eco-friendly photovoltaic materials [7–9]. Point contact solar cells are most important back contacted solar cells in which the metal contacts touch the Si only in an array of points. The major advantage of this point contact solar cells over inter-digitated back contacted solar cell is that it provides high output voltage. Low cost, good reliability and high PCE are the key advantages of back contacted solar cell design [10]. The material quality of mc-Si is limited by the crystal defects and metal impurities [11,12]. Different band-gap semiconductors can be used for the effective utilization of the solar spectrum for solar energy conversion. Based on this fact, various research groups have developed hetero-junction (HJ) SCs and HJ bipolar transistor SCs [13]. In 2013, B. Endres et al. [14] demonstrated a spin solar cell based on GaAs p-n junction. Multi-junction SCs are found to be effective in achieving high PCE compared with single junction (SJ) solar cells. The PCE of SJ-SCs are constrained by the Queisser-Shockley limit [15,16]. V_{oc} , J_{sc} , FF (fill factor), dark current density (J_0) and PCE are the key parameters that can be used for analyzing the PV performance of SCs. The PCE of solar cells can be computed as

$$PCE = \frac{J_{SE} \cdot V_{OC} \cdot FF}{I_0} \quad (1)$$

where I_0 represents the intensity of incident light.

The dark current density (J_0) of solar cells can be expressed as

$$J_0 = J_{SE} \exp\left(-\frac{qV_{OC}}{KT}\right) = \frac{qn_i W}{\tau} + qn_i(S_{front} + S_{back}) \quad (2)$$

where, n_i , W , τ , S_{front} and S_{back} represents intrinsic carrier concentration, depletion layer thickness, life time of minority carriers, velocity of surface recombination at front surface and velocity of surface recombination at back surface respectively.

The relationship between V_{OC} and light intensity (P) is given by

$$V_{OC}(P) = \frac{n k T}{q} \ln(P) + C \quad (3)$$

where n and C are ideality factor and a constant respectively.

The relationship between V_{OC} , energy of charge transfer state (E_{CT}), J_{SC} and dark current (J_0) is given below.

$$V_{OC} = \frac{E_{CT}}{q} + n \frac{kT}{q} \ln\left(\frac{J_{SC}}{J_0}\right) \quad (4)$$

The fill factor (FF) of solar cells can be computed as

$$FF = \frac{J_{MPP} V_{MPP}}{J_{SC} V_{OC}} \quad (5)$$

Where, J_{MPP} and V_{MPP} are maximum power point current density and maximum power point voltage respectively. The variation in J_{SC} and V_{OC} due to charge density changes significantly affects the FF of solar cells. The relationship between generation rate of free charges (G), J_{SC} and active layer thickness (L) is given by

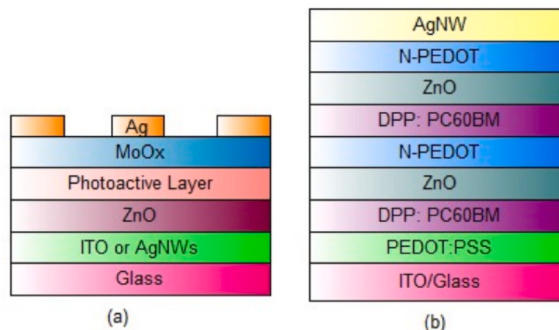


Fig. 1. Device structures of (a) SJ solar cell and (b) Triple junction (TJ) solar cell [15].

$$G = \frac{J_{SC}}{qL} \quad (6)$$

Fig. 1 shows the device structures of single and multi-junction SCs. In 2014, Ju-Hyung Yun et al. [17] from State University of New York successfully demonstrated an incident light adjustable periodic nanolens architecture based on Si solar cells. Nanowire or nanopillar arrays have been used for photovoltaic energy harvesting applications to enhance PCE. This is due to the ability of nanowire arrays to minimize surface light reflection and improve the charge collection efficiency [18–22].

2. Silicon solar cells

The PCE of a-Si:H/mc-Si HJ-SCs can be improved by using front electron-collector in rear-emitter [23]. Since high PCE can be achieved with simple fabrication processes and cost effective materials, silicon hetero-junction (SHJ) SCs have been gaining much attention in the photo-voltaic industry. Charge recombination is the critical factor that limits the performance of solar cells and therefore, a-Si:H/mc-Si interface should be passivated to minimize the recombination of carrier. a-Si:H SCs suffer from the low conductivity of amorphous silicon and therefore a TCO (transparent conductive oxide) can be used to enhance the lateral transport of carriers to metal contacts [24]. ITO (Indium tin oxide) and Al-doped ZnO are the most widely used TCO materials in Si solar cells. An overview of photovoltaic performance of state of the art Si SCs is given in Table-1. EWT (Emitter wrap through) solar cell design can be used to achieve high PCE even with poor quality light absorbing material [25]. Laser processing is the most powerful tool that can.

Be used for dielectric ablation and selective Si doping in cost effective high performance SCs. The performance of the Si-SCs with

Table 1
An overview of Photovoltaic performance of Si solar cells.

Ref.	Structure/Features	V _{OC} (mV)	J _{SC} (mA/cm ²)	FF (%)	PCE (%)
[26]	HIT solar cell on Si wafer	750	40.1	83.2	24.7
[25]	n-Type EWT Si Solar Cell	661	40.4	80	21.6
[27]	N-PERT BJ	668	39	76.1	19.85
[27]	BJBC	667	39.6	75.8	20
[28]	c-Si with thin ALD Al ₂ O ₃ +SiO _x	681	39.3	79.6	21.3
[28]	c-Si with ALD Al ₂ O ₃ +SiO _x	676	40.2	78.5	21.2
[28]	c-Si with PECVD AlO _x + SiO _x	678	39.7	79.4	21.3
[28]	c-Si with PECVD AlO _x	684	39.4	79.8	21.5
[28]	c-Si with thermal SiO ₂	685	39.2	79.8	21.4
[29]	Homogeneous Emitter	624	38.3	78.5	18.7
[30]	GaP window layer on Si	632	24.6	79.7	12.4
[31]	Ag Gridline based metallization	636	37.8	76.5	18.4
[32]	Mono-MWT-EBSE cell	639	39.01	78.6	19.61
[33]	Al-BSF/Ion implantation Emitter	643	37.52	80.4	19.39
[33]	PERC/Ion implantation Emitter	661	38.88	78.4	20.14
[34]	Structured Seed Layer based SHJ	728	38	80.1	22.2
[35]	Screen and Stencil-Printed contact	632	37.7	78.8	18.8
[36]	p-type MIS Si solar cell	710	5.94	58	2.47
[37]	p-Type Si/MoO _x rear contact	658	39.8	77.8	20.4
[38]	p-Type MWT-PERC	661	39.9	78.3	20.6
[39]	Large-Area Back-Contact BCBJ	630	41.4	77.6	20.2
[40]	Bifacial n-Type Cell	647.5	39.1	79.5	20.13
[41]	Industrial Al-BSF Si	645	38.64	79.3	19.76
[42]	c-Si HIT/inter digitated BC	740	41.8	82.7	25.6
[43]	c-Si PERC	645.9	38.6	79.1	19.76
[44]	n-Type High Performance mc-Si	683.9	41.5	82.2	23.3
[45]	Honeycomb/Al-BSF-Si	618.4	36.3	79.5	17.8
[45]	Isotextured Si solar Cell	618.3	35	79.3	17.3
[46]	n-Type Rear-Junction solar cell	669.7	39.41	78.3	20.65
[47]	PERC p-type Si	669.7	39.41	78.3	20.65
[48]	mc-Si surface nanotextured Si	631	37.5	79.1	18.72
[49]	Perovskite Tandems with Si	1430	15.3	75	16.2
[50]	Fully Ion Implanted n-type Si	655	39.52	79.1	20.5
[51]	c-Si/Metal-Free Back Reflectors	650	40.6	76.5	20.5
[52]	a-Si:H/c-Si SHJ solar cell	711	36.6	76.4	19.9
[53]	MWT SHJ solar cell	734	36.3	76.3	20.3
[54]	Full Back Contacted IBC Cell	655	40.5	73.9	19.65
[55]	Aluminum-Alloyed P + Emitter	624	40	78	19.1
[56]	Ag/ZnO back reflectors nc-Si:H	541	24.62	71.1	9.47
[57]	All-back-contact thin Si nanocone	623	29	76	13.7
[58]	Aluminium alloyed iron-silicide	425	18.5	63.5	5.1
[59]	ITO-Free SHJ/ZnO:Al/SiO ₂	729	39.9	79	23
[60]	c-Si/Phosphorous-Doped SiC	706	38	80.2	21.5
[61]	Photoluminescent employed Si	621	37.20	68.5	15.81

laser doped selective emitter is limited by passivation induced cavity defects [62]. Hybrid SCs, that is combination of homo-junction and HJ solar cells can be used to achieve higher J_{SC} and V_{OC} simultaneously [63]. In 2016, Nadine Wehmeier et al. [27] reported the fabrication of industrial type PERT BJ (Passivated-emitter and rear totally diffused back-junction) and BJBC (Back junction back contact) SCs on n-type wafers that have a PCE of approximately 20% using PECVD technique.

BCBJ architecture is the most successful technique that can be used for the bulk production of large area Si-SCs. Improvement of PCE and reduction of fabrication cost are the two primary concerns in the photovoltaic industry. PERC (passivated-emitter and rear solar-cell) structure is found to be effective in improving PCE by minimizing optical and recombination losses. SiO_2 , a-Si, a-SiN_x, a-SiC_x and Al₂O₃ are the popularly used passivation materials in Si solar cells [28]. Narrow grid lines, good quality contacts, excellent surface passivation and homogeneous high sheet resistance emitter are the key factors required for realizing high efficiency solar cells [29,64]. In classical Si solar cells, more than 45% of the incident photons cannot be utilized due to their relatively small energy compared with the band gap energy of Si. Therefore, it is required to transform the energy of those sub-band-gap photons into higher energy photon (up conversion) to enhance the PCE of SCs [30,65]. In 2012, Abasifreke Ebong et al. [31] investigated the effect of Ag dosages on the emitters of ink-jet full grid line cells and found that increasing the amount of Ag in emitter resulted in the enhancement of V_{OC} , J_{SC} , FF and PCE of SCs. Metal wrap through (MWT) technology is another attractive technique used in mc-Si SCs in order to improve the PCE [32]. In 2014, Mikio Taguchi et al. [26] studied the impact of substrate thickness on the performance of HIT (hetero-junction with intrinsic thin-layer) SCs and observed that thinning down the wafer thickness is essential to enhance the PV performance of HIT SCs. Interdigitated back contact (IBC), MWT, PERC, EWT and PERL are the key technologies reported in the development of Si-SCs to improve PCE [66–68].

In 2015, Vinodh Shammugam et al. [35] investigated the influence of stencil printed and screen printed metal contacts for Si-SCs and observed that stencil printing technology offers higher performance compared with screen printing technology. The V_{OC} of the Si solar cells can be enhanced by adopting a metal-insulator-semiconductor (MIS) structure [36]. James Bullock et al. [37] demonstrated that the use of transparent molybdenum oxide (MoO_x) films as hole collecting local rear contacts in mc-Si solar cells will help to improve PCE [37]. The main benefit of Si-SCs is that Si is an earth abundant material and therefore, Si solar cells are cheap and also low temperature process can be used for manufacturing Si-SCs. A significant part of global manufacturing of multi-crystalline p-type Si-SCs with Al-BSF is based on screen printing technology [38–40,69]. The J-V characteristics of some of the high performance Si solar cells are shown in Fig. 2 n-type Si solar cells are less sensitive to light induced degradation and superior in performance compared with p-type Si-SCs [70]. n-type Si solar cells also have excellent immunity to metal impurities. The PCE of multi-crystalline Si-SCs can be enhanced by reducing the surface reflectance. Deposition of an antireflection coating (ARC) and surface texturing using alkaline agents (KOH or NaOH) with organic additives are the two popular techniques used for minimize surface reflectance in multi-crystalline Si solar cells [45,46]. NiO_x and TiO_x are the widely used ARC materials. Innovative techniques such as selective emitter formation, patterning and metallization can be applied at the front side of both n-type and p-type Si-SCs for improving the photovoltaic performance. Screen printed Ag/Al metal contacts have recently gained tremendous attention for the front contacts of n-type Si-SCs due to its cost effectiveness. Front surface passivation and long bulk life time at the base of the cells are the two key requirements for a n-type rear junction Si solar cell. The bulk life time is decided by the bulk resistance of the material. In order to achieve a very small contact resistance and increase minority carrier life time by minimizing recombination, a phosphorous-diffused front surface field (FSF) potential barrier is widely used. An innovative combination of excellent dielectric passivation and FSF can effectively reduce the front surface recombination which leads to the enhancement of cell efficiency. FSF with low surface doping density also helps to improve the internal quantum efficiency (IQE) at high frequencies. Laser doping process, etch back process and double diffusion process are some of the popularly used methods to form a selective FSF [46].

For a laser doped screen printed n-type rear junction Si solar cell, the total saturation current density (J_{0tot}) can be computed as [71, 72].

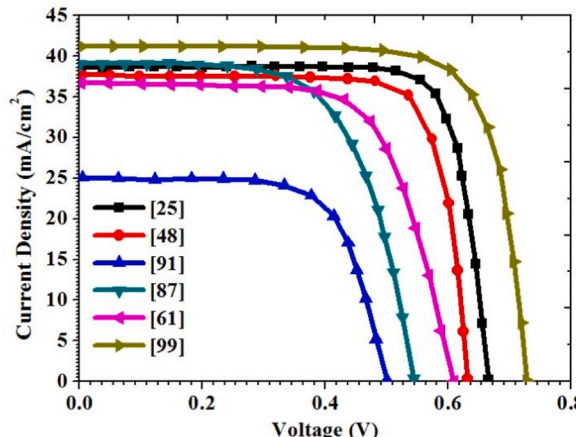


Fig. 2. J-V curves of some of the high performance Si-SCs.

$$J_{0tot} = j_{0e}(1-f) + J_{0e,metal}f + J_{0,nbulk} + J_{0FSF}(1 - F_{laser}) + J_{0FSF,metal} \cdot F_{metal} + J_{0laser}(F_{laser} - F_{metal}) \quad (7)$$

where, F_{metal} , F_{laser} and f represents FSF metallization fraction, front laser doping and rear metallization fraction respectively. The relationship between J_{0tot} , J_{SC} and V_{OC} are given in equation (8).

$$J_{0tot} = \frac{J_{SC}}{\exp\left(\frac{qV_{OC}}{nKT}\right)} \quad (8)$$

The components of J_{0tot} is shown in Fig. 3.

The PERC concept was first introduced by Blakers et al. [73] in 1989. Fig. 4 shows the PERC design of a p-type mc-Si solar cell. R. Preu et al. [74] has successfully demonstrated laser ablation of the rear passivation layers that propelled the industrialization of PERC cell structure. PECVD and ALD are the two popularly used rear passivation technologies [75]. Front and back electrodes, base, emitter, ARC coating and a BSF are the typical parts of c-Si-SCs. c-Si-SCs have a n^+ - p^+ structure that consists of a phosphorous doped emitter (n^+ -type) and p^+ -type BSF which can be obtained by sintering the screen printed Al paste on the back-side of the solar cell. The potential barrier introduced by the p - p^+ junction region at the cell back passivates the cell back by reflecting the free electrons (minority charges) towards the n^+ - p junction area [76]. In 2013, Ulrich Jager et al. [36] studied the performance comparison of homogeneous and selective-emitters on p-type mc-Si SCs with passivated surfaces and reported that the p-type cells with selective emitter exhibits a superior performance compared with homogeneous front side emitter. Low contact resistance, high FF and high V_{OC} are the major causes for the superior photovoltaic performance of selective emitter based cells. Cz-Si (Czochralski grown Si) and FZ-Si (Float-zone-Si) are commonly used for fabricating Si solar cells [47].

In 2016, Ping Feng et al. [48] successfully demonstrated a RIE (Reactive ion etching) based surface nano-texturing to improve the PCE of c-Si SCs by minimizing surface reflectance. Nano-surface texturing combined with ARC can effectively improve the light collection efficiency of all types of Si-SCs. Laser texturing, metal catalyzed chemical etching and plasma etching are the popular surface nano-texturing techniques [77,78]. In 2018, Robert L. Z. Hoye et al. [49] demonstrated the first two terminal (2T) perovskite tandem with p-type Si solar cell that enables the voltage addition between p-type Si bottom solar cell and perovskite top solar cell in a 2T tandem structure. Calvin S Fuller from Bell Lab demonstrated the first Si solar cell in 1954 which has a PCE of 8%. Making good metal contacts were the major issue at that time period [79,80]. Later in 1977 M. D. Lammert et al. developed an IBC (inter-digited back contact) Si solar cell which has the advantage of no shading loss [81]. The schematic of an IBC solar cell is depicted in Fig. 5. In 1984, R. M. Swanson et al. [82] reported the development of first point contact Si solar cells. Light trapping techniques can be used to enhance the efficiency of a-Si:H and c-Si:H SCs [53,83–88]. In 2017, R. Lopez-Delgado et al. reported the use of photoluminescent down shifting CdSe/CdS QDs for improving the PCE solar cells [87].

The I-V characteristics of solar cells can be expressed as [89,90].

$$I(V) = I_0 \left[\exp\left(\frac{qV}{n_i k_B T}\right) - 1 \right] - I_G \quad (9)$$

where, I_0 , k_B , T and I_G represents dark current, Boltzmann's constant, temperature and photo-generated current respectively. The V_{OC} of a p-type Si solar cell is given by [58].

$$V_{OC} = \frac{KT}{q} \ln \left[\frac{J_{ph}(N_A + \Delta p)\tau_{eff}}{qdn_i^2} \right] \quad (10)$$

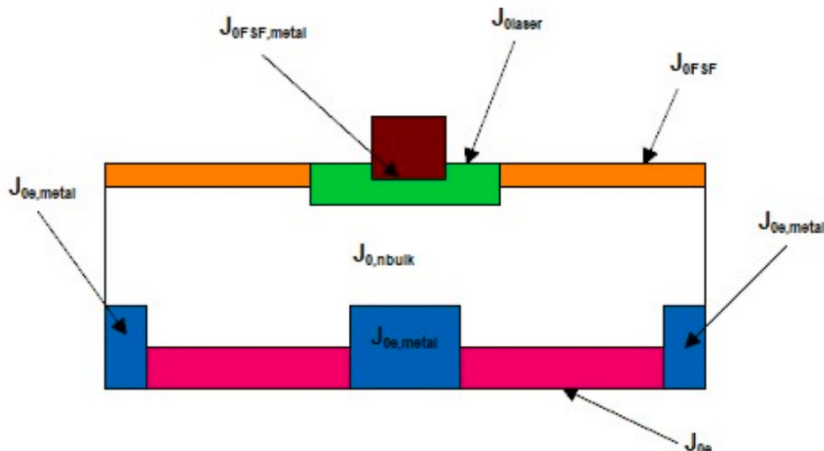


Fig. 3. Various components of J_{0tot} [46].

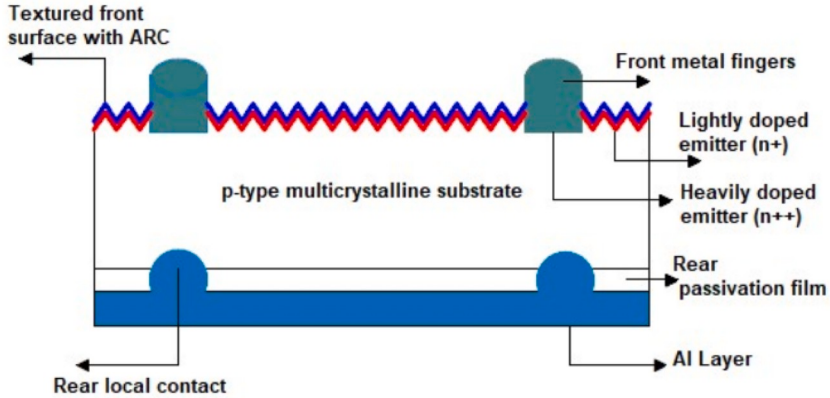


Fig. 4. PERC design of p-type mc-Si solar cell [66].

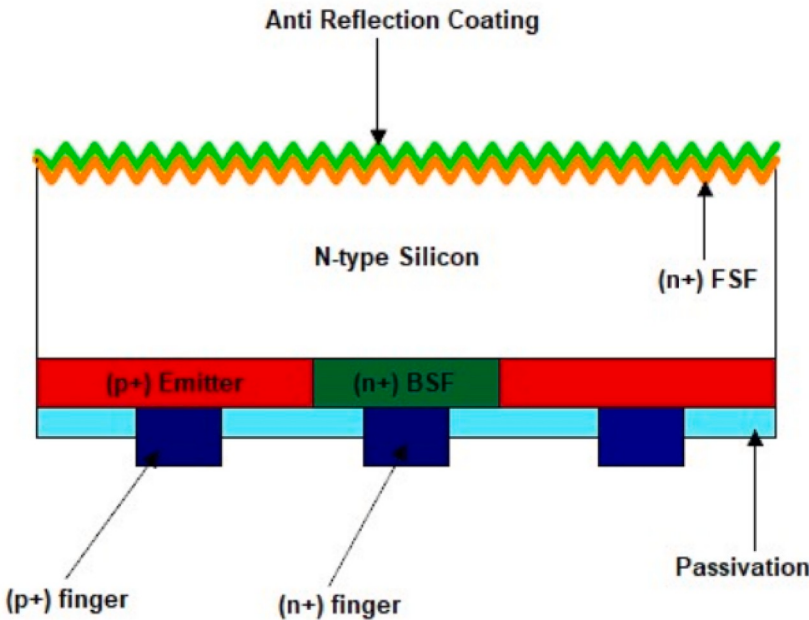


Fig. 5. Structure of an IBC solar cell [54].

where, J_{ph} , N_A , τ_{eff} , Δp , n_i and d represents photo current density, acceptor concentration, effective minority carrier life time, excess minority hole concentration, intrinsic carrier concentration and cell thickness respectively. The short circuit current density (J_{SC}) and dark current density (J_0) of a p-type Si solar cell is given in equations (11) and (12) respectively [91].

$$J_{SC} = J_0 \left(e^{qV_{oc}/KT} - 1 \right) \quad (11)$$

$$J_0 = q n_i^2 \left[\frac{1}{N_A} \sqrt{\frac{D_n}{\tau_n}} + \frac{1}{N_D} \sqrt{\frac{D_p}{\tau_p}} \right] \quad (12)$$

where, D_n , D_p , τ_n , τ_p , N_A and N_D represents electron diffusion constant, hole diffusion constant, electron life time, hole life time, acceptor concentration and donor concentration respectively. Auger recombination and Schockley-Read-Hall (SRH) are the two recombination-mechanisms which significantly degrades the photovoltaic performance of solar cells. The SRH recombination (R_{SRH}) and Auger recombination (R_{Aug}) mechanisms can be mathematically expressed as

$$R_{SRH} = \frac{(np - n_i^2)}{\tau_{n0}(p + p_1) + \tau_{p0}(n + n_1)} \quad (13)$$

$$R_{Aug} = (np - n_i^2)(C_{p0}p + C_{n0}n) \quad (14)$$

where

$$n_1 = n_i \exp\left(\frac{E_t - E_i}{KT}\right) \quad (15)$$

$$p_1 = n_i \exp\left(\frac{E_i - E_t}{KT}\right) \quad (16)$$

where, E_t , τ_{n0} , τ_{p0} , C_{p0} and C_{n0} are the trapping energy level, SRH electron life time, SRH hole life time, hole Auger coefficient and electron Auger coefficient respectively.

The total recombination current density of solar cells can be expressed as [92,93].

$$J_{rec}(V) = J_{rec,bulk} + J_{e,stack} + J_{h,stack} + J_{e,interface} + J_{h,interface} \quad (17)$$

where, $J_{rec,bulk}$, $J_{e,stack}$, $J_{h,stack}$, $J_{e,interface}$ and $J_{h,interface}$ represents recombination current density at bulk, recombination current through electron extraction stack, recombination current through hole extraction stack, recombination current at a-Si/c-Si interface of electron extraction stack and recombination current at a-Si/c-Si interface of the hole extraction stack respectively. In 2017, Wen-Chieh Lee et al. [94] demonstrated a RGO (reduced graphene oxide)/pyramidal Si cell with an efficiency of 5.21% for low cost environmental friendly applications. However, these RGO on pyramidal Si solar cell suffer from reduced efficiency. In 2018, Anupam Nandi et al. [95] reported a hybrid ITO/RGO bilayer based a-Si solar cell which exhibited a slightly higher efficiency of 7.64%. Anna B. Morales-Vilches et al. demonstrated an ITO free, ZnO:Al/SiO₂ front electrodes based SHJ solar cell which has an efficiency of 23% [59]. In order to suppress the recombination losses, phosphorous doped SiC based front contact can be used for developing c-Si solar cells [60]. In 2019, Rosendo Lopez-Delgado et al. [61] reported that photoluminescent materials like chlorophyll-A can be employed in Si solar cells for improving its PCE. Light trapping techniques such as plasmonic nanostructures, triangular gratings, photonic crystals, nanowires, nanocones, nanohole arrays and pyramidal gratings can be used for enhancing the efficiency of c-Si-SCs [96,97]. Light-induced-degradation (LID) in multi-crystalline Si-SCs can be eliminated with the help of fast regeneration process [98–104]. Sangmoo Jeong et al. [57] has investigated the influence of S_{eff} (Effective surface recombination velocity) and pitch (centre to centre distance between p⁺ and n⁺ regions) on the photovoltaic characteristics of Si nanocone SCs featuring all back contact design to prevent Auger recombination and a nanocone structure that effectively minimizes the surface area of the ultra-thin silicon solar cell. Fig. 6(a) indicate that increasing both S_{eff} and pitch leads to the severe degradation of fill factor. Fig. 6(b) reveals the fact that J_{sc} is inversely proportional to the pitch. The variation in pitch have no significant impact on the V_{oc} (Fig. 6(c)), but severely degrades the PCE of the ultra thin Si nanocone SCs (Fig. 6(d)).

Fig. 7(a) depicts the J-V curves of planar and nanostructured Si-SCs. Nanostructured Si solar cells exhibits higher J_{sc} and V_{oc} compared with planar Si solar cells which is evident from Fig. 7(a). The influence of graphene/planar Si and graphene/pyramidal Si

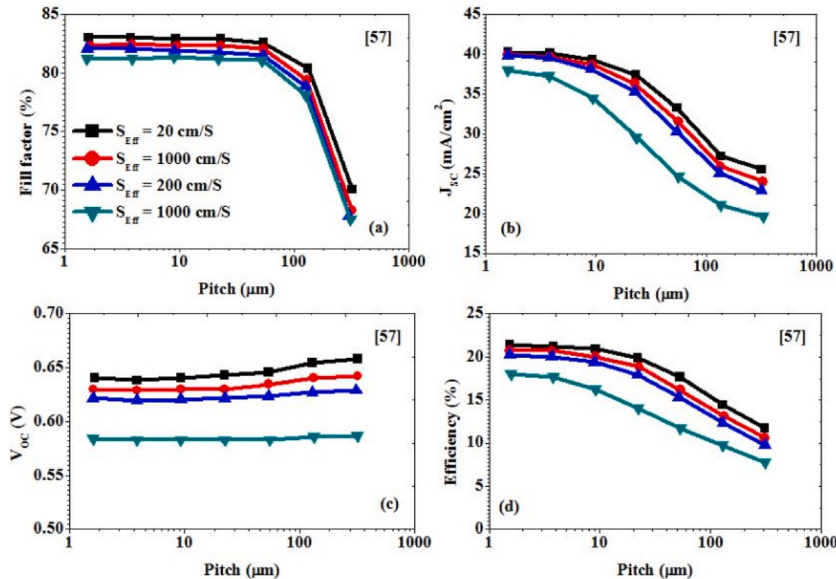


Fig. 6. Influence of S_{eff} and pitch variation on the PV characteristics of silicon nanocone cell (a) FF Vs Pitch characteristics (b) J_{sc} Vs Pitch characteristics (c) V_{oc} Vs Pitch characteristics (d) Efficiency Vs Pitch characteristics [57].

substrates on the J-V characteristics of SHJ cell is shown in Fig. 7 (b). From Fig. 7 (b) it is understood that SHJ solar cells on graphene/pyramidal substrate exhibits superior photovoltaic performance compared with SHJ solar cells on graphene/planar Si substrates. Fig. 7 (c) depicts the influence of variation in thickness of α -phase FeSi(Al) layer on the PV performance of α -phase FeSi(Al)/p + -Si/n-Si cells. Increase in thickness of α -phase FeSi(Al) layer results in the severe degradation of J_{SC} which is evident from Fig. 7 (c). The effect of rapid thermal annealing (RTA) process on the PV performance of α -phase FeSi(Al)/p + -Si/n-Si cells is shown in Fig. 7 (d). From Fig. 7 (d) it is very clear that a higher RTA temperature results in the improvement of both J_{SC} and V_{OC} of α -phase FeSi(Al)/p + -Si/n-Si cells.

The influence of length of nanowires on the photovoltaic performance of SiNWs based solar cell is plotted in Fig. 8. Fig. 8 reveals the fact that increasing the length of nanowires results in the severe degradation of J_{SC} , V_{OC} , and PCE of SiNWs based solar cells. In summary, there are three main types of Si cells and they are single crystal Si cells, poly crystal Si cells and amorphous Si cells. According to the NREL (National Renewable Energy Laboratory) efficiency chart, the highest PCE reported for Si cells is 27.6%. Single crystal cells are highly reliable and area efficient. Poly crystal cells require larger area and are less heat tolerant. Amorphous Si cells are flexible and light weight devices but exhibits less output power so not suitable for large scale applications.

3. Perovskite solar cells (PSCs)

The PCE of flat-plate SJ solar cell is approaching to its theoretical-efficiency limit due to the rapid advancements in fabrication processes, photovoltaic materials and solar cell structures [105]. Organometal trihalide PSCs have gained tremendous attention in the PV industry due to their unique characteristics such as good flexibility, low cost, good scalability, low temperature processability and comparable photovoltaic performance with traditional thin film inorganic SCs. Even though PSCs have the potential for performance enhancements, due to the inability of producing different colour appearances, it still remains difficult to integrate with building envelopes and automotive surfaces such as awnings, windows, walls and facades. Photonic crystal and Fabry-Perot cavity based nanostructured colour filtering techniques can be incorporated in PSCs to overcome the above mentioned challenges. The J_{SC} of PSCs can be computed as [105].

$$J_{SC} = \int_{400nm}^{800nm} \frac{e\lambda}{hc} QE(\lambda) I_{AM1.5}(\lambda) d\lambda \quad (18)$$

Where, $I_{AM1.5}$, λ , e , h and c represents AM1.5 solar spectral irradiance, wavelength, electron charge, Plank's constant and velocity of light respectively. Perovskite materials have a 3-D crystal-structure and it consist of three ions (A, B and X) with a stoichiometry of ABX_3 . A and B represents cations and X represents halide anions. For inorganic PSCs, caesium is commonly used as A-cation, tin or lead is used as B-cation and chlorine, bromine or iodine is used as X-anions. Methylammonium (MA) or Formamidinium (FA) has been used as A-cations for hybrid PSCs. The time is urged to think beyond SJ-SCs and intermediate band-gap solar-cells, hot-carrier collection, multi-exciton generation and singlet fission are the emerging concepts for beyond SJ solar cells [106]. Several key issues such as long term stability and reliability, recombination losses and challenges in scaling to large electrode areas needs to be addressed before industrialization.

Recombination losses in PSCs are commonly associated with the interface of the transport layer and perovskite bulk [107]. Light

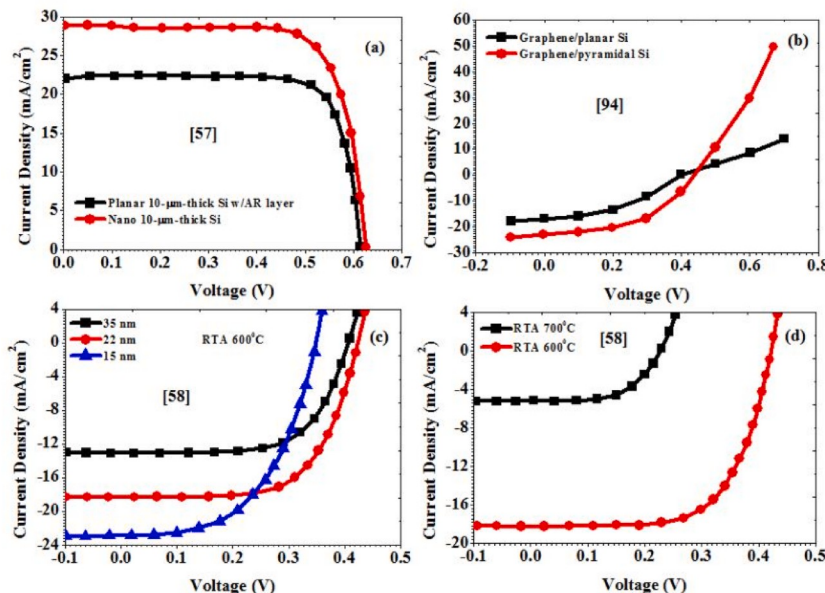


Fig. 7. (a) J-V characteristics of planar and nanocone structure based Si solar cell (b) Influence of graphene on planar Si wafer and pyramidal Si wafer (c) Effect of thickness of α -phase FeSi(Al) layer on the J-V characteristics (d) Effect of RTA temperature on the J-V curves.

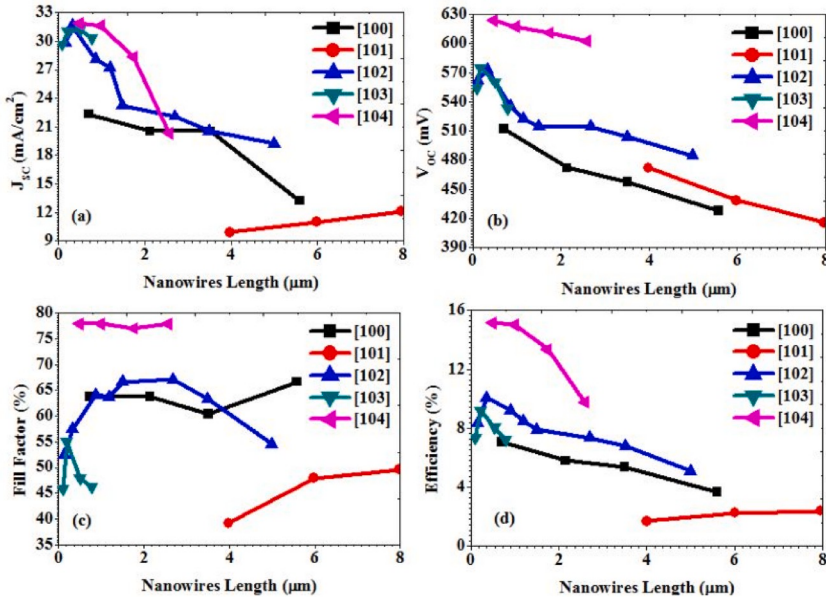


Fig. 8. Influence of length of nanowires on the PV-performance of SiNWs based cell.

weight, high stability, high efficiency and low cost are the key requirements of a light-absorbing material for SCs. A chemically inert ETL (electron transport layer) is essential to increase the efficiency of PSCs. In 2018, Makhsum I. Saidaminov et al. [108] demonstrated the use of small isovalent-ions to improve the stability of PSCs in air which undergoes degradation in the presence of trace water and oxygen. Compared with single MAPbI₃ or FAPbI₃ perovskite materials, mixed CsMAFA exhibits superior photovoltaic performance due to their large minority carrier life time and reduced trap densities [109]. Miyasaka et al. [110] demonstrated the first perovskite sensitized TiO₂ cell based on liquid electrolytes. Photovoltaic materials with long carrier diffusion lengths, relatively large absorption coefficient and flexible band-gap tuning are desirable for achieving large V_{OC} of solar cells which is evident from equation (19).

$$V_{OC} = \frac{KT}{q} \ln \left(\frac{J_{SC}}{J_0} \right) = \frac{KT}{q} \ln \left(\frac{J_{SC} N_D \tau_{eff}}{qn_i^2 d} \right) \quad (19)$$

where “d” represents the active layer thickness. There are mainly three types of PSCs namely planar n-i-p, mesoporous n-i-p and inverted p-i-n solar cells which is shown in Fig. 9. Spin coating technique is commonly used to grow thin perovskite films. Screen printing, inkjet printing, electro deposition, blade coating, spray coating, meniscus coating and slot-die coating are the popular scalable solution deposition techniques used for growing thin perovskite films [111–113]. In order to reduce defects thermal annealing is preferred after the deposition of thin perovskite films. The charge transport layers play an important role on the scalability of PSCs.

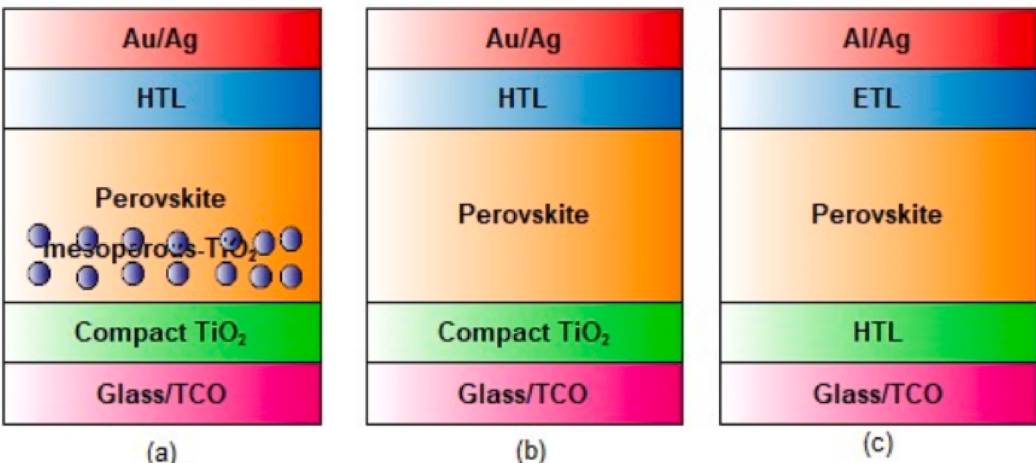


Fig. 9. (a) Mesoporous n-i-p (b) Regular planar n-i-p and (c) inverted planar p-i-n cell structures.

Charge transport layers can be made of either organic or inorganic materials.

TiO_2 , ZnO and SnO_2 are the popularly used ETL materials in n-i-p PSCs. Organic materials such as spiro-OMeTAD, PTAA (Poly-triarylamine), P3HT (Poly (3-hexylthiophene)) and inorganic materials such as CuI and CuSCN are the popularly used HTL (hole transport layer) materials in n-i-p PSCs [6,6].-phenyl-C₆₁-butyric acid methyl ester (PCBM) and Indene-C₆₀-bisadduct (ICBA) are the commonly used ETL materials in p-i-n PSCs. Organic materials such as PTAA and PEDOT:PSS and inorganic-materials such as CuSCN and NiO_x are the popularly used HTL materials in p-i-n PSCs [113]. External factors such as temperature, oxygen, mechanical stress, moisture and DC bias can affect the light absorbing layer and intermediate layers of PSCs which severely degrades its photovoltaic performance [114–117]. The J-V curves of some of the popular PSCs are shown in Fig. 10. In 2016, Wanyi Nie et al. [118] investigated the light activated photocurrent degradation in organo-metallic PSCs and reported that the solar cells can self-heal totally by placing them in the dark conditions [119–123]. In 2018, Chang Liu et al. [119] reported that by employing a CsPbI_3 quantum dot interface engineering layer, the stability and PCE of PSCs can be improved. In order to increase the stability and efficiency of CsPbI_3 cells, poly-vinylpyrrolidone (PVP) induced surface passivation technique can be used [124]. In 2016, Sang-Won Lee et al. [125] investigated the impact of UV light on PSCs and absorbed that increasing the time of UV light exposure results in the degradation of key parameters of PSCs like V_{OC} , J_{SC} , FF and PCE. In 2015, Wei Zhang et al. [126], illustrated that addition of HPA (hypophosphorous acid) in the precursor-solution can effectively increase the PCE of PSCs by significantly improving the perovskite film quality.

Fig. 11 (a) depicts the effect of different perovskite materials on the J-V characteristics of PSCs and from Fig. 11 (a) it is evident that solar cells with $\text{MAPbI}_{3-x}\text{Cl}_x$ (AlO_2) material exhibits higher J_{SC} and solar cells with p-type PIF8-TAA (indenofluorene triarylamine copolymer) material exhibits higher V_{OC} compared with other perovskite materials. The influence of metallic film thickness on the J-V curves of PSCs is shown in Fig. 11 (b). From Fig. 11 (b) it is understood that larger metallic film thickness results in the severe degradation of J_{SC} of solar cells. Fig. 11 (c) indicates that PSCs with fewer defects trap density exhibits superior J-V characteristics. Fig. 11 (d) shows that the introduction of CsPbI_3 QD interface engineering layer can effectively improve the PCE of PSCs.

In 2016 Qian Zhao et al. [127] demonstrated a chemical approach to improve the quality of methylammonium lead halide film by adding an appropriate amount of acetic acid that resulted in the enhancement of photovoltaic performance of PSCs. In 2018, Jae Choul Yu et al. [128] demonstrated that using a PEDOT:GO composite HTL can effectively improve the PCE and stability of inverted PSCs compared with PEDOT:PSS HTL based cells. For flexible applications inverted structure is highly suitable [129]. Bottom up approach is commonly used to fabricate PSCs. However bottom up approach involves the critical issues like growth rate, nucleation density and control of crystal size. In 2018, Johannes Schlipf et al. [130] reported a top down approach that can be used for fabricating single crystal PSCs. In 2017, Zhiping Wang et al. [131] reported a hetero-structured butylammonium-caesium-formamidinium lead halide perovskite based solar cells which outperform traditional MA (Methylammonium) based or FA ($\text{HC}(\text{NH}_2)_2$) based or a combination of FA and MA based PSCs in terms of stability and efficiency. In 2016, W. Heming et al. [132] analyzed the impact of a composite light harvesting layer ($\text{PTBT}(\text{Polymer})+\text{CH}_3\text{NH}_3\text{PbI}_3$ (Perovskite)) and a single perovskite light harvesting layer on the PV-performance of SCs and found that PSCs with composite light harvesting layer exhibit higher V_{OC} and PCE.

The influence of amount of acetate ions (HAc) on the photovoltaic characteristics of PSC is shown in Fig. 12 (a). Perovskite solar cell with 0.5 M HAc concentration exhibits the best photovoltaic performance compared with solar cells with 0 M and 1M HAc concentrations. Fig. 12 (b) indicates that PSCs with regular device architecture exhibits superior photovoltaic performance compared with solar cells with inverted cell architecture. The performance comparison of J-V characteristics for inverted cells manufactured on ITO-covered glass and PET substrates is plotted in Fig. 12 (c). From Fig. 12 (c) it is clear that solar cell with ITO coated glass substrate exhibits higher photovoltaic performance compared with solar cell with ITO-covered PET substrate. Fig. 12 (d) depicts the influence of FTO (Fluorine doped tin oxide) and Zn_2SnO_4 photoelectrodes (Zn_2SnO_4 paste-500, Zn_2SnO_4 paste-600 and Zn_2SnO_4 paste-700) annealed at different temperatures on the J-V characteristics of PSCs. Fig. 12 (d) indicates that compared with FTO-500, Zn_2SnO_4 photoelectrodes are found to be effective in improving the photovoltaic performance of PSCs.

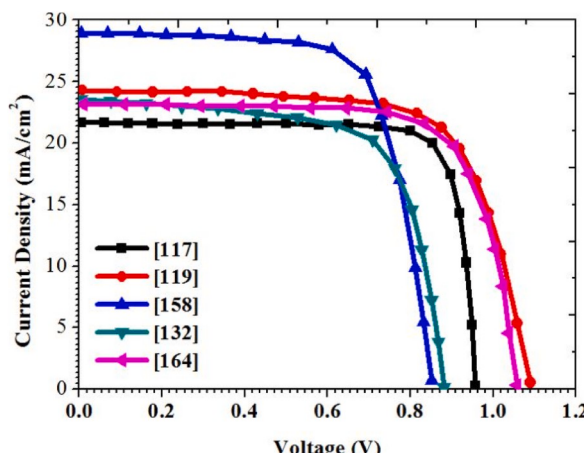


Fig. 10. J-V characteristics of some of the high performance PSCs.

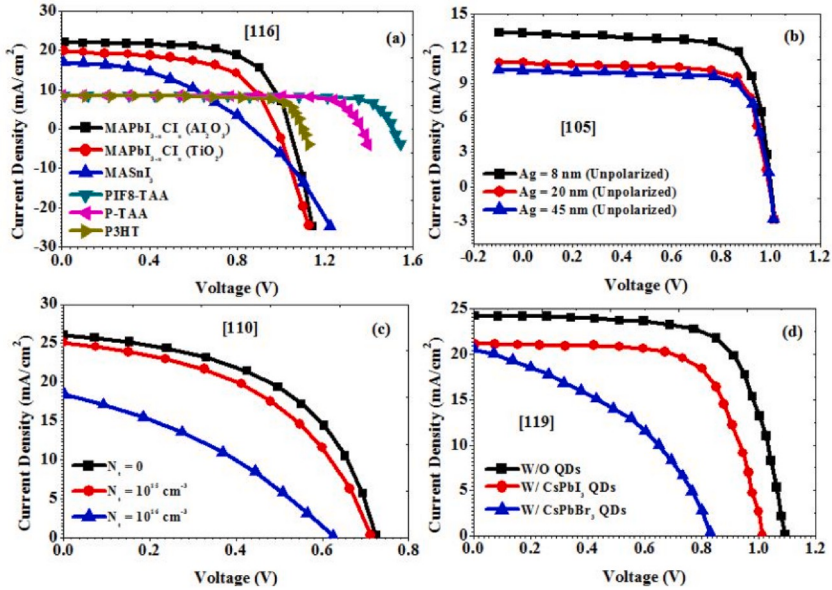


Fig. 11. (a) Influence of various perovskite materials on the J-V curves (b) The dependence of J-V characteristics on metallic film thickness (c) Impact of trap density (N_t) on the J-V curves and (d) The effect of quantum dots on the J-V curves of PSCs.

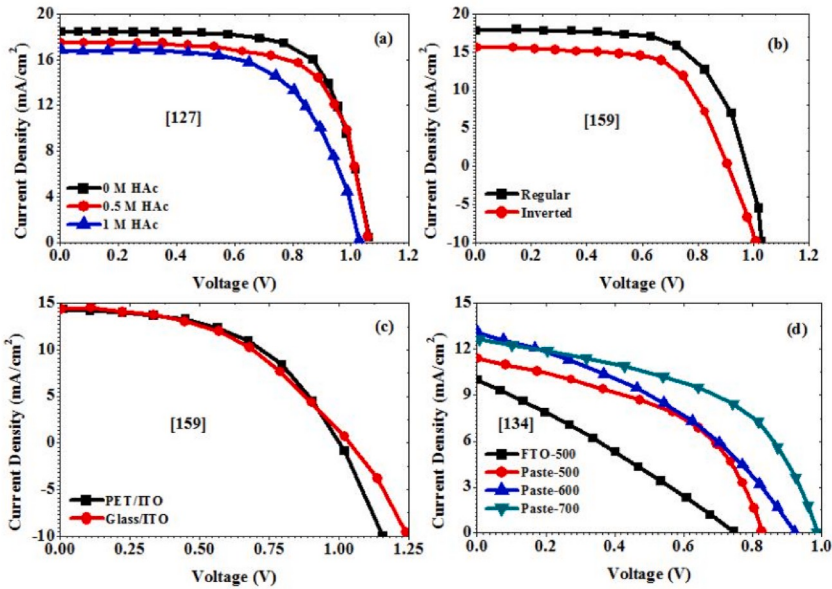


Fig. 12. (a) The influence of amount of acetate ions (HAc) on the J-V characteristics (b) Performance comparison of regular and inverted PSCs (c) J-V curves for inverted cells fabricated on ITO-covered glass and PET substrates (d) J-V characteristics of PSCs with various Zn₂SnO₄ photoelectrodes.

Fig. 13 (a) shows the effect of various HTL materials on the J-V characteristics of inorganic–organic hybrid hetero-junction solar cell and it indicates that PSCs with PTAA and mp-TiO₂ HTMs exhibits outstanding photovoltaic performance. **Fig. 13** (b) depicts the impact of poly [2-methoxy-5-(2-ethyl hexyloxy)-1,4-phenylenevinylene (MEH-PPV), Spiro-OMeTAD and P3HT HTMs dissolved in different solvents with varying concentrations on J-V characteristics of PSCs. From **Fig. 13** (b) it is evident that PSCs with Spiro-OMeTAD HTM dissolved in CB solution exhibits higher J_{SC} and cells with MEH-PPV HTM dissolved in toluene solution exhibits higher V_{OC} compared with other HTMs dissolved in different solvents. **Fig. 13** (c) shows the J-V performance of SCs with single CH₃NH₃PbI₃ and composite PTB7-CH₃NH₃PbI₃ perovskite materials and from this plot it is clear that the polymer-perovskite composite active layers help to increase the V_{OC} of the SCs. However, adding the polymer in the active layer leads to the minor degradation of J_{SC} . **Fig. 13** (d) plots the J-V performance of SCs using the A_{0.83}Cs_{0.17}Pb(I_{0.6}Br_{0.4})₃ and BA_{0.09}(FA_{0.83}Cs_{0.17})_{0.91}Pb(I_{0.6}Br_{0.4})₃

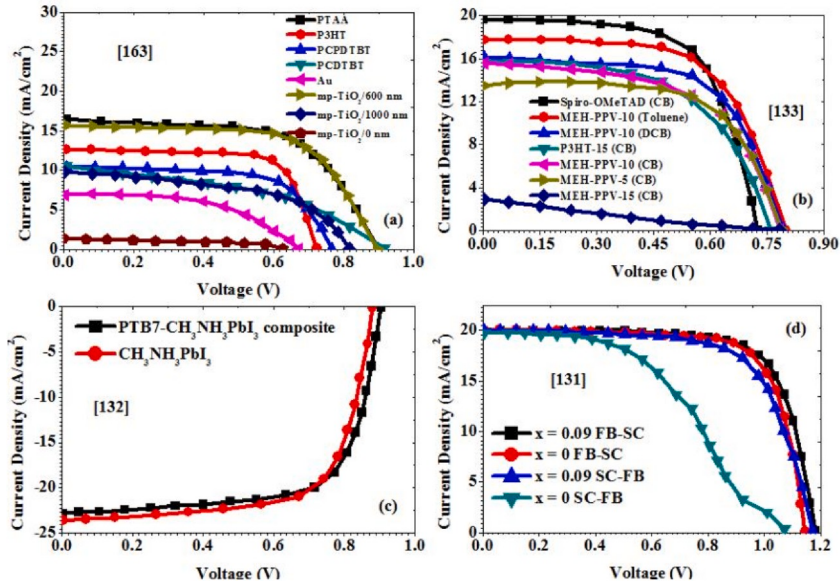


Fig. 13. (a) The effect of different HTLs on the J-V curves of inorganic-organic hybrid hetero-junction solar cells (b) J-V behaviour of PSCs with different HTL materials dissolved in various solvents with varying concentrations (CB: chlorobenzene, DCB: dichlorobenzene). (c) J-V characteristics of solar cells with single CH₃NH₃PbI₃ and composite PTB7-CH₃NH₃PbI₃ perovskite materials (d) J-V performance of SCs using the A_{0.83}Cs_{0.17}Pb(I_{0.6}Br_{0.4})₃ (marked as x = 0) and BA_{0.09}(FA_{0.83}Cs_{0.17})_{0.91}Pb(I_{0.6}Br_{0.4})₃ (marked as x = 0.09) perovskite active layers.

perovskite active layers. From Fig. 13 (d) it is clear that perovskite solar cell with BA_{0.09}(FA_{0.83}Cs_{0.17})_{0.91}Pb(I_{0.6}Br_{0.4})₃ active layer exhibits outstanding photovoltaic performance measured under FB (forward bias) to SC (short circuit) conditions.

Fig. 14 (a) shows the influence of PbS QD concentrations on the J-V curves of CH₃NH₃PbI₃/PbS hetero-junction PSCs. The introduction of PbS QDs significantly affects the photovoltaic performance of CH₃NH₃PbI₃/PbS hetero-junction PSCs and cells with 1.5 mg/ml PbS QD is found to be suitable for achieving high J_{SC} and V_{OC}. The introduction of PbS QD as an EBL helps to reduce the recombination losses at interfaces and it also enhances the carrier transport characteristics of the cells. Fig. 14 (b) demonstrates the influence of NiO Nanoparticles (HTM) on the J-V performance of carbon-based PSCs. From Fig. 14 (b) it is evident that solar cells with NiO nanoparticles based hole transport layer exhibits outstanding photovoltaic performance compared with PSCs without NiO

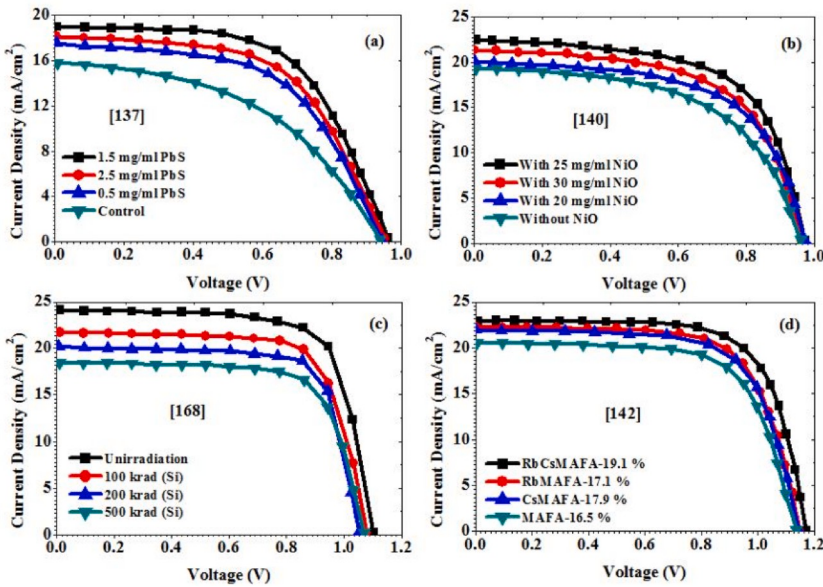


Fig. 14. (a)The influence of PbS QD concentrations on the J-V curves of CH₃NH₃PbI₃/PbShetero-junction PSCs (b) The influence of NiO Nanoparticles (HTM) on the J-V curves of carbon-based PSCs (c) The impact of gamma-ray irradiation dose on the J-V curves of PSCs (d) J-V performance of PSCs fabricated with perovskite films containingvarious cations.

nanoparticles. The introduction of NiO nanoparticles as HTL can effectively improves the extraction and separation of optically generated carriers and it can effectively minimize the losses due to recombination at the perovskite/carbon electrode interface, that results in the enhancement of PV-performance of the device. Fig. 14 (c) depicts the impact of gamma-ray irradiation dose on the photovoltaic performance of PSCs and it reveals the fact that increase in gamma-ray irradiation dose leads to the severe degradation of both J_{SC} and V_{OC} of the cells. This is mainly due to the factors such as phase transition of perovskite active layers that results in the reduction of absorbance of perovskite films and the colour appearance of the glass substrate induced by the gamma-ray-irradiation that leads to the degradation of transmittance of glass substrate. Fig. 14 (d) shows the J-V performance of PSCs manufactured with perovskite films containing various cations and this plot reveals that PSCs with RbCsMAFA cations exhibits outstanding photovoltaic performance compared with cells with other cations such as RbMAFA, CsMAFA and MAFA cations. RbCsMAFA cation is found to be effective in minimizing radiative recombination losses in PSCs.

In 2016, Hsin-Wei Chen et al. [133] demonstrated the effect of HTL materials like spiro-OMeTAD, P3HT and MEH-PPV dissolved in different solvents like chlorobenzene (CB) and dichlorobenzene (DCB) on the PV-performance of PSCs and observed that cells with HTL materials exhibits higher J_{SC} and PCE, cells with MEH-PPV exhibits higher V_{OC} . Equation (20) represents the relationship between dark current density (J_0), electroluminescence external quantum efficiency (EQE_{EL}), external quantum efficiency of photovoltaic (EQE_{PV}) and photon flux of the surroundings (ϕ_{BB}). Equations (21) and (22) can be used for computing J_{SC} and V_{OC} of PSCs as a

Table 2
Photovoltaic performance of state of the art PSCs.

Ref.	Structure/Features	V_{OC} (mV)	J_{SC} (mA/cm ²)	FF (%)	PCE (%)
[105]	Red/Plasmonic Nanoresonators	1000	13.17	77	10.12
[105]	Green/Plasmonic Nanoresonators	990	10.77	77	8.17
[105]	Blue/Plasmonic Nanoresonators	990	10	78	7.72
[112]	Glass/FTO/NiO _x /CsPbI _{3-x} Br _x /ZnO/Al	1010	8.65	63.6	5.57
[112]	Glass/FTO/NiO _x /CsPbI _{3-x} Br _x /ZnO/ITO	1000	7.92	59.2	4.29
[119]	CsPbI ₃ quantum dots interface layer	1050	24.28	71	18.14
[122]	CH ₃ NH ₃ PbI ₃ flexible perovskite	1010	18.1	70	13.9
[124]	Surface passivated CsPbI ₃ perovskites	1100	14.83	65	10.61
[125]	CH ₃ NH ₃ PbI ₃	1038	15.26	77.2	11.64
[126]	FTO/c-TiO ₂ /perovskite/spiro-OMeTAD/Ag	1070	20.4	74	16.2
[127]	CH ₃ NH ₃ Ac/Acetate treatment	1063	18.4	71	13.86
[158]	Mixed tin-lead iodide low-bandgap	1141	20.1	80	18.3
[159]	CH ₃ NH ₃ PbI _{3-x} Cl _x /polymer substrates	880	14.4	51	6.4
[159]	CH ₃ NH ₃ PbI _{3-x} Cl _x /glass substrates	920	14.4	47	6.3
[128]	ITO/PEDOT:PSS/perovskite/PCBM/ZnO	970	19.63	78.5	14.95
[128]	ITO/PEDOT:GO/perovskite/PCBM/ZnO	1020	21.55	82.3	18.09
[160]	CH ₃ NH ₃ PbI ₃ planar perovskite cell	1050	21.9	72	16.5
[161]	Vapour-deposited hetero-junction cell	1070	21.5	67	15.4
[161]	Solution-processed hetero-junction cell	840	17.6	58	8.6
[162]	CH ₃ NH ₃ PbI ₃ /mesoporous TiO ₂	970	19.05	66	12.54
[131]	FA _{0.83} Cs _{0.17} Pb(I _{0.6} Br _{0.4}) ₃	1140	19.8	75	16.9
[131]	BA(FACs)Pb(IBr) ₃	1180	19.8	73	17.2
[131]	BA(FACs)Pb(IBr) ₃	1140	22.7	80	20.6
[132]	CH ₃ NH ₃ PbI ₃ perovskite	860	20.88	70	14.3
[132]	PTB7-CH ₃ NH ₃ PbI ₃ composite	880	22.28	63	14.4
[133]	Spiro-OMeTAD (CB)	730	19.68	64	9.20
[133]	P3HT-(CB)	760	15.68	57	6.70
[133]	MEH-PPV-(CB)	800	15.62	64	7.21
[133]	MEH-PPV-(DCB)	800	16.18	62	8.06
[133]	MEH-PPV-(Toluene)	800	17.70	63	8.87
[134]	Zn ₂ SnO ₄ nanofiber photoelectrodes	986	12.68	59	7.38
[163]	Hybrid HJ solar cells	997	16.5	72.7	12
[164]	Planar HJ solar cells	1055	23.11	78	19
[165]	Planar solar cell	1072	21.6	69.6	16.1
[166]	NiO _x HTL solar cell	1070	17.8	63	11.9
[137]	TiO ₂ /CH ₃ NH ₃ PbI ₃ /PbS QDs.	970	19.03	61.3	11.32
[138]	CVD based Pb-free air-stableMBI layer	390	0.13	38.9	2
[167]	Planar cell with ionic liquid additives	1080	23.8	81	19.8
[140]	NiO Nanoparticles in C-based perovskite	970	22.49	62	12.7
[168]	FA _{0.945} MA _{0.025} Cs _{0.03} Pb(I _{0.975} Br _{0.025}) ₃	1100	24.04	71.4	19.03
[141]	Hybrid perovskite MAPbI ₃ solar cell	990	22.9	77.8	17.64
[141]	MAPbI _{3-x} Nd ³⁺ Hybrid perovskite cell	1040	24.33	83.6	21.15
[142]	RbCsMAFA	1170	22.4	73	19.1
[142]	CsMAFA	1140	21.9	72	17.9
[142]	RbMAFA	1150	22.2	67	17.1
[142]	MAFA	1140	21	69	16.5
[169]	CH ₃ NH ₃ PbI _{3-x} Cl _x on Al ₂ O ₃	1050	22.9	66	15.5
[157]	Plasmonic/planar hetero-junction cell	1044	22.10	72	17.38

function of EQE_{EL} , EQE_{PV} and φ_{BB} respectively [134–136].

$$J_0 = \frac{q}{\text{EQE}_{\text{EL}}} \cdot \int_0^{\infty} \text{EQE}_{\text{PV}}(E) \cdot \varphi_{\text{BB}}(E) dE \quad (20)$$

$$J_{\text{SC}} = q \int_0^{\infty} \text{EQE}_{\text{PV}}(E) \varphi_{\text{AM1.5}}(E) dE \quad (21)$$

$$V_{\text{OC}} = \frac{kT}{q} \ln \left(\frac{J_{\text{SC}} \cdot \text{EQE}_{\text{EL}}}{q \int \text{EQE}_{\text{PV}}(E) \cdot \varphi_{\text{BB}}(E) dE} \right) \quad (22)$$

In 2018, Gen Zhao et al. [132] demonstrated the use of a colloidal PbS QD electron blocking layer (EBL) for improving the stability and efficiency of PSCs. The critical issues preventing the commercialization of PSCs are lack of deposition techniques for highly stable large area and the toxicity of the widely used Pb-based perovskite materials. In 2019, S. Sanders et al. [138] demonstrated a Pb-free air stable organic-inorganic MBI (Methylammonium Bismuth Iodide) perovskite material based solar cell in which the perovskite film was deposited using chemical vapour deposition (CVD) process. Bismuth based perovskite materials provides outstanding stability. Compared with spin coating, CVD process offer excellent process control, good reproducibility and no substrate size limits [139]. Due to low cost and high thermal conductivity, carbon can be used as an electrode material in PSCs and in 2019, Chang Cai et al. [140] reported a highly efficient and stable carbon electrode based PSC in which NiO nanoparticles were used to enhance the hole extraction. Perovskite solar cells designed for space craft applications should have good radiation tolerance. In 2019, Kai Wang et al. [141] demonstrated a high performance inorganic-organic hybrid PSC that incorporated heterovalent neodymium cations (Nd^{3+}) in perovskite material. Addition of rare earth metal cations like Nd^{3+} , Eu^{3+} and Sm^{3+} improves the quality of perovskite films by reducing defects and chemical fluctuation. In 2019, Ankur Solanki et al. [142] demonstrated the impact of metal cations such as Rb^{3+} and Cs^{3+} on carrier dynamics in PSCs and found that solar cells with Rb^{3+} and Cs^{3+} metal cations added perovskite materials exhibited the highest PCE, FF, J_{SC} and V_{OC} . The stability of PSCs can be measured using tolerance-factor (t) which is given in equation (23) [143].

$$t = \frac{r_A + r_x}{\sqrt{2}(r_B + r_x)} \quad (23)$$

where, r_A , r_B and r_x are the radii of A-cation, B-cation and X-anion respectively. For a highly stable perovskite material the value of tolerance factor should be unity. High carrier mobility, low cost and superior chemical stability are the key requirements of a HTL material used in PSCs and inorganic materials such as NiO_x , CuO_x , CrO_x , CoO_x , CuI , CuS , VO_x , CuInS_2 , MoO_x , WO_x , CuAlO_2 , CuCrO_2 , CuZnSnS_4 , CuGaO_2 and CuBaSnS_4 are the widely used inorganic HTM in PSCs [144–156]. In 2019, Wenqiu Deng et al. [157] successfully demonstrated that the efficiency of hetero-junction planar SCs can be increased by using plasmonic effect of metal nanomaterials. Because of low production cost, simple fabrication processes and excellent photovoltaic performance the PSCs have been gaining tremendous attention in the PV-industry. It is also interesting to see that the PV-performance of PSCs can be further enhanced by introducing metal nanoparticles in the perovskite materials. According to NREL efficiency chart, the highest PCE obtained for PSCs is 25.2%. The long term operational stability and PCE of PSCs needs to be further improved for its commercialization. The Photovoltaic performance of PSCs is given in Table-2.

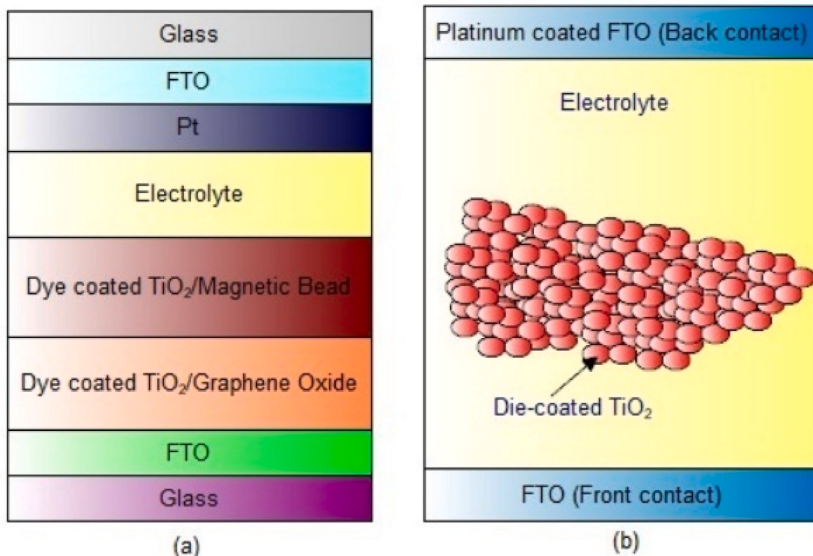


Fig. 15. (a) Architecture of DSSCs with GO and MB (b) Architecture of Liquid based DSSC.

4. Dye sensitized solar cells (DSSCs)

A DSSC is basically an electro-chemical cell in which a mesoporous and spongy dye-coated semiconductor is plunged into an electrolyte [170]. Nano particle made TiO_2 is the commonly used semiconductor in DSSCs. The TiO_2 paste is then deposited in a TCO which act as one electrode for the DSSCs. A Monolayer of molecules called dye is then covered on the surface of a mesoporous material. The dye act as the photoactive layer in DSSCs. The electrolyte normally contains an iodide/triiodide redox pair (I^-/I_3^-) in which the iodide and triiodide works like reducer and oxidant respectively. When sunlight falls on the dye, molecules absorbs the photons and gets photo excited. The structure of a DSSC is shown in Fig. 15. The first DSSC is introduced by O' Regan et al., in 1991 based on dye sensitized colloidal TiO_2 film [171]. In 2015, Jung-Chuan Chou et al. [172] demonstrated a DSSC which is fabricated with two layers of TiO_2 photo electrode composed of a TiO_2/GO (Graphene oxide) layer and a TiO_2/MB (Magnetic bead composed of Fe_3O_4). Spin coating was used to deposit TiO_2/MB layer on top of TiO_2/GO layer. The liquid electrolyte is made of a combination of 0.6 M 1-propyl-2, 3-dimethyl imidazolium iodide (DPMII), 0.05 M iodine, 0.5 M LiI (Lithium iodide), 0.5 M TBP (4-*tert*-butylpyridine) and 15 ml MPN (3-methoxy propionitrile). DSSCs can be fabricated on a variety of wafers such as glass, flexible materials and polymer materials. DSSCs utilize platinum counter electrodes (PtCE) for achieving high power conversion efficiency due to their outstanding electro-catalytic properties. However, the factors such as need for sophisticated equipments, high cost due to wastage of materials and high temperature requirements for the precursor thermal decomposition etc prevents them from using for mass production. In 2018, Idris K. Popoola et al. [173] reported a novel photo fabrication method to manufacture highly transparent PtCEs by UV irradiation of platonic acid ($\text{H}_2\text{PtCl}_6 \cdot 6\text{H}_2\text{O}$) on rigid FTO and flexible ITO on PET (Polyethylene terphthalate) substrate. Ruthenium based materials such as N719, N3, CYC-B11 and C106 have been considered as the most suitable dye materials for DSSCs. Large band-gap materials such as TiO_2 , SnO_2 or ZnO_2 can be used as sensitizing dye in DSSCs [174].

The PCE of DSSCs can be improved by two ways and the first method is by extending the light harvesting into near infrared and second method is to reduce the redox potential of liquid electrolyte to improve V_{OC} . Solid-state (SS) DSSCs use solid hole conductors made of small molecules like spiro-OMeTAD or PEDOT or P3HT instead of liquid electrolytes. Solution deposition techniques can be used for fabricating solid hole conductors [175,176]. Interface engineering can be used to reduce recombination solid state DSSCs to improve the photovoltaic performance. Light trapping techniques such as depositing large size Titania particles on top of a layer of normal size Titania, Photonic crystals and plasmonic effects can be used to enhance the light collection efficiency of DSSCs. In 2017, Min Ju Yun et al. [177] demonstrated a 3-D micro patterned photo anode for improving the PCE of DSSCs and also reported that increasing the pattern size of photo anodes results in the enhancement of photovoltaic performance of DSSCs. In 2016, Min Ju Yun et al. [178] reported the development of a textile based DSSC which can be used for wearable electronic devices. Ease of fabrication and environment friendliness makes the metal free and pure organic DSSCs more prominent in the scientific community. Arylamine, perylenes and anthocyanin are some of the popular metal free organic dyes. Due to tunable donor-acceptor mobilities and large molar absorption coefficient, arylamine organic dyes have gained tremendous attention in the last decade.

In 2017, Supratik Kar et al. [179] investigated the photovoltaic properties of organic lead dyes for DSSCs for future renewable energy technologies. 11 classes of organic lead dyes are triphenylamine (TPA), substituted TPA, planar and branched TPA, Fluorine based TPA, naphthalene based TPA, truxene based TPA, Indoline, N,N-Dialkylaniline, phenothiazine and phenoxazine, cabrazole and tetrahydroquinoline. In 2016, M. Klein et al. [180] reported that impact of magnetic field effects on photo-current generation in DSSCs can be controlled by spin coherence time and radius of electron-hole pairs. In 2008, Seigo Ito et al. [181] reported a novel bifacial DSSC architecture based on a liquid ionic electrolyte that offers high PCE. The incorporation of a SiO_2 between the electrodes results in the prevention of unnecessary back current generation that leads to the improvement of photovoltaic properties of ruthenium dye (Z907Na) based DSSC. Bifacial SCs are cost effective and power efficient compared with conventional DSSCs. In 2017, Yiming Cao et al. [182] demonstrated a 11% efficiency SS-DSSC with a HTL composed of $[\text{Cu}(4,4',6,6'\text{-tetramethyl-2,2'-bipyridine})_2]\text{bis}$

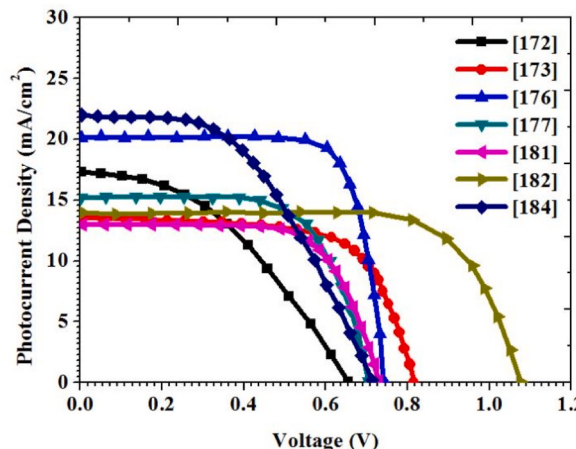


Fig. 16. J-V curves of some of the high performance DSSCs.

(trifluoromethylsulfonyl)imide) and $[\text{Cu}(4,4',6,6'\text{-tetramethyl-2,2'-bipyridine})_2](\text{bis}(\text{trifluoromethylsulfonyl})\text{imide})_2$. William Ghann et al. [183] demonstrated the photovoltaic performance of natural DSSCs with dyes extracted from pomegranate, blackberry, cranberry and blueberry. William Ghann et al. reported that fabricated natural DSSC with pomegranate exhibited higher PCE. In 2016, Joydip Dutta et al. [184] demonstrated the enhancement of PCE of DSSC with $\text{Y}_2\text{O}_3:\text{Ho}^{3+}/\text{Yb}^{3+}$ upconverting nanophosphors. In 2019, Jung-Chuan Chou et al. [185] illustrated that the PCE of DSSCs can be increased by using ZnO nanorod modified TiO₂ photoanode. In 2019, Jung-Chuan Chou et al. [186] showed that the charge transport properties and PCE of DSSCs can be increased with the help of a TiO₂ layer as ETL and a TiO₂/GO layer as light absorption layer. Cossensitization technique can be used in DSSCs for improving its efficiency. Cossensitization relies on sensitizing the same TiO₂ film with two dyes having complementary absorption spectra. In 2019, Vanessa A. El Bitar Nehme et al. [187] reported cossensitization of dyes in DSSCs with pyridine groups with carboxylic acid based dyes. The J-V performance of some of the high performance DSSCs are shown in Fig. 16. The Photovoltaic performance of state of the art DSSCs are given in Table 3.

Fig. 17 (a) depicts the influence of rear and front side irradiation with and without a porous SiO₂ spacer which indicates that the introduction of the porous SiO₂ spacer enhances the J_{SC} that leads to the improvement of PCE. Fig. 17 (b), Fig. 17 (c) and Fig. 17 (d) shows the influence of inter-weft spacing and the number of wires for photo-electrodes on the J-V curves of the mono-layered and monolithic structured textiles based DSSCs. Fig. 17 (b), Fig. 17 (c) and Fig. 17 (d) reveals that DSSCs with single wired photo-electrodes and higher inter-weft spacing offers superior photovoltaic behavior in terms of high J_{SC} , V_{OC} , FF and PCE. Fig. 18 (a) plots the influence of optical irradiation on the J-V curves of solid state DSSCs which reveals the fact that increase in optical irradiation in DSSCs increases its PCE [196]. Fig. 18 (b) shows that DSSCs with Y123 dye and spiro-OMedTAD HTL materials provides higher V_{OC} but suffer from very poor J_{SC} . DSSCs with ruthenium dye (CYC-B11) and iodide redox couple exhibits higher J_{SC} and suffer from very poor V_{OC} . However, DSSCs with Y123/Cobalt redox couple and co-sensitized donor-pi-acceptor dye YD2-o-C8 exhibits outstanding J_{SC} and V_{OC} compared with CYC-B11/iodide and Y123/spiro-OMeTAD dye based DSSCs. Fig. 18 (c) illustrates the impact of different electrodes on the J-V

Table 3

An overview of photovoltaic performance of DSSCs.

Ref.	Structure/Features	V_{OC} (mV)	J_{SC} (mA/cm ²)	FF (%)	PCE (%)
[172]	Glass/FTO/TiO ₂ /GO/TiO ₂ /MB	710	11.29	28.71	2.31
[172]	With 1.5 ml GO	650	12.93	46.32	3.92
[172]	With 0.5 ml MB	700	11.43	50.25	4.03
[172]	With 1.5 ml GO+0.25 ml MB	650	13.39	51.18	4.45
[172]	With 1.5 ml GO+0.5 ml MB	660	17.23	40.93	4.63
[172]	With 1.5 ml GO+0.75 ml MB	620	7.45	54.18	2.53
[188]	GO additive	820	10.82	65	5.72
[189]	RGO additive	770	12.51	62.40	6.01
[190]	ZnO additive	590	7.64	50.41	2.27
[191]	MoS ₂ additive	760	15.40	53	6.35
[173]	Pt CEs DSSC/UV 2 h (Pt-EG-FTO)	740	9.68	66.47	4.76
[173]	Pt CEs DSSC/UV 1h (Pt-EG-FTO)	750	10.31	64.9	5.01
[173]	Pt CEs DSSC/UV30min (Pt-EG-FTO)	690	10.59	38.49	2.81
[173]	Pt CEs DSSC/UV 1 h (Pt-EtOH-FTO)	810	13.53	66.56	7.29
[173]	Pt CEs DSSC/UV 30min(Pt-EtOH-FTO)	740	10.4	66.77	5.07
[173]	Pt CEs DSSC/UV 15min (Pt-EtOH-FTO)	750	9.79	53.1	3.92
[173]	Pt CEs DSSC/UV 1h(Pt-EtOH-PET-ITO)	710	8.67	53.35	3.26
[173]	Pt CEs DSSC/Pt-EtOH-FTO @ 450 °C	840	15.49	57.73	7.54
[192]	CYC-B11 Dye	743	20.1	77	11.5
[193]	YD2-o-C8 Dye	935	17.7	74	12.3
[194]	Y123 Dye	986	9.5	77	7.1
[177]	Uniform DSSC	700	13.21	72	6.66
[177]	100 μm patterned DSSC	750	10.76	70	5.6
[177]	200 μm patterned DSSC	720	14.08	68	6.95
[177]	300 μm patterned DSSC	710	14.44	68	6.64
[177]	600 μm patterned DSSC	720	14.80	66	7.12
[177]	1000 μm patterned DSSC	730	15.03	72	7.73
[181]	Bifacial DSSC without porous SiO ₂	736	12.6	66.2	6.13
[181]	Bifacial DSSC with porous SiO ₂	730	13.1	68.5	6.54
[182]	Solid-state DSSC with Cu (II/I)HTM	1080	13.87	73.3	11
[183]	Natural DSSC with Pomegranate	390	12.20	41	2
[183]	Natural DSSC with Blackberry	470	11.16	26	1.4
[183]	Natural DSSC with Cranberry	410	6.78	42	1.2
[183]	Natural DSSC with Blueberry	420	2.72	38	0.4
[195]	SM371 DSSC	960	15.9	79	12
[195]	SM315 DSSC	910	18.1	78	13
[184]	DSSC without UC nanophosphors	680	16.75	51.29	5.84
[184]	DSSC with UC nanophosphors	710	21.9	48.84	7.59
[185]	DSSC without TiO ₂ +ZnO	710	10.91	63.21	4.87
[186]	DSSC with TiO ₂ compact layer/GO	660	7.92	60	3.16
[187]	DSSC with T200 dye	751	11.8	61	5.4

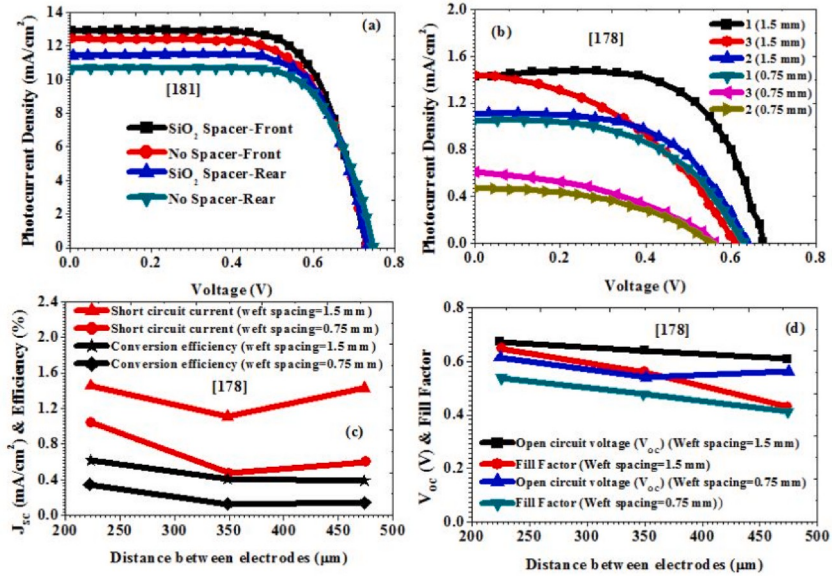


Fig. 17. (a) J-V performance of DSSCs without and with a porous SiO₂ layer under front and rear side irradiation (b) J-V characteristics of monolithic-structured single-layered textile based DSSCs based on number of wires for photoelectrodes and the inter-weft spacing (c) The impact of distance between electrodes and weft spacing on the J_{SC} of textile based DSSCs (d) The impact of distance between electrodes and weft spacing on the V_{OC} and FF of textile based DSSCs.

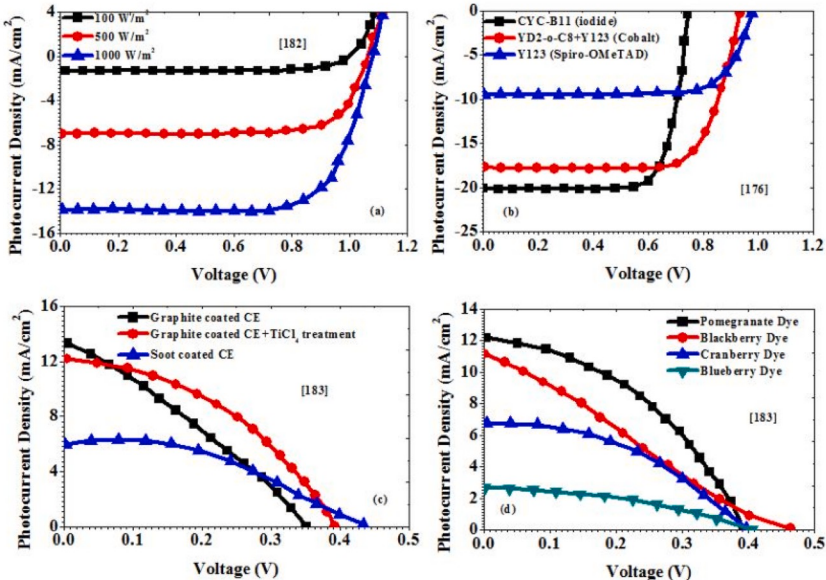


Fig. 18. (a) The influence of optical irradiation on the J-V performance of solid state DSSCs (b) J-V performance of solid-state DSSCs with Y123 dye and spiro-OMeTAD HTL materials (c) The impact of various electrodes on the J-V performance of natural dye based DSSCs (d) The influence of natural dyes on the J-V performance of DSSCs.

curves of the pomegranate DSSC which indicate that pomegranate DSSC with graphene coated CE (counter electrode) and TiCl₄ treatment offers higher J_{SC} and V_{OC} compared with DSSCs with only graphene coated or soot coated CEs. Fig. 18 (d) demonstrates the effect of natural dyes on the PV-performance of DSSCs which indicates that DSSCs with pomegranate dye exhibits superior photovoltaic performance compared with DSSCs with blackberry, cranberry and blueberry dyes.

Fig. 19 (a) and Fig. 19 (b) plots the impact of thermal stress on J-V curves and power density of Ruthenium-Based DSSCs respectively. The increase in thermal stress leads to the severe degradation of J_{SC}, V_{OC} and power density of ruthenium based DSSCs. The influence of graphene oxide (GO) and magnetic bead (MB) in TiO₂ photo-electrode of DSSCs is depicted in Fig. 19 (c). The

variation in GO and MB concentration significantly affects the photovoltaic performance of DSSCs. The effect of UV irradiation time and different photo-electrodes on the J-V curves of DSSCs is demonstrated in Fig. 19 (d). DSSCs with 1 h UV irradiation time and Pt-EtOH-FTO photo-electrodes on J-V curves of DSSCs are illustrated in Fig. 19 (d) which reveals the fact that DSSCs with 1 h UV irradiation and Pt-EtOH FTO photo electrodes exhibit superior photovoltaic performance. The effect of different dyes and co-sensitization on J-V performance of DSSCs is depicted in Fig. 20. Fig. 20 reveals that DSSCs with T220-BD dye exhibits superior J_{SC} and V_{OC} compared with DSSCs with BD and T220 dyes. In summary, good stability, non-toxicity, environmental friendliness, ease of fabrication and low cost production are the main features of DSSCs. DSSCs are also considered as an efficient leading thin film PV technology which can be used for generating electricity under different lighting conditions. The highest efficiency reported for DSSC is 12.3% and the stability of DSSCs can be further improved by replacing liquid electrolyte with solid state electrolytes.

5. III-V compound semiconductor based solar cells

III-V solar-cells (III-V SCs) have been considered as the most attractive way for generating cost effective photovoltaic electricity for space and terrestrial applications [198]. Excellent PCE with high radiation resistance and lower temperature coefficients are the major advantages of III-V SCs [199]. III-V SCs can be developed as single junction, two junction, triple junction (3J) and four junction (4J) cells. Among these 4J cells are found to be more efficient compared with other multi-junction SCs. The schematic of some of the III-V SCs are given in Fig. 21. III-V SCs can be fabricated with structures grown in a MOVPE are MOCVD or MBE reactors [200–202]. In 2010, Jae-Phil Shim et al. [203] proved that the PCE of InGaN/GaN SCs can be increased by using contact layers with high optical transparency. In 2013, Karen Derendorf et al. [204] reported a 3J-GaInP/GaAs/Si cell manufactured by using surface-activated direct wafer bonding. The major causes for the performance degradation of III-V SCs in space applications are due to the bombardment by sub-atomic particles such as neutron, proton etc. Due to the high irradiation resistance and tunable band-gap properties, InGaN/GaN solar cells are gaining attention for space applications [205]. The voltage versus photocurrent density characteristics of some of the most promising III-V SCs are shown in Fig. 22.

In 2014, Zhen Bi et al. [205] investigated the impact of proton irradiation on the PV-performance degradation of InGaN/GaN MQW (Multi-Quantum Well) cells and observed that increasing proton irradiation results in the degradation of photovoltaic performance of InGaN/GaN MQW cells which is demonstrated in Fig. 23 (a). The reason for this PV-performance degradation is that increase of proton irradiation decreases the EQE of solar cells due to irradiation induced defects. Compared with GaInP and GaAs, InGaN is highly immune to high energy proton irradiation damage. The proton irradiation in III-V semiconductors leads to the increase of resistivity which also leads to the PV-performance degradation of III-V SCs. In 2006, M. R. Lueck et al. [207] investigated the PV performance of GaInP/GaAs dual junction solar cells (2J-SCs) on SiGe and GaAs substrates under different illumination conditions (AM0 and AM 1.5G) and observed that GaInP/GaAs cells on GaAs wafer provides higher J_{SE} and V_{OC} compared with GaInP/GaAs 2J-SCs on SiGe substrate (Fig. 23 (b)). The high cost of III-V substrates is the main obstacle of their wide spread use for terrestrial photovoltaic energy harvesting applications.

Low temperature processing and low cost production are the key benefits of Si/III-V or SiGe/III-V hetero junction cells. Therefore,

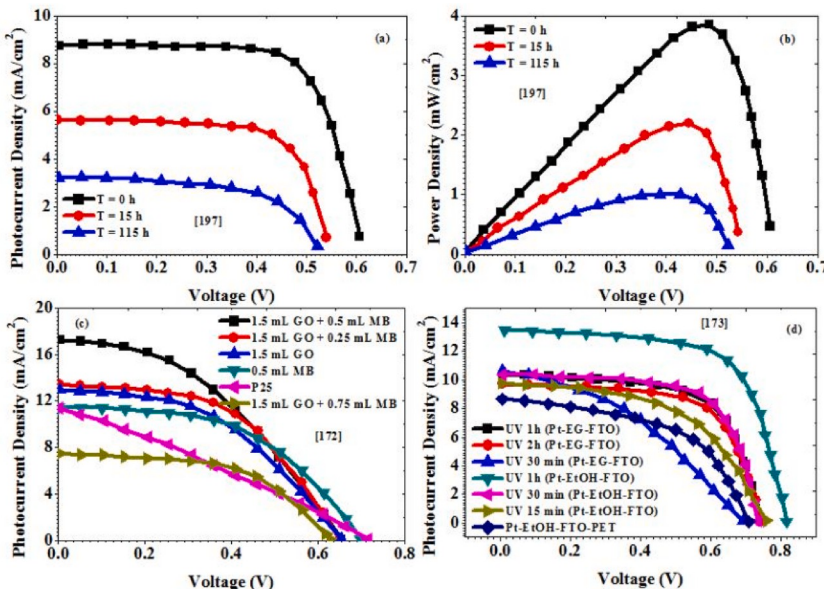


Fig. 19. (a) The impact of thermal-stress on J-V curves of Ruthenium-Based DSSCs [197]. (b) The impact of thermal stress on power density of Ruthenium-Based DSSCs [197]. (c) The influence of graphene oxide (GO) and magnetic bead (MB) in TiO₂ photo-electrode of DSSCs (d) The impact of UV irradiation time and photo-electrodes on the J-V curves of Bifacial DSSCs.

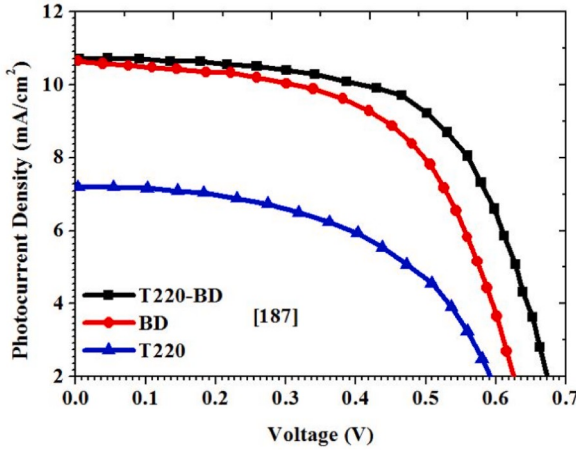


Fig. 20. The effect of different dyes and co-sensitization on the J-V curves of DSSCs.

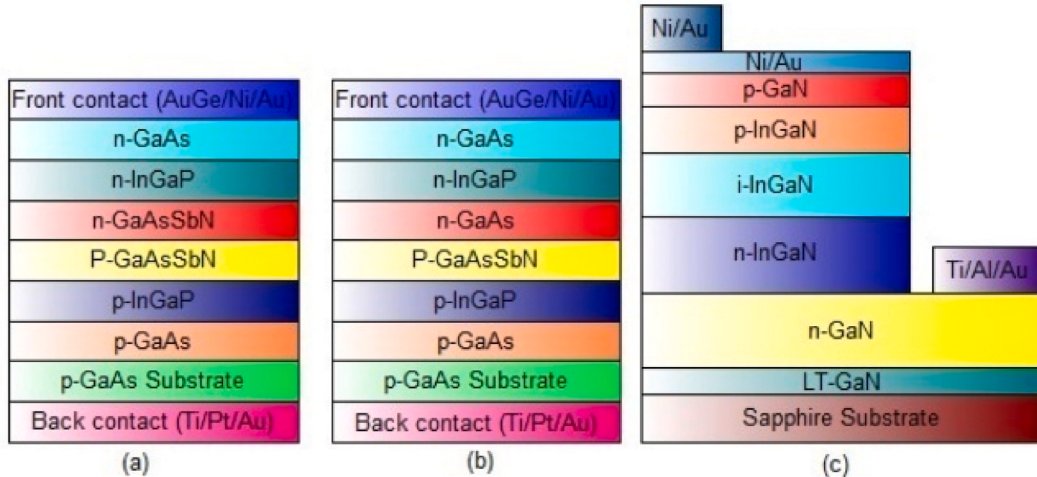


Fig. 21. III-V solar cell structures (a) GaAsSbN homo-junction solar cell [202] (b) GaAsSbN hetero-junction solar cell [202] (c) InGaN p-i-n solar cell [206].

high performance III-V SCs grown on SiGe or Si wafers are of gaining interest the photovoltaic industry for space and terrestrial applications due to their cost effectiveness, light weight and high thermal conductivity compared with III-V substrates. In 2010, Jae-Phil Shim et al. [203] studied the impact of transparent contact layers such as ITO and Ni/Au on the photovoltaic performance of InGaN/GaN p-i-n solar cells and found that InGaN/GaN p-i-n SCs with ITO current spreading layer provides higher J_{SE} and V_{OC} compared with solar cells without spreading layers and with Ni/Au spreading layer (Fig. 23 (c)). The reason for this is that InGaN/GaN p-i-n cells with ITO current spreading layer exhibits higher EQE compared with Ni/Au current spreading layer based solar cells. In 2010, Sheng-wei Zeng et al. [206] demonstrated the influence of Indium concentration on the PV-characteristics of InGaN/GaN p-i-n SJ-SCs and found that increasing the Indium concentration in InGaN results in the decrease of V_{OC} and increase of J_{SE} . However, it does not change the efficiency of solar cells because increasing Indium concentration in InGaN lowers its bandgap which leads to the increase of J_{SC} and reduction of V_{OC} . Si/III-V or SiGe/III-V hetero-junction solar cells have the drawback of poor V_{OC} .

The PCE of hetero-junction solar cells can be improved by using front grid contacts and TCO layer to reduce light scattering losses and external series resistances [208]. In 2014, Frank Dimroth et al. [209] successfully demonstrated that wafer bonding technique can be used to grow GaAs/GaInP 2J-SCs on silicon wafers to combine the benefits of high PCE of III-V SCs with low cost fabrication of silicon platform. Direct-epitaxial growth and wafer bonding based layer transfer are the two widely used fabrication techniques to grow III-V SCs on Si wafers [210]. One method to increase the PCE of III-V SCs is to introduce multiple quantum wells in the cell structure. This has the advantage of extending the absorption spectra of the cell into the infrared region that result in the increase of J_{SE} . In 2010, Bor Wen Liou from Wufeng Institute of Technology, Taiwan [211] studied the impact of MQW structure on the PV-characteristics of InGaN/GaN SCs on SiCN-Si substrates and found that InGaN/GaN solar cells with MQW exhibited higher photovoltaic performance compared with InGaN/GaN solar cells without quantum wells. Bor Wen Liou et al. also reported that

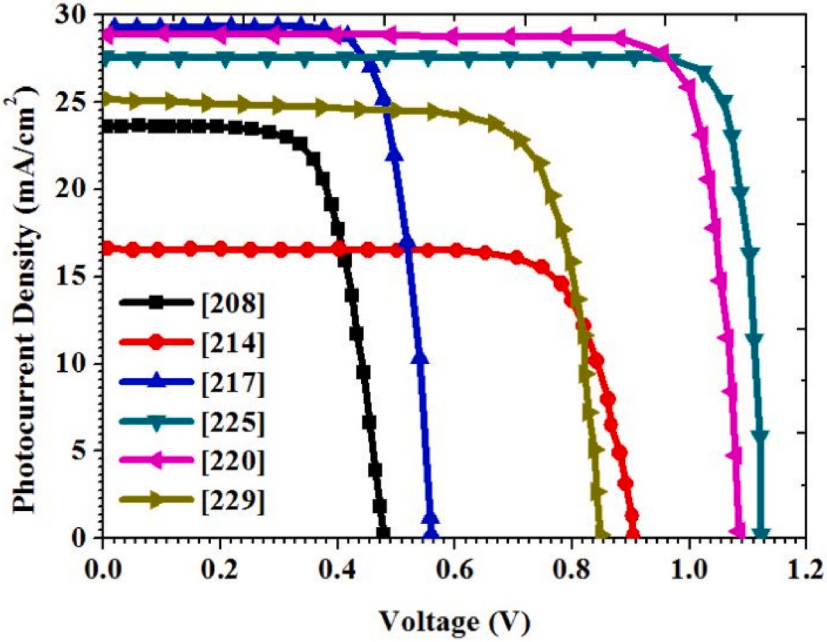


Fig. 22. J-V curves of some of the high performance III-V solar cells.

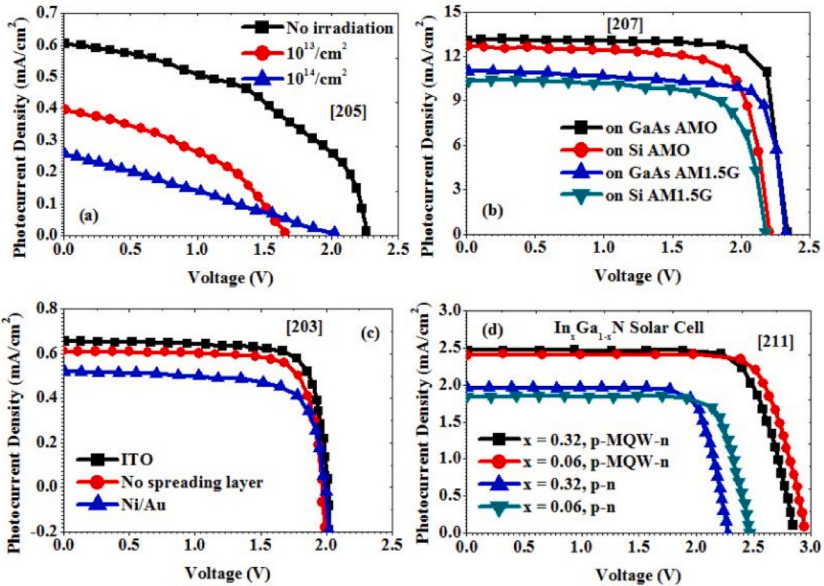


Fig. 23. (a) The impact of proton-irradiation on the J-V curves of GaN/InGaN MQW cells (b) Photovoltaic performance of GaAs/GaInP 2J-SCs on SiGe and GaAs substrates under different illumination conditions (AM0 and AM 1.5G) (c) The influence of transparent contact layers such as ITO and Ni/Au on the PV-characteristics of InGaN/GaN p-i-n cells (d) The impact of MQW structure on the PV-performance of InGaN/GaN cells on SiCN-Si substrates.

increasing the Indium concentration in InGaN layer leads to the increase of J_{SE} and decrease of V_{OC} due to the lowering of band gap of InGaN with increase in Indium content (Fig. 23 (d)). Fig. 24 (a) and Fig. 24 (b) shows the influence of Indium content in InGaN layer of GaN/InGaN p-i-n in SJ-SCs. Fig. 24 (a) indicates that a higher Indium content in InGaN layer of GaN/InGaN p-i-n cell is required to improve the J_{SC} . Fig. 24 (b) reveals the fact that increase in Indium content reduces the V_{OC} which also results in the decrease of maximum output power density. III-V materials with larger band gap (greater than 2.4 eV) are essential for achieving high PCE [212–214]. The major issues arises with the integration of III-V SCs on silicon wafers are the thermal expansion coefficient mismatches of silicon and III-V materials that leads to the introduction of strain which in turn creates cracks and bowing, the mismatch in lattice

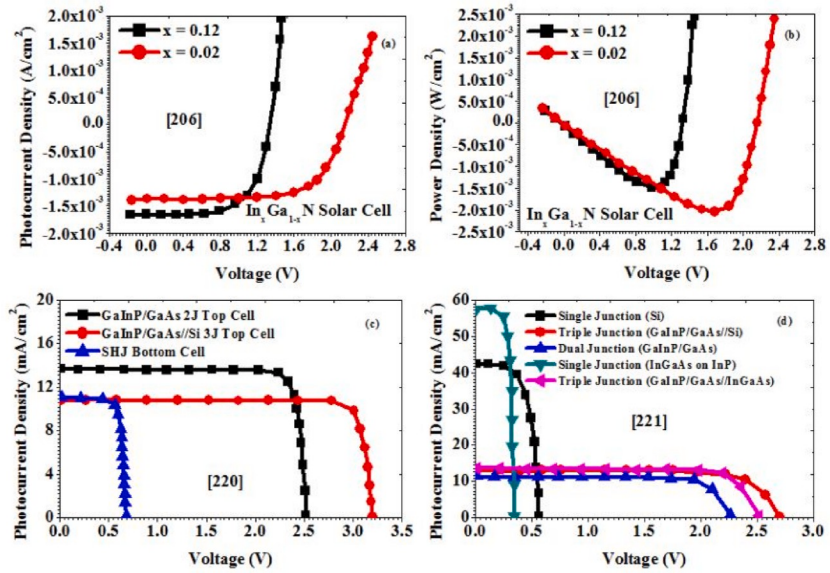


Fig. 24. (a) The influence of indium concentration on the J-V curves of InGaN/GaN p-i-n SJ-SCs (b) The influence of indium concentration on the power density of GaN/InGaN p-i-n SJ-SCs (c) J-V performance of Si/GaAs/GaInP 3J-SCs (d) Performance comparison of SJ, 2J and 3J cells.

constants of III-V and silicon materials induces recombination centers and dislocations and the transition between polar III-V crystals and non-polar silicon crystal creates antiphase domains [215–225]. The Shockley-Queisser limit of efficiency of classical PV cell is 31% [218,219]. In 2018, Dac-Trung Nguyen et al. [219] demonstrated that the efficiency of quantum well based cells can be enhanced with the help of hot carriers at room temperature. In 2017, Stephanie Essig et al. [220] reported that a Si/GaAs/GaInP 3J-cell which has a PCE of 35.9% (Fig. 24 (c)). In 2019, Yu-Cheng Kao et al. [221] compared the performance of SJ silicon cells with GaInP/GaAs 2J-SCs and GaInP/GaAs/InGaAs 3J-SCs and reported that triple junction solar cells are superior in photovoltaic performance compared with SJ and 2J solar cells (Fig. 24 (d)). However SJ silicon cells exhibited higher J_{SC} due to its lower band gap compared with GaInP material. In 2013, Peter Krogsstrup et al. [222] reported a GaAs single nanowire p-i-n structure solar cell grown in a silicon substrate that exhibited a PCE of 40%.

In 2016, Tzu-Neng Lin et al. [223] reported that the PCE of a III-V 3J-SCs can be improved by incorporating graphene quantum dots and Tzu-Neng Lin et al. also studied the impact of variation in graphene quantum dot concentration on the PV-characteristics of III-V

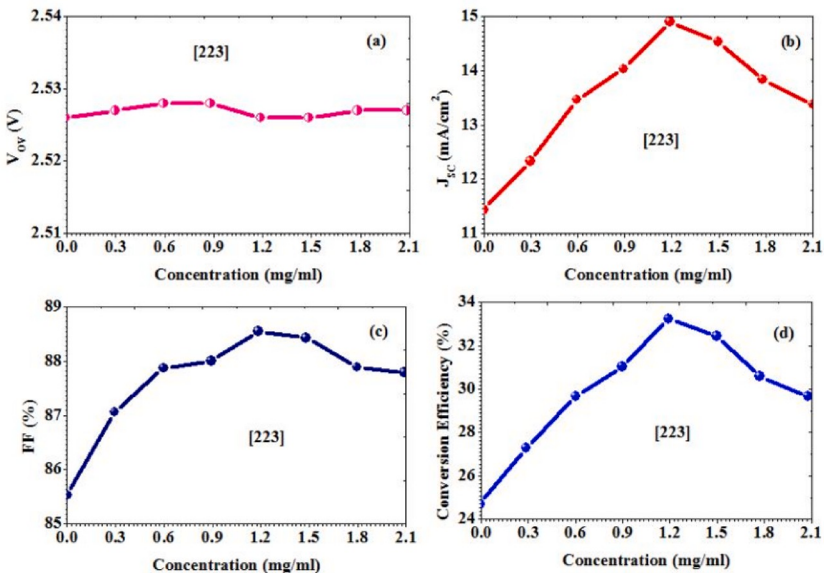


Fig. 25. The influence of graphene quantum dot concentration on the (a) V_{oc} (b) J_{sc} (c) FF and (d) Conversion-efficiency of III-V triple junction solar cells.

3J-SCs. Fig. 25 (a) depicts the influence of graphene quantum dot on the V_{OC} of III-V 3J-SCs. Fig. 25 (a) indicates that the variation in graphene quantum dot concentration does not influence the V_{OC} of III-V 3J-SCs significantly. However, Fig. 25 (b) reveals that the J_{SC} of III-V 3J-SCs initially increases with increase in graphene quantum dot concentration, reaches the peak and then decreases with further increase in graphene quantum dot concentration. Fig. 25 (c) and Fig. 25 (d) also reveals that the FF and PCE of III-V 3J-SCs initially increases with increase in graphene quantum dot concentration, reaches the peak and then decreases with further increase in graphene quantum dot concentration [223].

Fig. 26 (a) and Fig. 26 (b) depicts the influence of Indium concentration on the dark and photogenerated current density of InGaN/GaN p-i-n and InGaN/GaN MQW cells. Fig. 26 (a) and Fig. 26 (b) indicate that GaN/InGaN cells with higher Indium concentration enhances the J_{SC} and degrades the V_{OC} due to reduction of band gap. In 2019, Gaurav Siddharth et al. [224] analyzed the impact of temperature on the J_{SC} and PCE of InGaN/GaN p-i-n and InGaN/GaN MQW cells and observed that J_{SC} of both InGaN/GaN p-i-n and InGaN/GaN MQW cells were increased with respect to increase in temperature (Fig. 26 (c)) and the PCE of both the type of SCs decreases with increase of temperature (Fig. 26 (d)). Fig. 27 (a) indicates that increasing the number of quantum wells in GaN/InGaN MQW cells results in the increase of its PCE. V_{OC} of both p-i-n and MQW cells decreases with increase in temperature [219]. Fig. 27 (b) shows the impact of annealing temperature on the J_{SC} and V_{OC} of GaInP/GaAs/GaInNAsSb 3J-SCs which indicates that annealing of 3J-SCs significantly improves the J_{SC} and V_{OC} of the SCs. Fig. 27 (c) demonstrates the impact of surface conditions like bare surface, surface with nanorod based anti-reflective coating and surface with nano-needle anti-reflective coating on the J_{SC} of GaInP/GaAs/Ge 3J-SCs. Fig. 27 (d) indicates that triple junction solar cells with nano-needle coated anti-reflective surface provide higher J_{SC} and V_{OC} . This is due to the fact that, nano-needle like surface exhibits low reflectance and high EQE compared with bare and nanorod surfaces. Fig. 27 (d) plots the influence of solar concentration ratio on the PCE of GaInP/GaAs/Ge 3J-SCs which indicates that PCE of triple junction solar cells is directly proportional to solar concentration ratio and it also reveals the fact that compared with bare and nanorod based surfaces, nano-needle structured surface exhibits better PCE. The PV-performance of III-V SCs are given in Table-4. In summary, III-V SCs grown on Si wafer are considered as the most suitable PV technology for future space and terrestrial applications due to their excellent irradiation resistance and bandgap tenability. However, the large costs of III-V wafers have been the main obstacle for their widespread use for terrestrial applications. To date, the best III-V PV cells have attained a PCE of 53.8%.

6. Recent developments in flexible solar cells

The demand for self-powered portable electronic devices is increasing day by day and flexible solar cells remains the most attractive solution to meet this demand. Light weight, wearability, bendability, conformability and roll to roll processing are the main advantages of flexible solar cells [231]. By 2030, solar cells are expected to account for 30% of global electrical energy generation. For future flexible photovoltaic devices, the key requirement is transparent conducting electrodes (TCE) with outstanding mechanical strength. ITO has been considered as the most popularly used TCE for flexible SCs. In 2016, Hyeon-Gyun Im et al. [232] reported a hybrid crystalline ITO/metal nano wire TCE for future flexible solar cells. The J-V performance of some of the popular flexible solar cells is shown in Fig. 28. J_{SC} of over 35 mA/cm² and V_{OC} of over 1V have been reported for flexible solar cells.

The influence of bending cycles and bending radius on the PCE of c-ITO/metal nano wire-glass fabric reinforced plastic

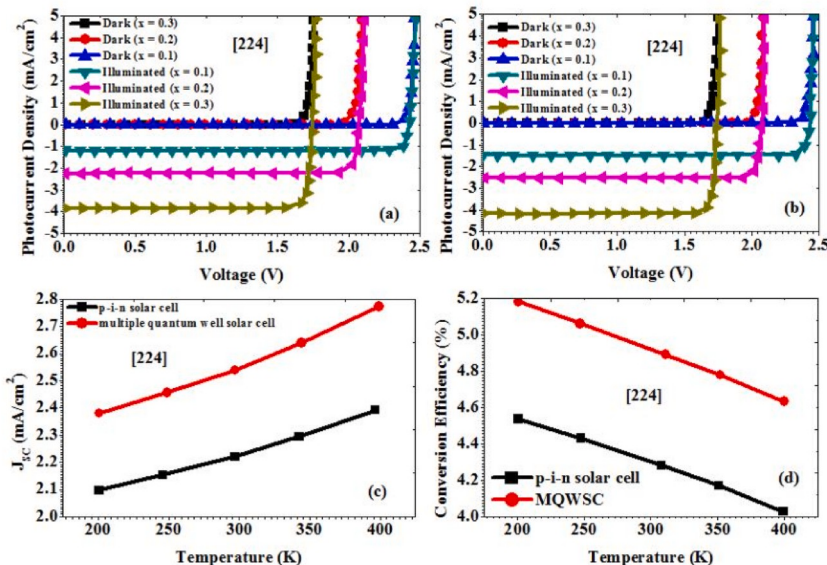


Fig. 26. (a) the influence of Indium concentration on the dark and photogenerated current density of InGaN/GaN p-i-n cells (b) the influence of Indium concentration on the dark and photogenerated current density of GaN/InGaN MQW cells (c) The impact of temperature on the J_{SC} of GaN/InGaN p-i-n and GaN/InGaN MQW cells (d) The impact of temperature on the PCE of GaN/InGaN p-i-n and GaN/InGaN MQW cells.

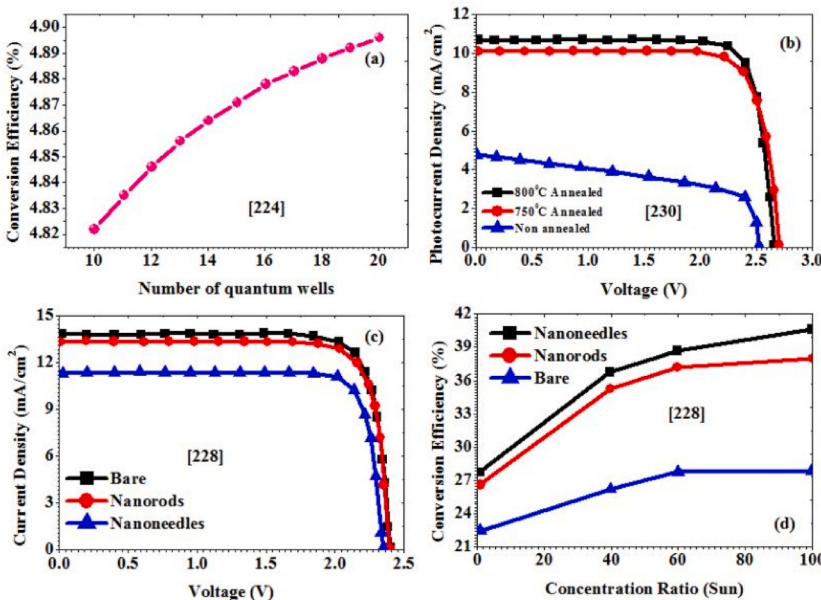


Fig. 27. (a) The influence of number of quantum wells on the efficiency of GaN/InGaN MQW cells (b) Impact of annealing-temperature on the J_{SC} and V_{OC} of GaInP/GaAs/GaInNAsSb 3J-SCs (c) The impact of surface conditions on the J_{SC} of GaInP/GaAs/Ge 3J-SCs and (d) The influence of solar concentration ratio on the PCE of GaInP/GaAs/Ge 3J-SCs.

Table 4
An overview of PV performance of III-V solar cells.

Ref.	Structure/Features	V_{OC} (mV)	J_{SC} (mA/cm^2)	FF (%)	PCE (%)
[200]	InP-based four junction solar cell	4376	14.2	86.7	53.8
[200]	Ge-based four junction solar cell	4170	13.8	86.2	49.5
[200]	GaSb-based four junction solar cell	4412	13.4	86.9	51.5
[202]	GaAsSbN/Ge Double-Junction Solar Cell	830	11.59	72.58	7
[204]	GaInP/GaAs//Si Solar Cells	2780	8.56	86.3	20.5
[203]	InGaN p-i-n Cells with ITO layer	2010	0.644	79.5	1
[203]	InGaN p-i-n Cells with Ni/Au layer	1980	0.507	73.9	0.75
[203]	InGaN p-i-n Cell w/o spreading layer	1960	0.599	79.2	0.93
[207]	GaInP/GaAs/SiGe/Si double junction	2340	13.08	82.5	18.6
[206]	InGaN p-i-n Homojunction Solar Cells	2150	1.4	67.8	3.7
[208]	a-Si:H/GaAs Heterojunction Solar Cells	4970	23.2	69.3	8
[209]	Wafer bonded GaInP/GaAs/Si	2390	12.7	85.9	26
[209]	GaInP/GaAs: Upright on GaAs wafer	2450	13.15	84.2	27.1
[209]	GaInP/GaAs: Upright direct growth on Si	1940	11.20	75.3	16.4
[226]	InGaP/InGaAs/Ge Triple-Junction	2200	—	82.77	23.23
[211]	InGaN/GaN MQW cell on SiCN–Si wafer	2960	2.40	76.5	5.43
[227]	Standard GaAsP/Si cell	524	12.6	80.8	5.33
[227]	LT-BSF GaAsP/Si cell	543	13.5	81.3	5.96
[227]	PERC- GaAsP/Si cell	561	14.8	79	6.56
[227]	PERL - GaAsP/Si cell	586	14.9	79.2	6.92
[227]	HIT - GaAsP/Si cell	628	15	79.6	7.50
[215]	GaInP/GaAs/Si triple junction solar cell	3046	11.9	83	30.2
[217]	n-GaP/p-Si hetero-junction solar cell	561	29.2	75.7	12.4
[217]	n-GaP/n-Si/p-Si homo-junction solar cell	619	24.1	80.3	12
[222]	GaAs nanowire p-i-n solar cell	430	180	52	40
[228]	GaInP/GaAs/Ge 3J cell with bare AR	2350	11.32	84	22.4
[228]	GaInP/GaAs/Ge 3J cell with nanorods AR	2390	13.32	83	26.6
[228]	GaInP/GaAs/Ge 3J cell with nanoneedles AR	2400	13.82	83	27.7
[223]	InGaP/InGaAs/Ge 3J cell with GQD	2530	14.9	88.5	33.2
[229]	Lattice matched InGaAsP/InGaP QW cell	1126	18.5	72.3	14.7
[230]	Inverted lattice matched 3J cell	2719	14.03	81.58	31.1
[221]	Single-junction InGaAs solar cell	350	57.65	71.24	14.37
[221]	Dual-junction InGaAs solar cell	2270	11.44	79.25	20.58
[221]	Triple-junction InGaAs solar cell	2520	13.66	78.30	26.95

(GFRHybrimer) films and on ITO/PET film is shown in Fig. 29. PCE decreases with increase in bending cycles. Bending radius should be maximized for achieving high PCE. The critical challenges remain in the use of flexible solar cells for practical applications are their poor PCE, stability, mechanical flexibility, optical transparency and scalability [233]. Transition-metal-dichalcogenides have been considered as attractive materials for flexible solar cell development because of their excellent mechanical flexibility with outstanding semiconducting properties. In 2017, Toshiki Akama et al. [233] reported the development of a WSe₂ and WS₂ layers based high performance schottky solar cell with Pd–Ni electrode. CN-MEH-PPV, MDMO-PPV, PCBM, C₆₀ and P3HT are some of the popularly used materials in flexible conjugated polymer based SCs. Flexible conjugated polymer SCs are considered as most suitable photovoltaic devices for indoor applications [234].

In 2005, Gilles Dennler et al. [234], reported the development of a flexible MDMO-PPV:PCBM cell fabricated on a ITO coated PET substrate. Conjugated polymer based flexible SCs are attractive due to the following properties such as low-temperature processing, solution based deposition, cost effective, roll-to-roll processing and the suitability of large scale production. Recently, flexible solar cells are gaining interest in e-clothing applications to provide electricity for wearable electronic devices [235]. CIGS (Copper Indium Gallium diselenide) SCs are one of the most attractive thin film flexible SCs in the photovoltaic industry. ZnO, CdS and CIGS are the widely used active layers of flexible CIGS solar cells. Sputtering is suitable for the growth of ZnO at room temperature and chemical/deposition can be used for growing CdS layer and Co-evaporation technique can be used for developing CIGS layer. In order to enhance the PCE of flat CIGS cells, high temperature annealing treatment is required. The high temperature annealing treatment helps to improve the crystal quality of active layers. However, high temperature annealing treatment may create porous holes or cracks at the interfaces of active layers [236,237]. In 2019, Hansung Kim et al. [235] investigated the thermo-mechanical stress on CIGS flexible cells and noticed that the stress increases with the increase of bending-displacements. The photocurrent density of CIGS flexible solar cells decreases with increase in delamination length. In 2019, Collin R. Brown et al. [238] demonstrated a flexible CIGS cell for outer planetary applications. Collin R. Brown et al. investigated the impact of temperature on the J_{SC} and V_{OC} of CIGS flexible cells and found that the solar cells exhibited higher V_{OC} at lower temperature which is evident from Fig. 30 (a) and Fig. 30 (b).

The impact of proton irradiation on the dark current density of flexible CIGS solar cell reported in Ref. [238] is shown in Fig. 31 (a). The proton-irradiation degrades the PV-performance of CIGS flexible SCs. The impact of annealing-treatment on the PV-performance of flexible CIGS cell is shown in Fig. 31 (b). Increasing the annealing time leads to the improvement of PV-performance of CIGS flexible SCs which is evident from Fig. 31 (b). The impact of annealing time on V_{OC} and J_{SC} of CIGS flexible cell is plotted in Fig. 31 (c) and Fig. 31 (d) respectively. Both Fig. 31 (c) and Fig. 31 (d) indicate that increasing the annealing time is required for enhancing the key parameters of solar cells such as V_{OC} and J_{SC}. In 2019, Huben Lu et al. [239] demonstrated a high performance flexible solar cell on PET substrate that features flip-Ag nanowire TCE. ITO and FTO are the commonly used TCEs for flexible solar cells. Metal nanowires, graphenes, carbon nanotubes and conductive polymers are the recently developed TCE materials for fabricating flexible SCs. Due to the ease of processing, high thermal conductivity, high chemical stability, excellent flexibility and electrical conductivity, Ag nanowires have been considered as the most promising TCE for replacing traditional ITO and FTO TCEs for future flexible solar cells. Spin coating, Mayer rod coating, spray coating, electrohydro-dynamic spray deposition, drop coating, doctor blade coating, dip coating and brush painting are the various fabricating methods used for Ag nanowire based TCEs. PET is the most suitable substrate for Ag nanowire TCE based flexible solar cells.

The impact of bending time on the J_{SC} and PCE of PET/flip-Ag nanowire TCE based flexible solar cell is illustrated in Fig. 32 (a) and Fig. 32 (b) respectively. Fig. 32 (a) and Fig. 32 (b) clearly pointed out that as the bending time increases, both J_{SC} and PCE of flexible solar cells decreases. Fig. 32 (c) plots the impact of different in-curved cycles on the J-V characteristics of PET/flip-Ag nanowire TCE based flexible solar cells. As the in-curved cycles increases the J_{SC} of flexible solar cells decreases. Fig. 32 (d) depicts the variation of series resistance (R_S) of PET/flip-Ag nanowire TCE based flexible solar cells with bending time. Fig. 32 (d) reveals that the series resistance is directly-proportional to the bending times. Low cost flexible substrates and low cost kesterite materials such as CIGS (Cu

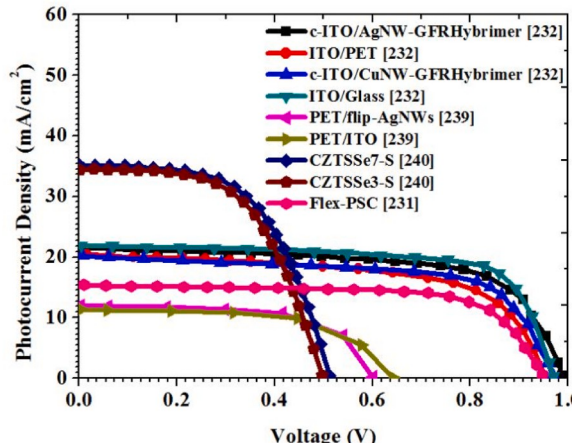


Fig. 28. The J-V performance for some of the popular flexible cells.

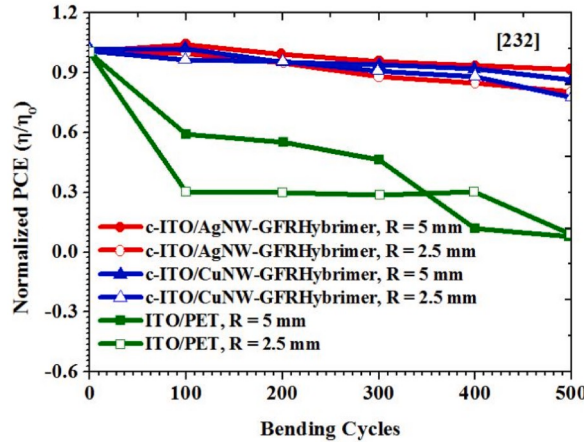


Fig. 29. The influence of bending cycles and bending radius on the PCE of c-ITO/metal nano wire-glass fabric reinforced plastic films and on PET/ITO film.

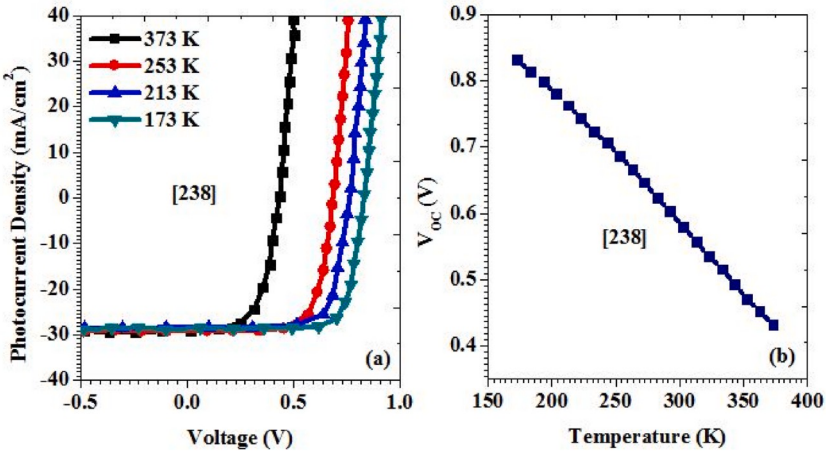


Fig. 30. The impact of temperature on the J_{SC} and V_{OC} of CIGS flexible SCs.

(In,Ga)Se₂), CZTS (Cu₂ZnSnS₄), CZTSSe (Cu₂ZnSn(S,Se)₄) and CZTSe (Cu₂ZnSnSe₄) can be used for manufacturing low cost thin film flexible SCs. Flexible CIGS SCs on Polyimide substrates exhibited an efficiency of 20.4%, CIGS cells on stainless steel foil substrates exhibited an efficiency of 17.7%. The efficiency of flexible kesterite solar cells on Mo foil substrate exhibited an efficiency of 7.04%.

The impact of compressive strain on the J-V performance of flexible PSCs is illustrated in Fig. 33 (a). From Fig. 33 (a), it is clear that both V_{OC} and J_{SC} of flexible PSCs increase with increase in compressive strain. Fig. 33 (b) depicts the tensile strain effects on the J-V performance of flexible PSCs and it also indicate that increase of tensile strain leads to the enhancement of both J_{SC} and V_{OC} . Fig. 33 (c) shows that V_{OC} of flexible perovskite solar cell increases with increase in tensile strain. However, when flexible PSCs are subjected to compressive strain its V_{OC} decreases with increase in compressive strain which is evident from Fig. 33 (d). In future, electronic products will be wearable and flexible. Flexible solar cells are attractive for wearable electronics and as roofing materials for the production of electricity for home applications. To date, the highest efficiency reported for flexible PV cells is 15.38%. An overview of PV-performance of flexible SCs is given in Table-5.

7. Recent developments in tandem solar cells

Tandem SCs can be developed in two ways and they are four terminal (4T) mechanically stacked tandem SCs and two terminal (2T) series connected tandem SCs [241]. The 4T mechanically stacked tandem SCs requires semi-transparent contacts to reduce absorption losses. The two terminal series connected tandem SCs needs the matching of band gap of top and bottom sub cells in order to minimize current losses. In order to match the band gap of bottom and top cells, in two terminal series connected tandem cells, intermediate layers can be used. These intermediate layers electrically connect the top and bottom sub cells. In 2015, Zhengshan J. Yu et al. [242] introduced the concept of using photovoltaic mirror for enhancing the PCE of tandem SCs. One method to improve the PCE of tandem SCs at low cost is to combine high performance c-Si SCs with low cost thin film solar cell technology in a mechanically stacked manner

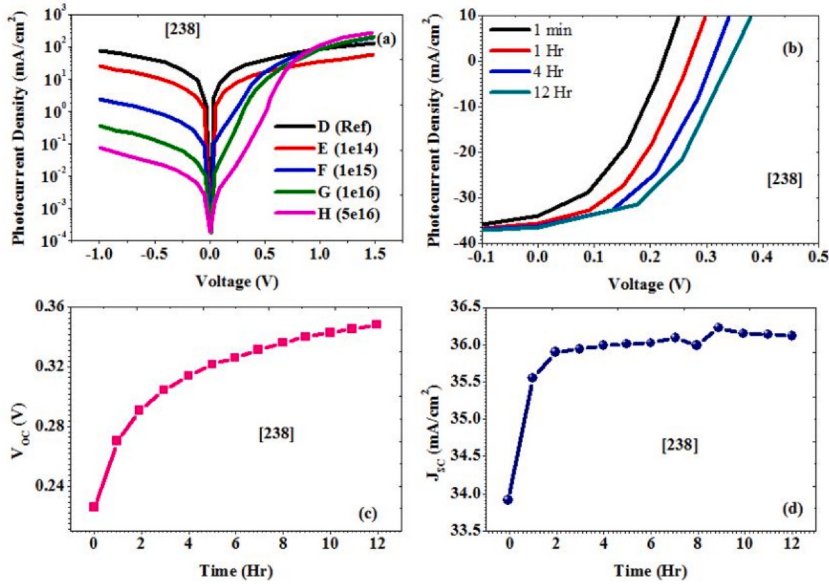


Fig. 31. (a) The influence of proton irradiation on the dark current density of flexible CIGS solar cell (b) Annealing treatment effects on the PV-performance of flexible CIGS cell (c) The influence of annealing time on V_{oc} of CIGS flexible solar cell (d) The impact of annealing time on J_{sc} of CIGS flexible cell.

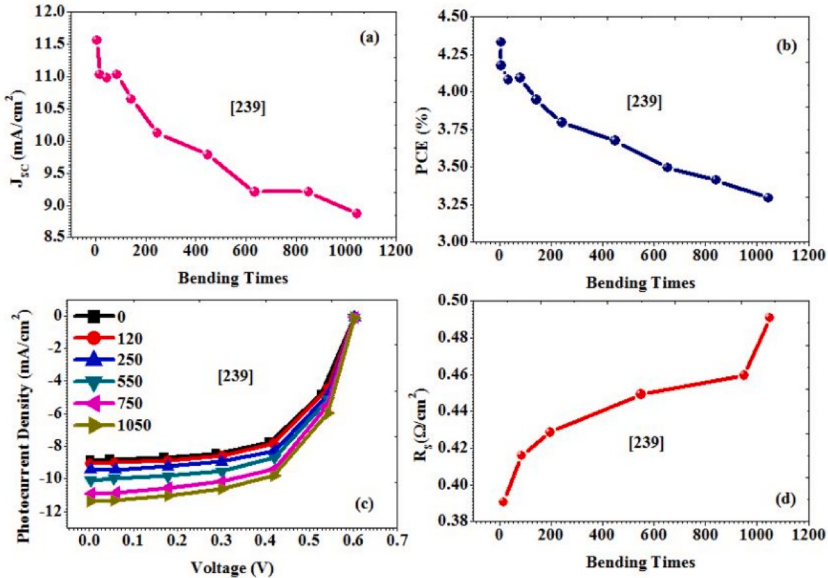


Fig. 32. (a) The impact of bending time on the J_{sc} of PET/flip-Ag nanowire TCE based flexible solar cell (b) The impact of bending time on the PCE of PET/flip-Ag nanowire TCE based flexible solar cell (c) The impact of different in-curved cycles on the J-V characteristics of PET/flip-Ag nanowire TCE based flexible solar cells (d) The variation of series resistance (R_s) of PET/flip-Ag nanowire TCE based flexible solar cells with bending time.

[243]. In 2015, Li Wang et al. [244] illustrated that the PCE of a 3T GaAsP/SiGe tandem SCs grown on silicon wafer can be improved by adding an antireflection coating combined with the improvement of material quality of III-V semiconductor layers. III-V SCs are commonly used as top cells due to the wide band gap of III-V semiconductors. Some of the popular tandem solar cell structures are given in Fig. 34.

Fig. 35 (a) demonstrates the influence of anti-reflection coating on the J-V characteristics of 3T GaAsP/SiGe/Si tandem SCs. In 2012, Sambit Pattnaik et al. [245] reported a novel hybrid-amorphous (a-Si, C):H/organic (P3HT:PCBM) tandem cell whose J-V characteristics is shown in Fig. 35 (b). Fig. 35 (c) shows the J-V characteristics of a-Si/P3HT:PCBM hybrid organic/inorganic cell reported by T. Kim et al. [246] in 2011. The poor PV-performance of (a-Si, C):H/organic (P3HT:PCBM) tandem cell is due to the

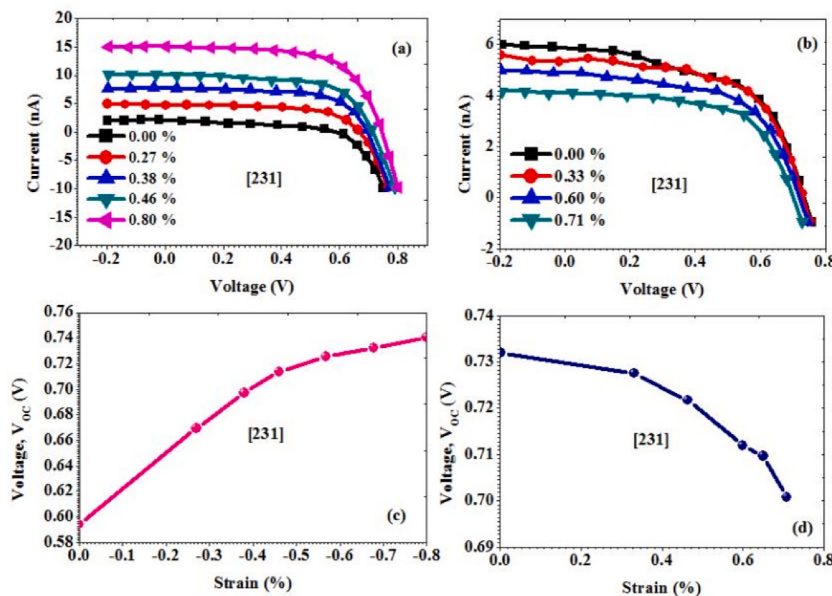


Fig. 33. Compressive and tensile strain effects on the PV-performance of flexible PSCs.

Table 5

An overview of PV-performance of flexible solar cells.

Ref.	Structure/Features	V _{OC} (mV)	J _{SC} (mA/cm ²)	FF (%)	PCE (%)
[232]	AgNW-GFRHybrimer/c-ITO	990	21.53	66	14.15
[232]	CuNW-GFRHybrimer/c-ITO	970	20.09	66	12.95
[232]	Glass/ITO	970	21.82	73	15.38
[232]	PET/ITO	960	20.50	62	12.08
[234]	PET/ITO/PEDOT:PSS/MDMO-PPV:PCBM	650	1.75	38	5
[238]	CIGS – Saturn R	782	0.463	71.1	–
[238]	CIGS – Saturn M	770	0.469	63.7	–
[238]	CIGS – Jupiter R	782	1.54	77.2	–
[238]	CIGS – Jupiter M	772	1.53	75.8	–
[238]	CIGS – Mars R	654	17.8	71.1	–
[238]	CIGS – Mars M	646	17.7	68.1	–
[239]	PET/ITO	640	10.84	60.75	4.21
[239]	PET/Flip-Ag NW	610	11.93	65.21	4.72
[240]	CZTSSe3-Small cell	497	34.78	56.69	9.8
[240]	CZTSSe7-Small cell	513	35.23	57.22	10.34
[240]	CZTSSe3-Large cell	512	32.27	50.90	8.40
[240]	CZTSSe7-Large cell	538	32.29	49.59	8.61

absence of ITO intermediate layer. Fig. 35 (b) and Fig. 35 (c) shows that, a hybrid inorganic/organic tandem solar cell requires an ITO intermediate layer to enhance the PCE. Hybrid organic-inorganic all perovskite tandem cells are considered as the most attractive photovoltaic device technology for future indoor and outdoor applications due to their ease of manufacturing and high PCE [247]. In 2019, Ajay Singh et al. [247] illustrated that the PCE of 2T tandem SCs increases with increase in the work function of top cell cathode materials. Ajay Singh et al. [247] also demonstrated that the PCE of two terminal tandem SCs decreases with increase in work function of bottom cell cathode materials. In 2018, Kevin L. Schulte et al. [248] reported that inverted metamorphic multi junction (IMM) solar cell design can be used to achieve high PCE by introducing multiple active junctions with different band gaps in a vertically stacked series connected design. The reason for excellent efficiency of IMM cells is that the reduction of thermal losses by absorbing highly energetic photons in the higher band gap junctions. Tandem cells are also considered as the leading photovoltaic technology for space applications due to their high PCE [249]. Fig. 35 (d) shows that both V_{OC} and J_{SC} of tandem cells degrades severely due to irradiation.

In 2013, Jingbi You et al. [250] studied the effect of light intensity on the PV-characteristics of polymer tandem solar cells and found that the J_{SC} increases with increase in light intensity (Fig. 36 (a)) and (Fig. 36 (b)). Fig. 36 (c) indicates that the V_{OC} of polymer tandem cells increases with increase in light intensity. However, increase in light intensity degrades the fill factor of polymer based tandem solar cells which is evident from Fig. 36 (d). Thin film solar cells are gaining attention to meet the challenges for future renewable energy technologies [251]. The researchers are aiming to minimize the cost of production of high-performance PV devices.

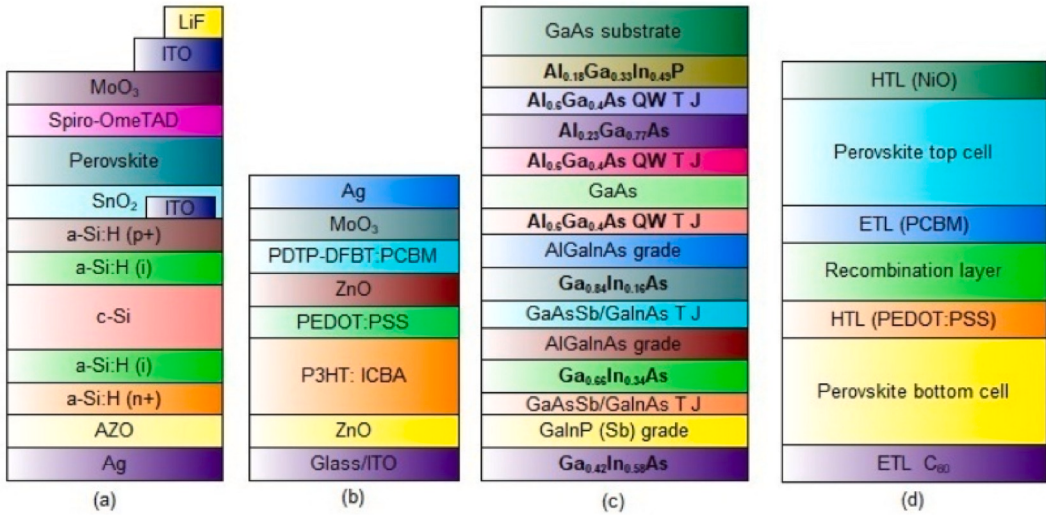


Fig. 34. Tandem solar cell structures (a) 2T tandem solar cell [241] (b) Glass/ITO/ZnO/P3HT:ICBA/PEDOT:PSS-/ZnO/PDTP-DFBT/PCBM/MoO₃/Ag [250] (c) 6J metamorphic multijunction (IMM) tandem solar cell design [248] (d) All-perovskite two terminal tandem solar cell architecture [247].

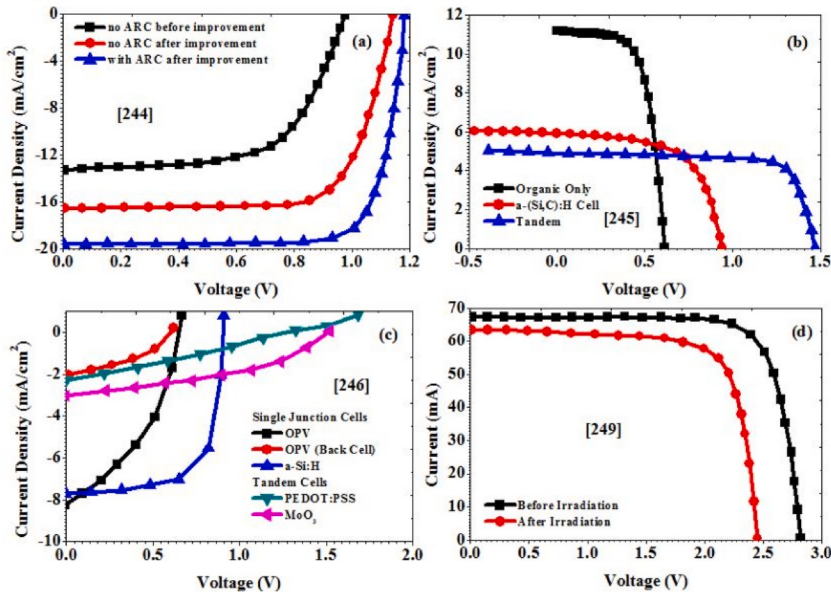


Fig. 35. (a) The influence of ARC on the J-V characteristics of 3T GaAsP/SiGe/Si tandem SCs (b) Performance comparison of organic only, amorphous only and hybrid tandem solar cells (c) J-V performance of a-Si/P3HT:PCBM hybrid organic/inorganic solar cell (d) Influence of irradiation on the J-V performance of tandem SCs.

In this scenario organic/inorganic hybrid solar cells containing solution processable active organic materials and amorphous inorganic semiconductors are becoming popular because of their cost effectiveness and ease of fabrication. In 2014, Taehee Kim et al. [251] compared the photovoltaic performance of single junction, double junction and triple-junction hybrid organic/inorganic cells and observed that hybrid organic/inorganic 3J cells exhibited superior photovoltaic performance compared with homo-junction and double junction cells (Fig. 37 (a)).

Taehee Kim et al. [251] also demonstrated that compared with PEDOT only triple junction hybrid solar cells, UVO (Ultra Violet Ozone) treated interface engineered PEDOT hybrid solar cells exhibits higher PCE. In 2015, Wilson Jose da Silva et al. [252] illustrated that the PCE of polymer tandem cells can be improved by appropriate and careful interface engineering of carrier transport layer. Thinner active-layers are normally required to obtain good PV-performance for polymer tandem cells because the use of thinner active layer enhances the EQE of solar cells. However, Wilson Jose da Silva et al. [252] demonstrated that polymer tandem solar cells with

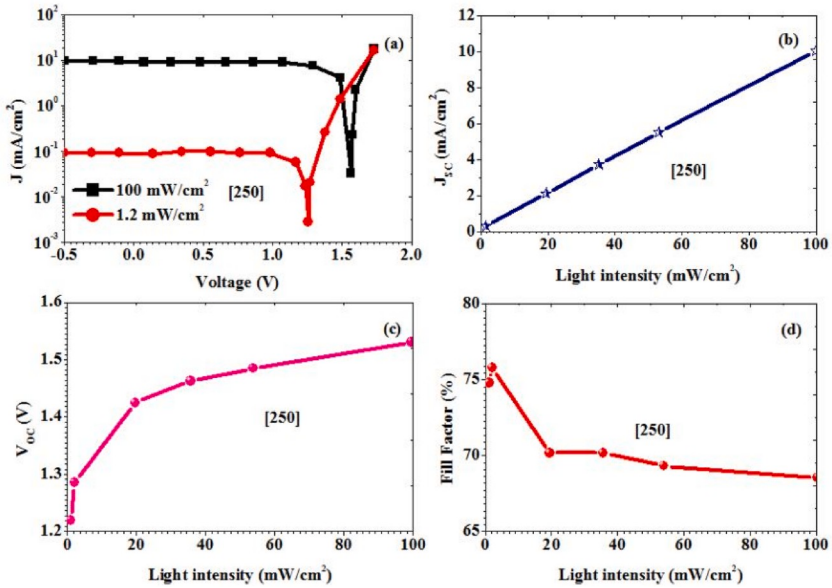


Fig. 36. Influence of intensity of light on the PV-performance of polymer tandem cells.

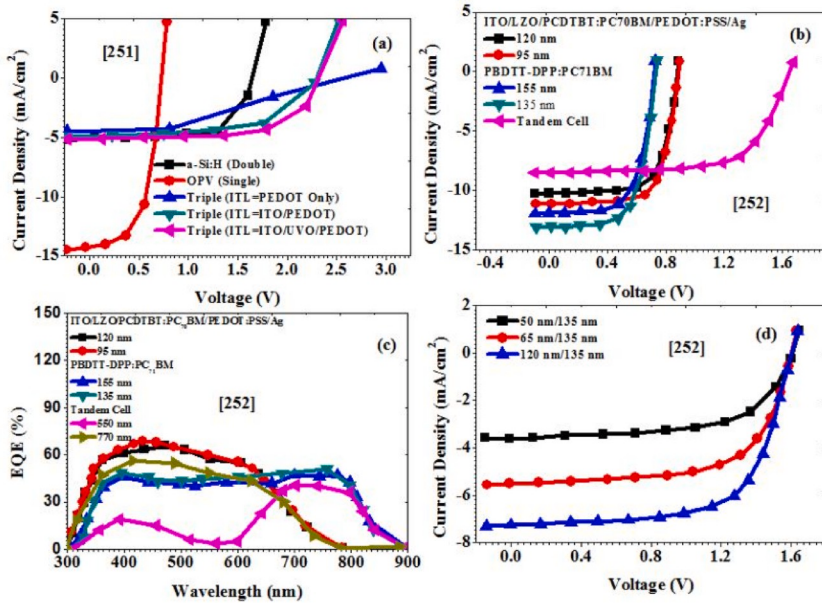


Fig. 37. (a) Performance comparison of SJ (Single junction), 2J (double junction) and 3J (triple junction) organic/inorganic SCs (b) Influence of sub-cell thickness on J-V curves of polymer tandem cells (c) Influence of active layer thickness on the EQE of polymer tandem cells (d) Influence of active layer thickness on J-V performance of polymer tandem cells.

higher sub-cell thickness exhibited superior photovoltaic performance (Fig. 37 (b)). The polymer tandem solar cells with higher active layer thickness exhibited higher EQE (Fig. 37 (c)) and (Fig. 37 (d)) which helped to improve the PV-performance. The influence of various interconnecting layers on the PV-performance of inverted tandem polymer solar-cell is shown in Fig. 38 (a) which reveals that inverted tandem polymer cells with P:CNT (Carbon NanoTube)/LZO (Lithium Zinc Oxide) interconnecting layer exhibits superior photovoltaic performance compared with inverted tandem polymer cells with P:NiO_x/LZO, P:rGO/LZO, P/LZO and P:WO_x/LZO interconnecting layers [252].

In 2019, Martina Trahms et al. [253] reported a LPC-Si (Liquid Phase Crystalline Silicon)/Perovskite-tandem cell with an efficiency of 19.3%. Fig. 38 (b) shows the photovoltaic performance of LPC-Si, filtered LPC-Si and perovskite solar cells. Fig. 38 (b) indicates that the perovskite materials are attractive for increasing the PCE of tandem SCs. The influence of CIS (CuInSe₂), ACIS (Ag(CuInSe₂)), CIGS

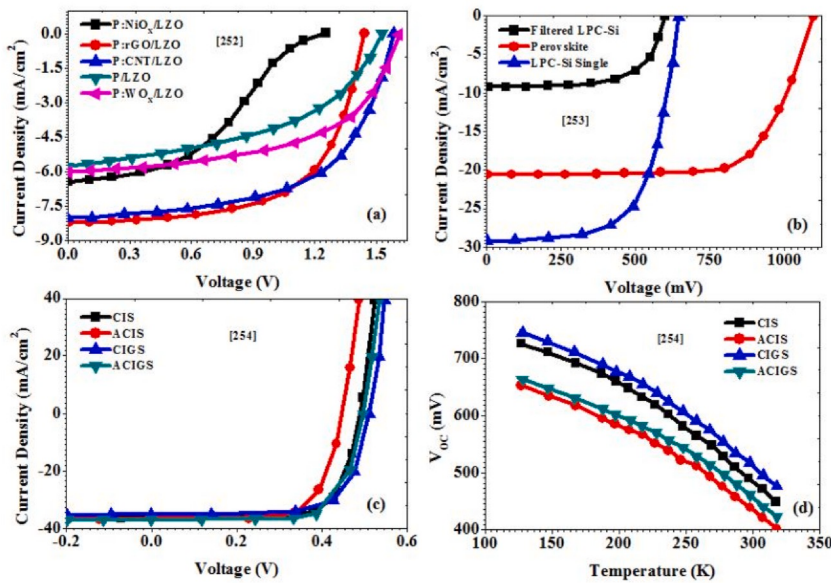


Fig. 38. (a) Influence of various interconnecting layers on the PV performance of inverted tandem polymer SCs (b) PV performance of LPC-Si, filtered LPC-Si and perovskite solar cells (c) The impact of different materials on the PV- performance of CIS based SCs (d) Thermal-stability of cells with different materials.

Table 6
Photovoltaic performance of state of the art tandem cells.

Ref.	Structure/Features	V _{OC} (mV)	J _{SC} (mA/cm ²)	FF (%)	PCE (%)
[241]	Perovskite Silicon Tandem SCell	1770	12.26	63	13.86
[244]	3- T GaAsP/SiGe/Si tandem cell	1190	19.6	79	18.4
[245]	a-(Si:C):H/P3HT:PCBM hybrid solar cell	1500	5	77	5.7
[255]	GaInP/GaAs/Ge 3J tandem solar cell	2630	17.14	85.9	28.7
[256]	PFDTBT:PC ₆₁ BM/PTBEHTT:PC ₆₁ BM	1400	0.9	99	0.57
[257]	P3HT:PC ₇₁ BM/PCPDTBT:PC ₆₁ BM	1240	7.8	67	6.5
[258]	P3HT:ICBA/PSBTBT:PC ₇₁ BM	1470	7.6	63	7
[259]	PCDTBT:PC ₇₁ BM/PMDPP3T:PC ₇₁ BM	1480	9.64	59	8.44
[259]	PCDTBT:PC ₆₁ BM/2 × PMDPP3T:PC ₇₁ BM	2090	7.34	63	9.64
[260]	P3HT:PC ₆₁ BM/PSBTBT:PC ₇₁ BM	1200	7.84	54.1	5.1
[261]	P3HT:SF (DPPB) ₄ /PTB7-Th:IEIC	1970	8.28	52	8.48
[250]	P3HT:ICBA/PDTP-DFBT:PC ₇₁ BM	1530	10.1	68.5	10.6
[251]	PEDOTonly triple junction solar cell	2330	4.50	50.7	5.32
[251]	ITOITL/PEDOT triple junction solar cell	2310	4.91	60.1	6.80
[251]	ITOITL/UVO/PEDOT 3J solar cell	2350	5.13	64.9	7.81
[252]	Inverted tandem solar cell	1600	8.53	66.14	9.02
[252]	Inverted polymer tandem solar cell	1600	7.30	66	7.72
[262]	4T IBC c-Si FA _{0.75} MA _{0.15} Cs _{0.10} Rb(I _{0.66} Br _{0.33}) ₃	1120	19.4	73	26.4
[263]	4T SHJ c-Si MAPbI ₃	1070	20.1	76	25.2
[264]	4T SHJ c-Si FA _{0.83} Cs _{0.17} Pb(I _{0.6} Br _{0.4}) ₃	1100	19.9	71	19.8
[265]	4T TI mc-Si MAPbI ₃	1030	17.5	71	17
[266]	2T SHJ c-Si FA _{0.83} Cs _{0.17} Pb(I _{0.83} Br _{0.17}) ₃	1650	18.1	79	23.6
[267]	2T n-type HJ c-SiCs _{0.07} Rb _{0.03} FA _{0.765} MA _{0.135} Pb(I _{0.85} Br _{0.15}) ₃	1750	17.6	73	22.5
[268]	2T SHJ c-Si Cs _{0.19} MA _{0.81} PbI ₃	1750	16.8	77.5	22
[269]	2T SHJ c-Si MAPbI ₃	1690	15.9	80	21.2
[270]	2T SHJ c-Si MAPbI ₃	1760	14	77	18.1
[271]	2T n-type, HJ MAPbI ₃	1580	11.5	75	13.7
[272]	4T FA _{0.6} MA _{0.4} Sn _{0.60} Pb _{0.40} I ₃ FA _{0.8} Cs _{0.2} Pb(I _{0.7} Br _{0.3}) ₃	1200	17.5	74	22.9
[158]	4T FA _{0.6} MA _{0.4} Sn _{0.60} Pb _{0.40} I ₃ MAPbI ₃	1140	20.1	80	21
[273]	4T FA _{0.75} Cs _{0.25} Sn _{0.50} Pb _{0.50} I ₃ FA _{0.82} Cs _{0.17} Pb(I _{0.83} Br _{0.17}) ₃	970	20.3	79	20.3
[274]	2T MASn _{0.50} Pb _{0.50} I ₃ MA _{0.9} Cs _{0.1} Pb(I _{0.6} Br _{0.4}) ₃	1980	12.3	73	18.5
[273]	2T FA _{0.75} Cs _{0.25} Sn _{0.50} Pb _{0.50} I ₃ FA _{0.83} Cs _{0.17} Pb(I _{0.50} Br _{0.50}) ₃	1660	14.5	70	17
[275]	2T MAPbI ₃ Fa _{0.85} CsPb(I _{0.30} Br _{0.70}) ₃	2290	9.8	80	18.1
[276]	2T MAPbI ₃ MAPbI ₃	1890	6.6	56	7

and ACIGS ($\text{Ag}(\text{Cu}(\text{In},\text{Ga})\text{Se}_2)$) materials on the PV-performance of CIS based SCs are depicted in Fig. 38 (c). From Fig. 38 (c) it is evident that materials with Ga exhibits higher V_{OC} and addition of Ag enhances J_{SC} but reduces V_{OC} (Fig. 38 (d)). From Fig. 38 (d) it is very clear that CIGS and CIS based solar cells are thermally stable compared with ACIS and ACIGS based solar cells [254]. CIS, CIGS, ACIS and ACIGS materials are considered as attractive for making bottom cells of high performance tandem solar cells [277–282]. In summary, the PV performance of tandem cells depends on the way in which the sub-cells are configured in it. Based on the sub-cell types, the tandem cells can be classified as perovskite/Si tandem cells, organic tandem cells, perovskite/CIGS tandem cells and all perovskite tandem cells. According to NREL efficiency chart, the highest efficiency attained by perovskite/Si, organic and perovskite/CIGS tandem cells are 29.1%, 14.2% and 24.2% respectively. An overview of PV-performance of tandem cells is given in Table-6.

8. Quantum dot solar cells

Quantum dot SCs realized using semiconductor nanocrystals are emerging as one of the leading photovoltaic technologies for commercial solar-energy harvesting applications. The rapid developments in nanotechnology have made it possible to fabricate uniform quantum dot SCs from a wide range of semiconductor nanocrystals. The band gap of quantum dot is determined by its size and therefore, the main advantage of quantum dot cell is that its band gap can be precisely controlled by varying its size. The IBSE (intermediate band SCs) have been considered as the most attractive method of solar energy harvesting because these solar cells can generate electricity by absorbing photons with lower energy (energy less than the band gap of silicon). Quantum dot cells exhibit higher J_{SC} without degrading V_{OC} [283]. Vapour phase-epitaxy and solid source molecular beam-epitaxy are the two most commonly used techniques to grow InAs quantum dots on InGaP/GaAs material system. InGaP act as a spacer layer. InAs quantum dots are always associated with quantum well islands. It is very difficult to grow InAs quantum dot without quantum well islands due to the specific growth mechanism of InAs [284]. For achieving high efficiency, usually n-i-p structure is preferred for quantum dot solar cells. A two step photon up conversion process is utilized in IBSC solar cells. That is, initially an electron transit from VB (Valence Band) to IB (Intermediate Band) by absorbing a below-energy band gap photon and this electron jump from IB to CB (Conduction Band) by absorbing another below-band gap energy photon. This two step photon up conversion process enhances J_{SC} without degrading V_{OC} . The schematic of a two step photon up conversion InAs quantum dot cell [285] is depicted in Fig. 39.

The J-V curves of some of the high performance quantum-dot cells are plotted in Fig. 40. Solution processible inorganic-semiconducting nanosrstals known as colloidal nanocrystal quantum-dots are gaining tremendous attention for future solar energy harvesting applications for renewable-energy technology due to their unique properties of size tunable band gap [286]. Colloidal nanocrystal quantum dots can be made from different materials such as PbSe, PbS, CdS and CdSe. The different quantum dot solar cell configurations are quantum dot bulk nano-hetero-junction, metal oxide/quantum dot bilayer hetero-junction, quantum dot organic bulk hetero-junction and quantum-dot sensitized SCs. However, metal oxide/quantum-dot bilayer HJ-cells are considered as the most efficient quantum dot solar cell technology. In 2015, Zhenhua Sun et al. [286] demonstrated that the J_{SC} and V_{OC} of PbS–CuInS₂ quantum dot solar cell can be enhanced by incorporating a Zn–CIS quantum dot into the PbS quatum dot matrix. Addition of Zn–CIS quantum dots in PbS quantum dot matrix enhances both J_{SC} and V_{OC} by minimizing carrier recombination losses. The influence of Zn–CIS quantum dot on PbS–CIS quantum dot SCs is depicted in Fig. 41.

The Zn–CIS concentration significantly affects the PV performance of PbS–CIS quantum-dot SCs and it was observed that 10% Zn–CIS quantum dot is best for achieving high photovoltaic performance. Increasing or decreasing Zn–CIS concentration from 10% significantly degrades the PV-performance of PbS–CIS quantum dot SCs. In 2018, Tapan Kumar Das et al. [287] reported a QDSWSC (Quantum-Dot Sensitized Whisperonic Solar-Cell) based on CdSe quantum-dots. Tapan Kumar Das et al. [287] studied the impact of size of CdSe quantum dots on the PV-performance of QDSWSC and found that the photovoltaic performance increases with increase in size of the CdSe quantum dots. In 2014, Hau-Vei Han et al. [288] investigated influence of quantum-dot size and dilution factor on the PV-performance of hybrid colloidal quantum-dot GaAs cell and found that at a fixed quantum-dot size, cell with a dilution factor of 5 exhibited higher J_{SC} and V_{OC} compared with quantum dot solar cells with dilution factors of 1, 10 and 15. It was also found that hybrid colloidal quantum-dot GaAs SCs with higher quantum dot size exhibited superior photovoltaic performance. In 2016, Yiming Cao et al. [289] demonstrated that the application of thermal treatment enhances both J_{SC} and V_{OC} of PbS quantum dot solar cells by enhancing their EQE. Nanorod films can be used for multiple-exciton generation in PbSe quantum-dot SCs for improving its PCE [290]. In 2017, Zhenyu Yang et al. [291] reported the first mixed quantum-dot cell which has a PCE of 10.4%. This mixed quantum-dot cell consists of methyl ammonium lead triiodide (MAPbI₃) quantum-dots and thioglycerol-PbS quantum-dot. In order to analyze the influence of quantum dot size on the PV-performance of mixed quantum dot solar cell, Zhenyu Yang et al. [291] varied the thickness of quantum dot film from 200 nm to 450 nm and observed that mixed quantum dot solar cells with 350 nm active layer thickness exhibited superior photovoltaic performance. In 2017, T. Kada et al. [292] studied the impact of internal electric field on the PV-performance of InAs/GaAs quantum dot superlattice (QDSL)-IBSCs and found that the photovoltaic performance of InAs/GaAs QDSL-IBSCs degrades at higher internal electric field due to the decrease of EQE. The carrier life time in PbS quantum dot SCs can be increased by adopting a bulk nano-heterojunction structure [293]. The enhancement of carrier lifetime improves the charge transportation properties which results in the enhancement of PCE. In 2016, Jianjun Tian et al. [294] reported that the PCE of PbS quantum dot solar cells can be enhanced by adding methanol in the electrolyte. The addition of methanol in the electrolyte improves the stability of PbS quantum dot SCs. In 2016, María Bernechea et al. [295] reported an environmental friendly AgBiS₂ nanocrystal based quantum dot cell which has a PCE of 6.3%. In 2019, Dang Huu Phuc et al. [296] reported that the photoelectrodes plays a significant role on determining the PV-performance of quantum-dot sensitized SCs. In summary, the PV performance of quantum dot PV cells depends on factors such as transport of charges across the junction, effective insertion of sensitizer on photo-anode and material quality of photo-anode. Novel PV

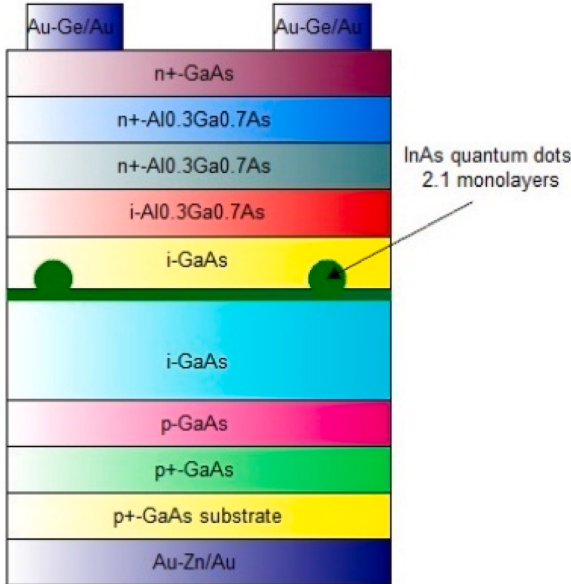


Fig. 39. The schematic of a two step photon up conversion InAs QD solar cell [285].

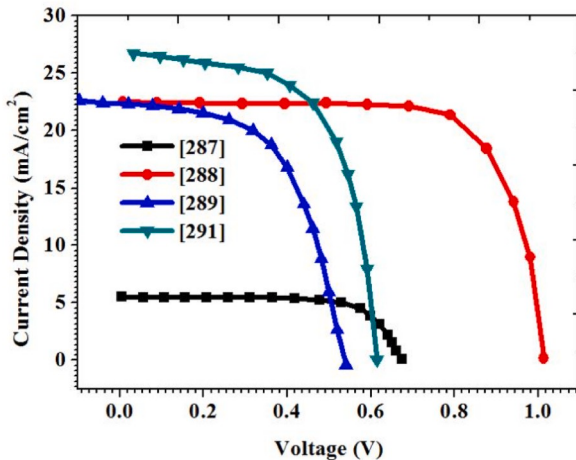


Fig. 40. The J-V performance of some of the high performance quantum dot SCs.

cell architectures and improvement of electronic properties of colloidal quantum dots are highly essential for the improvement of PV performance of quantum dot cells. To date, the highest efficiency reported for the quantum dot PV cell is 18.05%. The photovoltaic performance of state of the art quantum dot SCs is given in Table-7.

9. CIGS and similar materials based solar cells

The developments of economic and environment friendly materials are required for solar energy harvesting applications to generate electricity for future renewable and sustainable energy technologies. CdTe, CZTSSe ($\text{Cu}_2(\text{Zn},\text{Sn})(\text{S},\text{Se})_4$) and CIGSSe are the three commonly used semiconductor materials for thin film SCs [299]. Among these two, CZTSSe is stable, non-toxic and earth abandoned material but it offers poor PCE compared with CIGSSe material. In 2105, Bart Vermang et al. [299] introduced a novel rear surface passivation technique in CZTS solar cells for improving its efficiency by minimizing rear interface recombination. Nano-structured Al_2O_3 was used for rear surface passivation. Reducing the absorber layer thickness of CZTS SCs results in the increase of interface recombination velocity and degradation in bulk quality that severely degrades both J_{SC} and V_{OC} . The schematic of thin film solar cells are given in Fig. 42. The J-V characteristics of some of the popular thin film SCs are shown in Fig. 43.

Fig. 44 (a) reveals that CZTS thin film SCs with rear surface passivation exhibits superior photovoltaic performance compared with CZTS thin film SCs without passivation. The reason for this is that rear surface passivation reduces the interface-recombination velocity

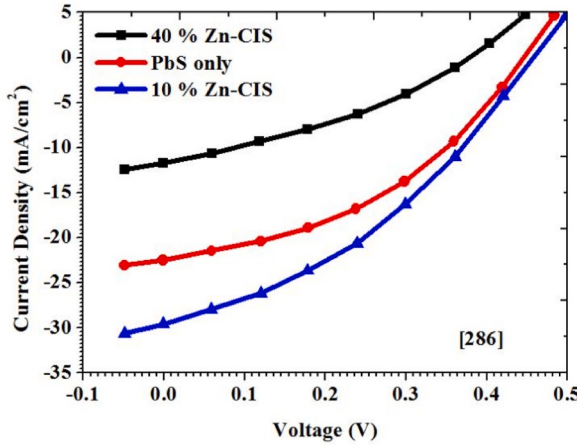


Fig. 41. The influence of Zn-CIS quantum dot on PbS-CIS quantum dot solar cells.

Table 7
Photovoltaic characteristics of state of the art Quantum Dot SCs.

Ref.	Structure/Features	V _{OC} (mV)	J _{SC} (mA/cm ²)	FF (%)	PCE (%)
[286]	PbS-CuInS ₂ Quantum Dot Solar Cells	340	1.54	45	7.74
[288]	QD-hybrid GaAs solar cell: QD460nm_1X	1000	21.45	75.89	16.21
[288]	QD-hybrid GaAs solar cell: QD460nm_5X	990	22.21	76.34	16.85
[288]	QD-hybrid GaAs solar cell: QD460nm_10X	1010	20.41	77.07	15.9
[288]	QD-hybrid GaAs solar cell: QD460nm_15X	1000	20.41	77.24	15.79
[288]	QD-hybrid GaAs solar cell: QD530nm_1X	1020	22.87	73.31	18.05
[288]	QD-hybrid GaAs solar cell: QD530nm_5X	1000	20.17	76.35	15.47
[288]	QD-hybrid GaAs solar cell: QD530nm_10X	1000	19.81	74.27	14.75
[288]	QD-hybrid GaAs solar cell: QD530nm_15X	970	19.34	74.64	14.06
[288]	QD-hybrid GaAs solar cell: QD640nm_1X	1020	20.69	78.28	16.54
[288]	QD-hybrid GaAs solar cell: QD640nm_5X	1030	20.38	79.71	16.69
[288]	QD-hybrid GaAs solar cell: QD640nm_10X	1030	19.88	78.76	16.05
[288]	QD-hybrid GaAs solar cell: QD640nm_15X	1020	19.46	75.52	15.01
[289]	PbSQuantum Dot solarcell	460	17.37	44	35
[290]	Lead selenide (PbSe) nanorod solar cell	290	21	41	2.52
[297]	CH ₃ NH ₃ PbBr ₃ perovskite QD solar cell	1110	14.07	73	11.40
[294]	PbS QD cell without methanol	410	11.68	49.86	2.41
[294]	PbS QD cell with 30% methanol	430	18.34	50.86	4.01
[295]	AgBiS ₂ QD solar cell	450	22.1	6.31	63
[296]	TiO ₂ /CdS QD solar cell	410	4.79	76	1.52
[296]	TiO ₂ /CdSe QD solar cell	430	15.32	36	2.38
[296]	TiO ₂ /CdS/CdSe/ZnS QD solar cell	430	16.72	35	2.55
[296]	TiO ₂ /CdS/CdSe:Cu/ZnS QD solar cell	500	20.01	42	4.31
[296]	TiO ₂ /CdS/CdSe:Mn/ZnS QD solar cell	520	19.04	38	3.79
[298]	TiO ₂ /CdS/CdSe:Mn/ZnS QD solar cell	740	12.6	44	4.14

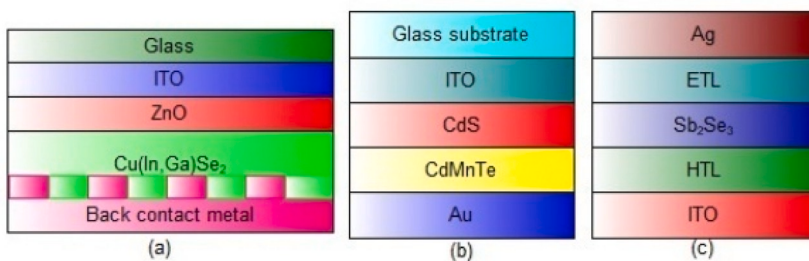


Fig. 42. The schematic of thin film SCs (a) Schematic of Cu(InGa)Se₂ superstrate thin film solar cell design with diffraction gratings [305] (b) CdMnTe thin film solar cell [320] (c) Architecture of Sb₂Se₃ thin film solar cell [329].

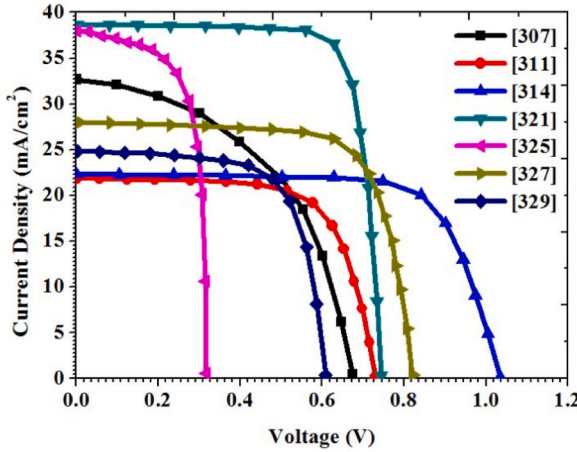


Fig. 43. The J-V characteristics of some of the popular thin film SCs.

and also enhances the bulk quality of the material [300]. The influence of thick and thin InGaN layers on the PV-performance of p-i-n InGaN/GaN thin film SCs is depicted in Fig. 44 (b). A thin InGaN layer enhances the V_{OC} , J_{SC} and PCE of p-i-n InGaN/GaN thin film SCs [304].

In 2013, P. M. P. Salome et al. [301] investigated the influence of NaF on the thin film CIGS SCs on alkali-free glass wafers and observed that increase in NaF content leads to the increase of V_{OC} without degrading J_{SC} (Fig. 44 (c)) [301]. Post deposition KF (Potassium Flouride) treatment and rear surface passivation can be used for improving the front interface of CIGSSe absorber layers which is essential for increasing the PCE of CIGS thin film SCs. The KF treatment improves the bandgap, increases the junction depth and reduces the thickness of CdS buffer layer. In 2014, Bart Vermang et al. [302] introduced the concept of Si PERC rear contact design for enhancing the PCE of CIGSSe thin film SCs. Interdigitated metallization patterns also play a crucial role on the PV-performance of thin film SCs [303]. Introduction of a Chromium silicide (CrSi) layer between the doped layers and metal electrodes of a n-i-p a-Si:H SCs helps to improve its PV-performance which is evident from Fig. 44 (d). Enhancing the light-trapping capacity in thin film SCs also result in the improvement of PV-performance [305–310]. A high density of traps and defects in the absorber layers of thin film SCs leads to the reduction of carrier mobility and increase of carrier recombination rate which results in the severe degradation of PCE of thin film SCs [304]. In 2018, Chang Yan et al. [311] illustrated that the PCE of CZTS thin film SCs can be enhanced by a simple hetero-junction heat treatment process. This is due to the elemental diffusion and formation of new phases. In 2013, Lukas Kranz et al. [312] realized a CdTe thin film solar cell on flexible metal foil substrate.

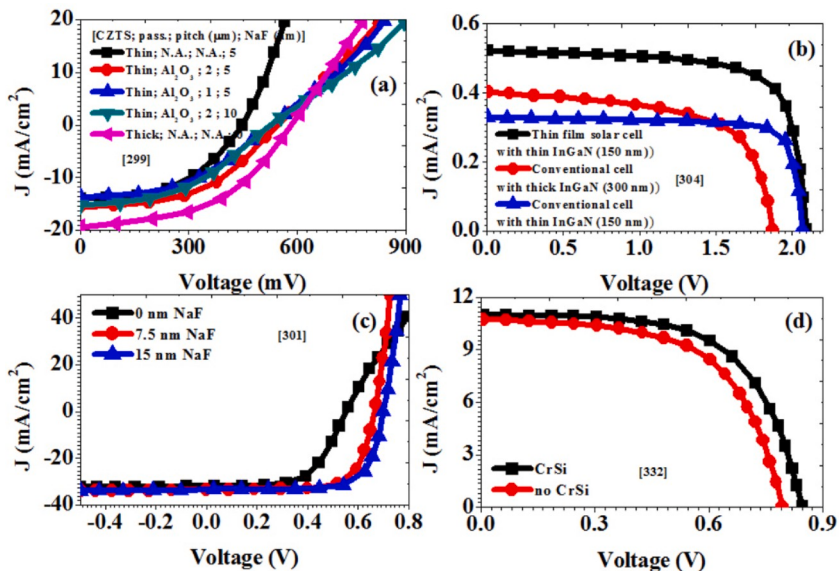


Fig. 44. (a) The effect of rear surface passivation on CZTS thin film SCs (b) The impact of thick and thin InGaN layers on the PV-performance of p-i-n GaN/InGaN thin film SCs (c) Influence of NaF on the thin film CIGS SCs on alkali-free glass wafers (d) The influence of Chromium silicide (CrSi) layer on the J-V curves of thin film SCs.

M. H. Liao et al. [307] studied the impact of Ge concentration on Si-SiGe hetero-structure thin film cell and observed that increase of Ge concentration results in the enhancement of J_{SC} but degrades V_{OC} (Fig. 45 (a)). The influence of glass and metal foil substrates on the J-V characteristics of thin film CdTe cell is plotted in Fig. 45 (b). CdTe thin film SCs on glass substrate provides higher V_{OC} compared with CdTe thin film SCs on flexible steel and Molybdenum foil substrates. In 2015, Hongmei Dang et al. [313] realized a nanowire CdS-CdTe thin film cell with transparent MoO₃/Au back contact. In 2016, Yuan Zhao et al. [314] reported a mono crystalline CdTe/MgCdTe double hetero-structure thin film cell with a V_{OC} and PCE of over 1 V and 17% respectively. In 2016 Jonathan D. Poplawsky et al. [315] analyzed the effect of thickness of CdSe and CdS window layers on the PV-performance of CdTe thin film cell and observed that CdTe thin film SCs with CdS window layer provides higher J_{SC} and V_{OC} compared with CdSe window layer (Fig. 45 (c)). Plasmonic based metallic nanostructures, dielectric nanosphere arrays, patterned transparent conductive oxides and high refractive indexed scatterers are some of the innovative light-trapping structures used to enhance the light collection efficiency of thin film SCs [316–319]. In 2019, Subhash Chander et al. [320] studied the impact of annealing on the PV-performance of CdMnTe thin film cell and observed that the heat treatment significantly affects the PV-performance of CdMnTe thin film SCs. A high temperature annealing enhances the V_{OC} of CdMnTe thin film SCs but degrades the J_{SC} . Therefore care must be taken to fix the annealing temperature in order to achieve the desired PV-performance of thin film SCs (Fig. 45 (d)). In 2018, Takuya Kato et al. [321] reported that the PCE of Cu(In,Ga)(Se,S)₂ thin film SCs can be improved by enhancing the quality of absorber layer with Cs based alkali treatment. The Cs based alkali treatment helps to improve the absorber layer quality by minimizing defect density. Cs based alkali treatment also found to be effective in suppressing carrier recombination rate. In 2019, Nicholas H. Valdes et al. [322] analyzed the impact of Ag alloying and KF treatment on the PV-performance of CuInSe₂ thin film SCs and observed that the addition of Ag in CIS leads to the degradation of PV-performance of thin film CuInSe₂ SCs. The KF treatment in CIS enhances its PCE, but KF treatment in ACIS leads to severe degradation of photovoltaic performance [322]. The influence of Ag alloying and KF treatment on the J-V characteristics of CuInSe₂ thin film solar cell is depicted in Fig. 46 (a). The PCE of Cu(In,Ga)Se₂ thin film SCs can be improved by minimizing the optical losses by introducing a nanopatterned dielectric structure passivation and rear optical reflection [323]. The dielectric layer can effectively minimize the rear interface recombination rate. The influence of various nanopatterned metal/dielectric structures on the J-V characteristics of Cu(In,Ga)Se₂ thin film SCs are plotted in Fig. 46 (b). Cu(In,Ga)Se₂ thin film SCs with Mo/Al₂O₃ structure provides higher J_{SC} and V_{OC} compared with other structures. The quality of buffer layers in Cu(In,Ga)(Se,S)₂ thin film SCs plays a significant role on the PV-performance because the buffer layer quality determines the shunt resistance, series resistance and EQE [324–326]. The PV-performance of CIGS and CZTSSe thin film SCs can be improved by introducing alkali doping. In 2019, Yixuan Wu et al. [325] reported a rubidium (Rb) doped CZTSSe thin film solar cell which outperform conventional CZSSe solar cells (Fig. 46 (c)). The influence of sulphur (S) to Selenium (Se) ratio ($S/(S + Se)$) on the J-V characteristics of CZTSSe thin film solar cell is depicted in Fig. 46 (d). Fig. 46 (d) indicates that CZTSSe thin film solar cells with lower $S/(S + Se)$ ratio exhibits superior photovoltaic performance [326].

In 2019, Jian Huang et al. [327] illustrated that the PCE of CdTe thin film SCs can be improved by introducing a CuCl buffer layer with thermal annealing treatment. The PCE of Cu(In,Ga)Se₂ thin film SCs can be improved by introducing a double Ga-grading in the absorber material [328]. The influence of CdSe and CdS window layers on the photovoltaic performance of CdSe/Sb₂Se₃ (antimony chalcogenide) thin film cell is plotted in Fig. 47(a). A Sb₂Se₃ solar cell with CdSe window layer provides higher J_{SC} , FF and PCE. Sb₂Se₃ have been emerged as an environment friendly alternate semiconducting material for CdTe thin film SCs due to their unique

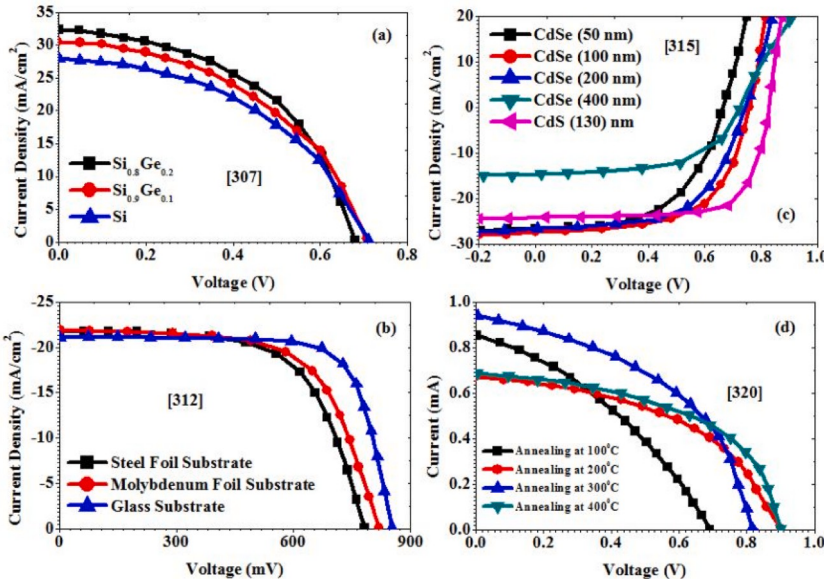


Fig. 45. (a) Influence of Ge concentration on Si-SiGe heterostructure thin film cell (b) The impact of glass and metal foil substrates on the J-V performance of thin film CdTe solar cell (c) Influence of thickness of CdSe and CdS window layers on the PV-performance of CdTe thin film cell (d) Impact of annealing-temperature on the PV-performance of thin film SCs.

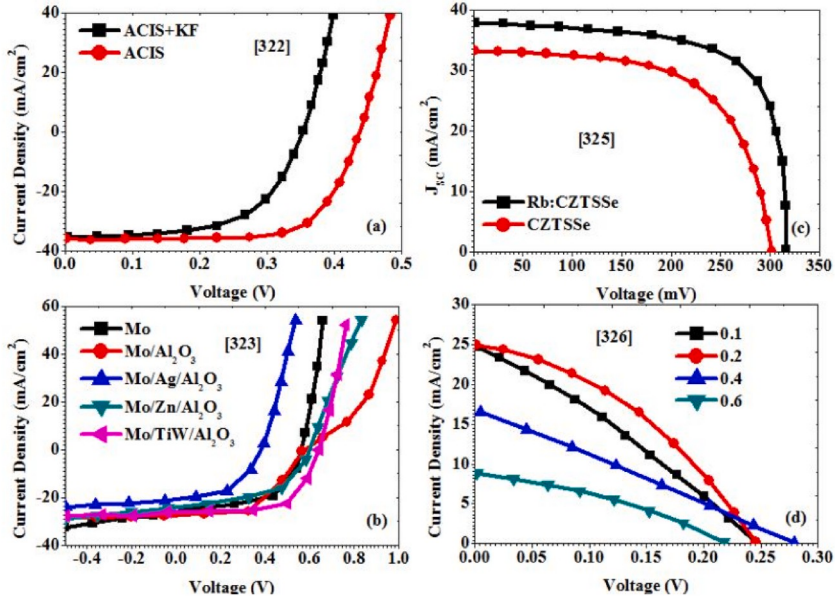


Fig. 46. The influence of Ag alloying and KF treatment on the J-V performance of CuInSe₂ thin film solar cell (b) The influence of various nanopatterned metal/dielectric structures on the J-V characteristics of Cu(In,Ga)Se₂ thin film SCs (c) The influence of Rb doping in CZTSSe thin film cell (d) The influence of sulphur (S) to Selenium (Se) ratio (S/(S + Se)) on the J-V performance of CZTSSe thin film cell.

characteristics such as large optical absorption coefficient, low toxicity, low cost, favourable band gap (1.1 eV), high electrical conductivity and high charge carrier mobility [329]. The influence of various hole transport layer materials such as NiO, CuI and Cu₂O on the PV-performance of Sb₂Se₃ thin film solar cell is depicted in Fig. 47 (b). Sb₂Se₃ thin film SCs with NiO HTL exhibits higher V_{OC}, J_{SC}, FF and PCE compared with CuI and Cu₂O hole transport materials. The effect of acceptor concentration (Na) of hole transport layer on the J-V characteristics of Sb₂Se₃ thin film solar cell is plotted in Fig. 47 (c). Increasing the acceptor concentration in hole transport layers leads to the enhancement of both V_{OC} and J_{SC}. The influence of defect density on the PCE of Sb₂Se₃ thin film solar cell is depicted in Fig. 47 (d) which indicates that the PCE of Sb₂Se₃ thin film solar cell degrades severely with increase in defect density. The global market for thin film solar cell is expected to increase at a rate of approximately 10% over the next few years due to their widespread use in institutional and residential buildings. According to NREL efficiency charts, the highest PCE reported for CIGS, CdTe and amorphous

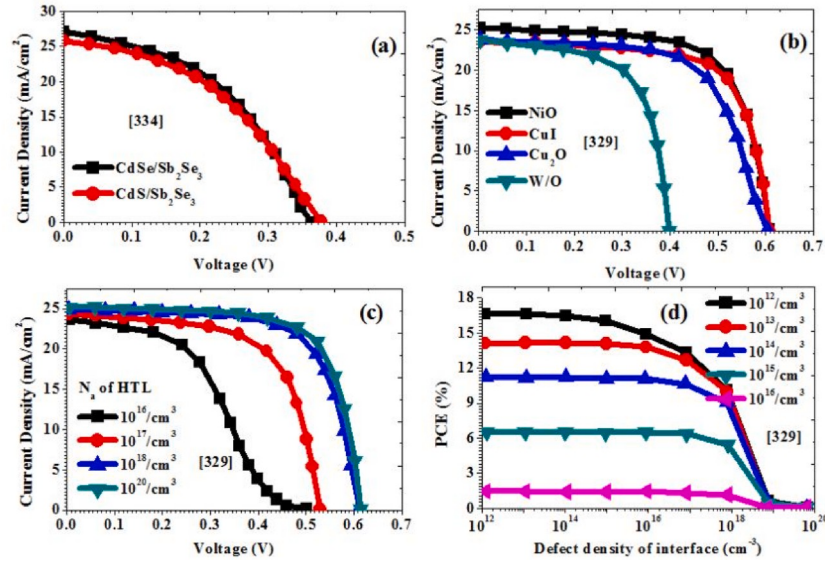


Fig. 47. (a) Influence of CdSe and CdS window layers on the PV-characteristics of CdSe/Sb₂Se₃ (antimony chalcogenide) thin film solar cell (b) Influence of various HTL materials on the PV-performance of Sb₂Se₃ thin film solar cell (c) The effect of acceptor concentration (N_a) of HTL on the J-V performance of Sb₂Se₃ thin film solar cell (d) The influence of defect density on the PCE of Sb₂Se₃ thin film cell.

Si thin film PV cells are 23.4%, 22.1% and 14% respectively. An overview of PV-performance of thin film SCs are given in Table-8.

10. Organic solar cells

The two most important benefits of organic photovoltaic devices (OPV) based on organic semiconductors compared with inorganic photovoltaic devices are the cost effective fabrication facilities and the possibility of producing organic SCs on flexible substrates [335]. Low cost solution-processes like roll-to-roll processing, spin coating and printing methods can be used for industrial-fabrication of polymer based organic SCs. The optical absorption coefficient and band gap energy of polymers depends on functional group and the length of polymers. Thin film technology can significantly reduce the cost of organic solar cells [336]. Low carrier mobility and poor optical absorption coefficient are the two most critical issues in the production of polymer based thin film organic SCs. Light trapping techniques and anti reflection techniques can be used for enhancing the PCE of organic SCs. The optical absorption efficiency of organic SCs can be improved by using techniques such as use of metallic nanostructures to scatter incident sunlight and by plasmonic nanostructures with different shapes in the absorbing layer. The schematic of organic SCs are given in Fig. 48. The J-V performance of some of the high performance organic SCs are shown in Fig. 49.

In 2013, Dong Liu et al. [337] reported a n-Si/PEDOT:PSS organic-inorganic hybrid cell with a PCE of 11%. Dong Liu et al. [337] studied the influence of different passivation materials such as PEI (polyethylenimine), PVA (polyvinylalcohol) and PMMA (poly (methyl methacrylate)) on the PV-performance of n-Si/PEDOT:PSS organic-inorganic hybrid cell and observed that hybrid solar cell with PEI passivation exhibited the highest PCE of 11% compared with hybrid solar cell with PVA and PMMA passivation materials. The passivation layer thickness also plays a crucial role on the PV-performance of organic SCs (Fig. 50 (a)). The PCE of organic SCs can be enhanced by using multiple optical absorbing materials. The use of multiple light absorbing materials widens the absorption spectrum which results in the enhancement of PCE of organic SCs [338]. The influence of multiple absorbing materials such as BTR

Table 8

Photovoltaic performance of thin film SCs.

Ref.	Structure/Features	V _{OC} (mV)	J _{SC} (mA/cm ²)	FF (%)	PCE (%)
[299]	Rear passivated CZTS solar cell	540	15.4	49.9	4.1
[302]	Cu (In, Ga) Se ₂ with Si PERC rear contact	659	23.3	77	11.8
[303]	Polycrystalline Si/Glass solar cell	447	14.5	66	4.1
[330]	CdTe solar cell	872	28	78	19
[331]	a-Si:H/nc-Si:H/nc-Si:H 3J solar cell	1936	8.96	71.5	12.41
[304]	p-i-n GaN/InGaN solar cell	2090	0.52	73.1	0.80
[332]	a-Si:H without Chromium Silicide Layer	796	10.95	59.76	5.2
[332]	a-Si:H with Chromium Silicide Layer	850	10.96	62.05	5.65
[311]	Cu ₂ ZnSnS ₄ solar cell with heat treatment	672.5	20.65	56.29	7.82
[311]	Cu ₂ ZnSnS ₄ solar cell without heat treatment	730.6	21.74	69.27	11.01
[312]	CdTe solar cell on flexible substrate	852	21.2	75.3	13.6
[312]	CdTe solar cell on Mo foil substrate	821	22	63.9	11.5
[312]	CdTe solar cell on steel foil substrate	785	21.8	63.9	10.9
[313]	CdS–CdTe with MoO ₃ /Au back contact	755	25.1	52.1	9.97
[313]	CdS–CdTe with MoO ₃ /Au annealing	752	25.6	57.1	11
[314]	CdTe/MgCdTe double heterostructure	1040	22.3	73.6	17
[315]	CdTe/CdS solar cell	810	23.8	75.4	14.5
[317]	a-Si:H without scatter	857	11.41	82.9	8.10
[317]	a-Si:H with flat scatter	862	13.08	83.2	9.37
[317]	a-Si:H with stepped scatter	863	13.76	83.3	9.89
[321]	Cs-Treated Cu(In,Ga)(Se,S) ₂ solar cell	746	38.5	79.7	22.92
[322]	CuInSe ₂	482	36.7	72.3	12.8
[322]	CuInSe ₂ +KF	485	36.9	73.3	13.1
[322]	Ag/CuInSe ₂	455	36.6	71.8	12
[322]	Ag/CuInSe ₂ +KF	411	37.2	68.3	10.4
[322]	CuInSe ₂ +KF + annealing	526	41	74.4	16
[323]	Cu (In, Ga) Se ₂ /Mo/TiW/Al ₂ O ₃	635	25.80	67.2	11
[325]	CZTSSe solar cell without Rb doping	300.4	33.2	62.6	6.25
[325]	CZTSSe solar cell with Rb doping	317	37.8	70.2	8.41
[333]	Cu ₂ ZnTi(S:Se) ₄ solar cell	505	9.5	40.1	1.96
[327]	CuCl treated CdTe solar cell	800	26.95	75.24	16.21
[327]	CuCl treated CdTe solar cell after annealing	822	27.96	72.59	16.69
[329]	Sb ₂ Se ₃ solar cell	396	23.84	64.60	6.12
[329]	Sb ₂ Se ₃ solar cell with NiO HTL	611	25.06	68.93	10.56
[329]	Sb ₂ Se ₃ solar cell with CuI HTL	606	23.48	70.57	10.04
[329]	Sb ₂ Se ₃ solar cell with Cu ₂ O HTL	606	23.79	64.76	9.34
[334]	CdSe/Sb ₂ Se ₃ CdSe window	377	25.68	43	4.16
[334]	CdSe/Sb ₂ Se ₃ CdSe window	354	27.57	46.13	4.51
[328]	Cu (In, Ga) Se ₂ solar cell	691	29.8	76.5	15.7
[328]	Cu (In, Ga) Se ₂ with double Ga grading	725	34.1	74.7	18.5
[328]	Ga graded Cu (In, Ga) Se ₂ with ARC	731	36.6	75.9	20.3

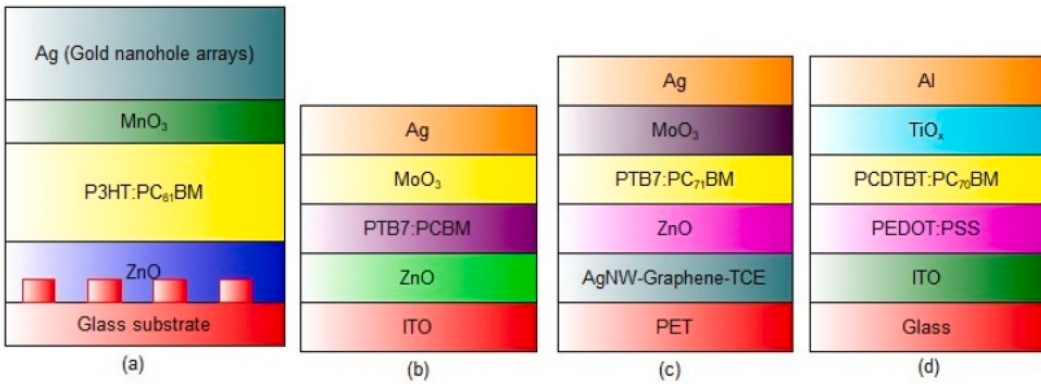


Fig. 48. The schematic of organic solar cells (a) Gold nanohole arrays based P3HT: PC₆₁BM organic solar cell [348] (b) Gold nanohole arrays based PTB7:PCBM solar cells [348] (c) Schematic of the inverted organic solar cell [374] (d) bulk hetero-junction (BHJ) organic solar cell [358].

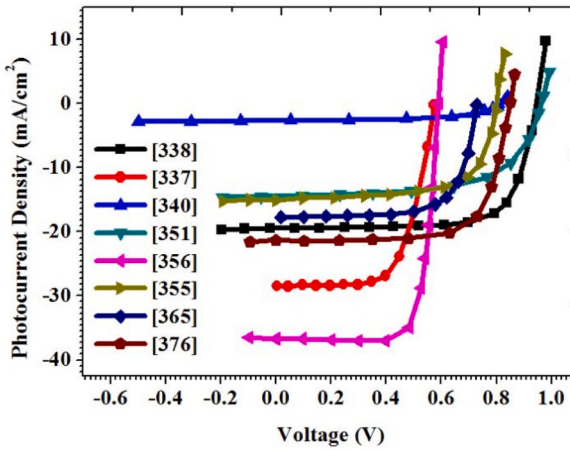


Fig. 49. The J-V performance of some of the high performance organic SCs.

(Benzodithiophene Terthiophene Rhodanine), NITI (molecular acceptor) and PC₇₁BM on the J-V characteristics of organic solar cell is plotted in Fig. 50 (b).

BTR:NITI:PC₇₁BM material system based ternaryorganic solar cells exhibits superior photovoltaic performance compared with BTR:NITI and BTR:PC₇₁BM material system based binary organic solar cells which is evident from Fig. 50 (b). The V_{OC} of organic solar cells mainly depend on the charge transfer state at the acceptor/donor interface. V_{OC} of organic SCs can be computed as [339].

$$V_{OC} = E_G - k_B T \ln \left(\frac{N_{ETL} N_{HTL}}{n_e n_h} \right) \quad (24)$$

where, E_G, N_{ETL}, N_{HTL}, n_e and n_h represents band gap, density of electronic state of electron transport level, density of electronic state of hole transport level, electron concentration and hole concentration respectively. The influence of various electron donor (D)/Electron acceptors (A₁ and A₂) interfaces on the PV-performance of PEDOT:PSS planar HJ organic SCs are shown in Fig. 50 (c). From Fig. 50 (c) it is understood that organic solar cell with D/C₆₀ interface provides higher J_{SC} but suffers from poor V_{OC}. On the other hand, a planar HJ organic cell with D/A1 provides higher V_{OC} but suffer from low J_{SC} [340]. The acceptor and donor molecular orientation significantly affects the PV-performance of organic SCs [341]. Fullerenes are the commonly used electron acceptors in high performance bulk HJ-SCs. Non-fullerene acceptors offers advantages such as crystallinity, planarity and band gap tenability compared with fullerene acceptors and therefore, organic SCs with non-fullerene acceptors are considered as future of organic photovoltaics [342]. PDI (Perylene diimide), BT (Benzothiadiazole) and Naphthalene diimide (NDI) based non-fullerene acceptors are the widely used materials for fabricating organic photovoltaic devices [343–345]. The absorptance (a_{eff} (E)) of the light absorbing layer can be calculated as [346].

$$a_{eff}(E) = 1 - \exp(-2\alpha_{eff}(E)d) \quad (25)$$

Where, α_{eff} and d are effective absorption-coefficient and light absorber layer thickness respectively. The J_{SC} of organic solar cell with

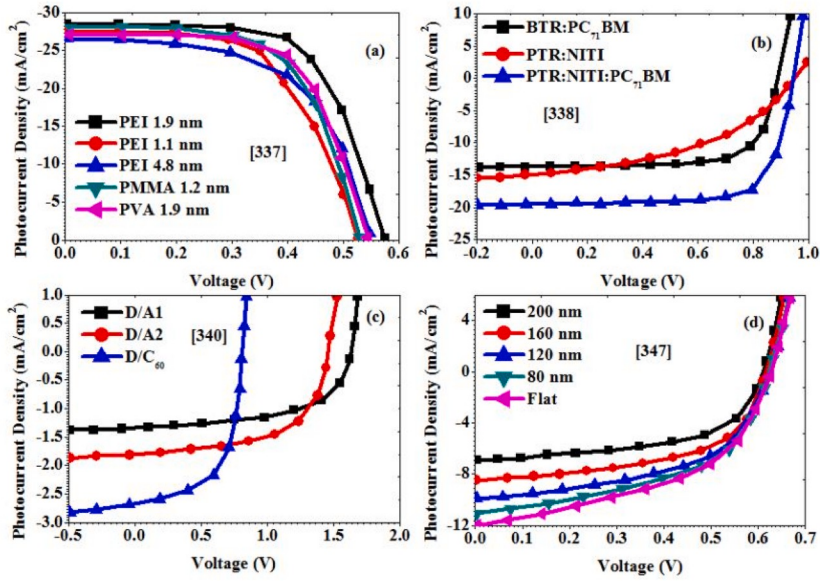


Fig. 50. (a) The influence of thickness of passivation layer on the PV-performance of organic SCs (b) The impact of multiple absorbing materials on the J-V characteristics of organic solar cell (c) The influence of various electron donor (D)/Electron acceptors (A₁ and A₂) interfaces on the PV-performance of PEDOT:PSS planar HJ organic SCs (here A₁ is 8Cl-controlled hexabenzocoronene (cHBC) and A₂ = 12Cl-cHBC) (d) The effect of height of the pillar on organic SCs.

non-fullerene acceptors is given by [346].

$$J_{SC} = q \int_0^{\infty} a_{eff}(E) \varphi_{sun}(E) dE \quad (26)$$

Where, $\varphi_{sun}(E)$ is the AM1.5 solar spectrum. In 2017, Mina Mirsafaei et al. [347] reported that organic solar cells with rectangular grating nanostructure electrodes exhibits superior photovoltaic performance compared with organic solar cells with planar grating electrode structures (Fig. 50 (d)). From Fig. 50 (d) it is evident that J_{SC} and V_{OC} decrease with increase in height of the pillar. Also as the

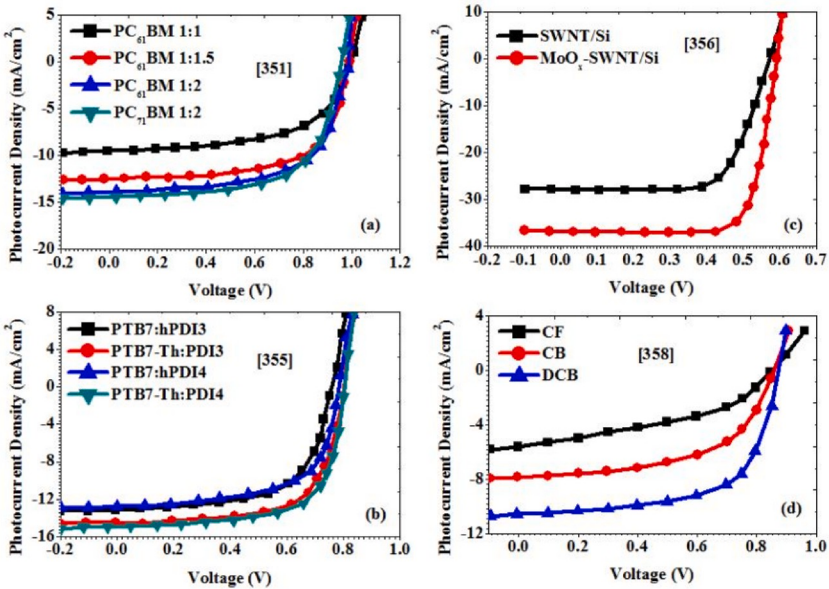


Fig. 51. (a) Influence of polymer to PCBM weight (p/n) ratios on the J-V performance of PNO₄T/PCBM organic polymer SCs (b) J-V characteristics of PTB7:hPDI₃, PTB7-Th:PDI₃, PTB7-hPDI₄ and PTB7-Th:PDI₄ for polymer organic solar cells (c) The PV-performance of SWNT/Si hybrid solar cell and MoO_x coated SWNT/Si hybrid solar cell (d) The impact of various solvents on the J-V characteristics of PCDTBCT:PC₇₀BM bulk HJ organic SCs.

height of the pillar increases fill factor increases and PCE decreases [347]. A transparent conducting electrode like ITO offers high transmittance of over 90% but it has the disadvantages like high cost, scarcity and very brittle. Metal nanohole arise, cracked or printing templates, metal grids formed by lithography, carbon nanotubes, solution processed metal nanowires and thin film metals can be used as an alternate for ITO in organic SCs [348–354]. In 2018, Chawloon Thu et al. [353] demonstrated that, the use of Sn of doping in ZnO nanowires of ITO/ZnO/P3HT/Ag organic solar cell improves the PCE compared with organic SCs with undoped ZnO layer.

The J_{SC} of the SCs are directly proportional to the thickness of active layers. In 2015, Kazuaki Kawashima et al. [351] investigated the influence of polymer to PCBM weight (p/n) ratios on the J-V performance of PNO₂4T/PCBM organic polymer SCs (Fig. 51 a) and found that PNO₂4T/PC₇₁BM SCs exhibited higher J_{SC} and V_{OC} compared with PNO₂4T/PC₆₁BM organic polymer SCs. Polymer SCs with higher polymer to PCBM ratio are required for achieving high PV-performance. The high performance bulk HJ organic SCs use derivatives of fullerene such as PC₇₁BM and PC₆₁BM as electron acceptors due to their outstanding charge separation capability over non-fullerene based electron acceptors. Yu Zhong et al. [355] in 2015 introduced two different molecular helical perylene diimides namely hPDI₃ and hPDI₄ as electron-acceptors for bulk HJ-SCs. Yu Zhong et al. [355] used PTB7 and PTB7-Th as polymer semi-conducting electron-donor materials. Fig. 51 (b) shows the J-V characteristics of PTB7:hPDI₃, PTB7-Th:PDI₃, PTB7-HPDI₄ and PTB7-Th:PDI₄ for polymer organic SCs. Fig. 51 (b) indicates that polar organic solar cell in the PTB7-Th as electron donor material and hPDI₄ as electron acceptor exhibited superior J_{SC} and V_{OC} compared with other combinations of bulk HJ-SCs. The PV-performance of single walled carbon nanotube (SWNT)/Si hybrid solar cell and MoO_x anti-reflection layer coated SWNT/Si hybrid solar cell shown in Fig. 51 (c). The SWNT/Si hybrid solar cell with MoO_x anti-reflection coating exhibits higher J_{SC} and V_{OC} compared with SWNT/Si hybrid solar cell without MoO_x anti-reflection coating. The MoO_x layer improves the hole transport properties which results in the improvement of FF and PCE of hybrid solar cells. MoO_x coated SWNT/Si hybrid solar cells have outstanding transmittance over SWNT/Si solar cell without MoO_x coating [356]. O-IDTBR (brominated indacenodithiophene) and EH-IDTBR materials can also be used as non-fullerene electron acceptors for organic SCs [357]. The influence of DCB (Dichlorobenzene), CB (Chlorobenzene) and CF (Chloroform) solvents on the J-V performance of PCDTBCT:PC₇₀BM bulk HJ organic solar cell is depicted in Fig. 51 (d). From Fig. 51 (d) it is clear that PCDTBCT:PC₇₀BM bulk HJ organic solar cell in which PCDTBCT:PC₇₀BM films dissolved in DCB exhibited superior photovoltaic performance [358]. Fig. 52 (a) depicts the influence of PID2 (Poly-3-oxothieno[3,4-d]isothiazole-1, 1 dioxide/benzo-dithiophene) concentration on the J-V characteristics of PTB7:PID₂:PC₇₁BM ternary bulk HJ organic solar cell. Fig. 52 (a) reveals that PTB7:PID₂:PC₇₁BM ternary bulk HJ organic solar cell with 10% PID₂ concentration is most suitable for achieving maximum PCE. Fig. 52 (b) shows the influence of binary additives such as CN (1-chloronaphthalene), DIO (1,8-diiodooctane) and a combination of both in the dichlorobenzene solution on the photovoltaic performance of PBDTTT-CT:P(NDI20D-T2) all polymer organic solar cell. From Fig. 52 (b) it is understood that addition of CN4 helps to improve V_{OC} but its J_{SC} is poor. On the other hand addition of DIO3CN1 improves J_{SC} but degrades V_{OC} [359]. Rylene diimides such as PDIs (Perylene diimides) and nDIs (naphthalene diimides) based small molecules are popularly used as non-fullerene electron acceptors in organic SCs [360–368]. Fig. 52 (c) indicates that PTB7-Th:PID₂:PC₇₁BM ternary organic solar cell with lower PID concentration exhibited higher photovoltaic performance. Stability is one of the most critical issues which needs to be addressed before polymer organic SCs enter the photovoltaic market [369,370]. Over the years the

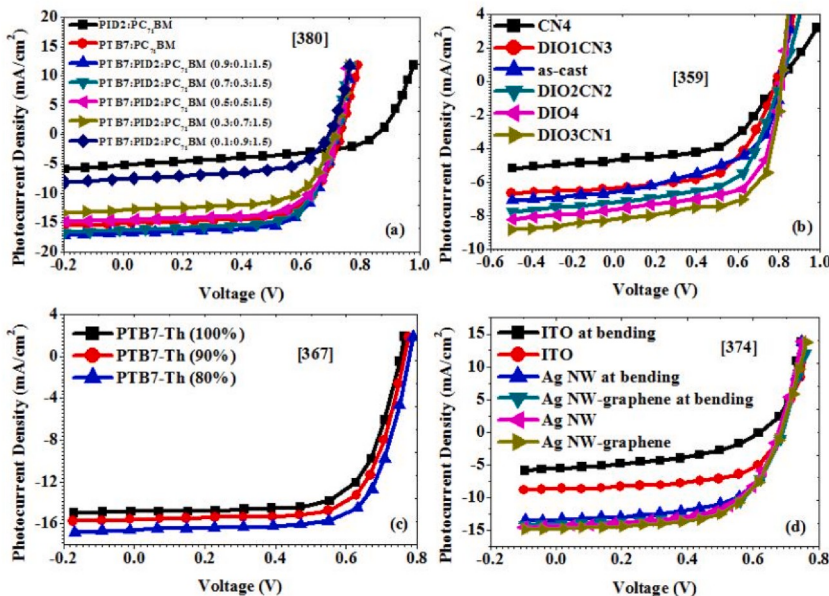


Fig. 52. (a) Impact of PID₂ concentration on the J-V characteristics of PTB7:PID₂:PC₇₁BM ternary bulk HJ organic SCs (b) Influence of various binary additives on the PV-performance of PBDTTT-CT: P(NDI20D-T2) all polymer organic SCs (c) J-V curves of PTB7-Th:PID₂:PC₇₁BM organic solar cells with 0, 10 and 20% PID₂ concentration (d) Influence of various transparent conducting electrodes (TCEs).

PCE of organic solar cells have been increased to above 13%. This outstanding result is mainly due to the development of controlled nanostructure morphology of donor-acceptor molecules, tandem organic solar cells, interface charge collecting materials and the development of low band-gap polymers [371].

In 2019, Ishan C. Ghosekar et al. [371] reported that the incorporation of a 3-hexyl thiophene buffer layer between the blended polymer and HTL using solution processing can significantly improves the PCE of organic SCs. The two factors that leads to the degradation of performance of organic solar cells are intrusion of air and moisture and thermal inter diffusion of constituent elements inside the organic SCs [372]. In 2018, Nikhil Chandar et al. [373] investigated the reliability and stability of PTB7:PC₆₁BM and PTB7:PC₇₁BM inverted organic SCs and found that PTB7:PC₆₁BM solar cells have a relatively better stability and reliability than PTB7:PC₇₁BM solar cells. Fig. 52 (d) shows the influence of transparent conducting electrodes (TCEs) such as ITO, silver nanowire (Ag NW) and silver nanowire graphene on the J-V performance of organic SCs. Organic SCs with Ag NW-graphene hybrid TCE exhibits superior photovoltaic performance compared with organic solar cells with other TCEs such as ITO and Ag NW. Ag NW have been emerged as one of the most promising TCE to replace traditional ITO [374]. Fig. 53 (a) shows the influence of different fabrication conditions of PTB7-Th:BAF-2HDT NFA based bulk hetero-junction organic solar cell. Fig. 53 (a) reveals the fact that PTB7-Th:BAF-2HDT bulk hetero-junction organic solar cell fabricated under additive DIO (1,8-diiodooctane) with solvate vapour annealing conditions exhibits superior J_{SC} and V_{OC} compared with organic solar cells fabricated under vacuum and thermal annealing conditions. Similarly Fig. 53 (b) plots the influence of different fabrication conditions with CN (1-Chloronaphthalene) additives on the J-V performance of PTB7-Th:BAF-4CN NFA based bulk HJ organic solar cell. From Fig. 53 (b) it is evident that PTB7-Th:BAF-4CN bulk HJ organic solar cell fabricated under solvent vapour annealing conditions with CN additive exhibits higher J_{SC} and V_{OC} compared with bulk HJ solar cells fabricated under vacuum and thermal annealing conditions [375]. In 2019, Hao Huang et al. [376] reported high performance organic SCs with non-covalently fused ring electron acceptors such as DOC2C6-2F, DOC2C6-IC, DOC8-IC, DC6-IC and DOC6-IC (Fig. 53 (c)). Fused ring electron-acceptors for organic SCs have gained tremendous attention in the photovoltaic industry due to their intense and broad light absorption ability, easy structural modulation and high PCE of over 14%. The molecular structures of DOC2C6-2F, DOC2C6-IC, DOC8-IC, DC6-IC and DOC6-IC fused ring electron acceptors are given in Ref. [377]. In 2019, Xiaojin Zhang et al. [377] reported that the PCE of organic SCs can be enhanced by introducing fluorine dimmers based cathode inter layers. The influence of PFN, FN-FN and (FN-E)₂ cathode interface layers on the J-V characteristics of organic solar cell is shown in Fig. 53 (d). From Fig. 53 (d) it is clear that bulk HJ organic SCs with (FN-E)₂ cathode interface layer provides better photovoltaic performance. The PCE of bulk HJ organics SCs can also be improved by isopropyl alcohol treatment [378,379]. In summary, reliability and operational stability are the key requirements for commercialization and scaling-up of organic PV technology. The PV performance of PTB7 based organic SCs are severely degraded by presence of oxygen and moisture. The highest efficiency reported for organic tandem PV cell is 13.76%. The PV-performance of state of the art organic SCs is given in Table-9. Finally, the absorption range of solar cells plays a critical role in determining the PCE. The bandgap of active layer material determines the absorption range and PCE. The bandgap comparison of some of the very popular solar cell active layer materials is given in Table-10. Active layer materials with low bandgap can effectively absorb higher wavelength lights. On the other hand active layer solar materials with larger bandgap can significantly absorb smaller wavelength lights in the absorption spectrum. Solar cells with narrow bandgap active layer materials exhibits higher J_{SC} but suffer from reduced V_{OC} . On the other hand, solar cells with wide bandgap active layer materials provide higher V_{OC} and lower J_{SC} .

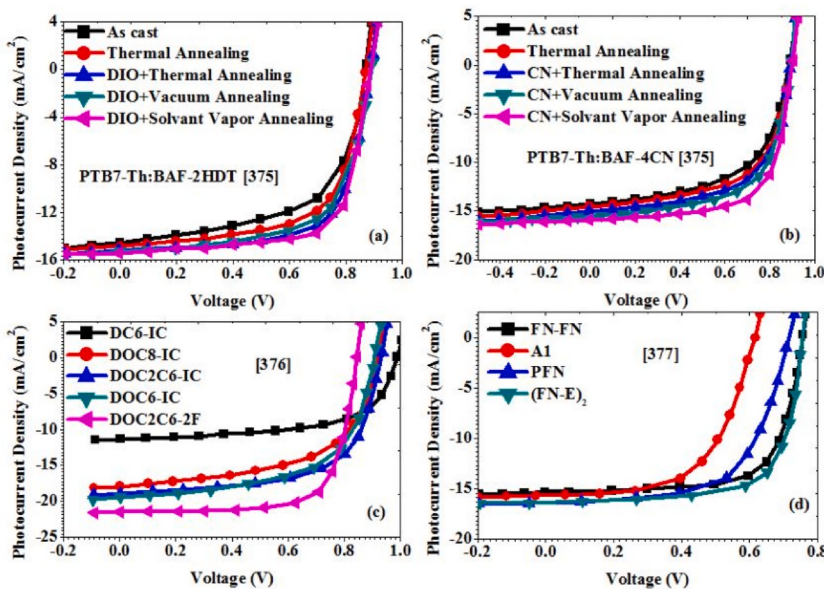


Fig. 53. (a) Influence of different fabrication conditions of PTB7-Th:BAF-2HDT NFA based bulk HJ organic solar cell (b) Influence of different fabrication conditions with CN additives on the J-V performance of PTB7-Th:BAF-4CN NFA based bulk HJ organic solar cell (c) Influence of fused ring electron acceptors (d) Influence of various cathode interface layers.

Table 9

An overview of photovoltaic performance of Organic SCs.

Ref.	Structure/Features	V _{OC} (mV)	J _{SC} (mA/cm ²)	FF (%)	PCE (%)
[337]	n-Si/PEDOT:PSS without passivation	520	28.15	59.3	8.75
[337]	n-Si/PEDOT:PSS with PEI passivation	574	28.6	67	11
[384]	Organic tandem solar cell	1642	14.35	73.7	17.36
[337]	n-Si/PEDOT:PSS with PVA passivation	540	27.1	67	9.8
[337]	n-Si/PEDOT:PSS with PMMA passivation	530	28	63	9.35
[338]	BTR:NiT _x :PC ₇₁ BM	940	19.5	73.83	13.63
[341]	P3HT/PCBM bi-layer device	320	2.38	51.8	0.387
[347]	ITO/PEDOT:PSS/P3HT:PC ₆₀ BM/Al with planar grating	623	12.3	48.8	3.74
[347]	ITO/PEDOT:PSS/P3HT:PC ₆₀ BM/Al with 200 nm square pillar	629	12.3	56.5	4.37
[347]	ITO/PEDOT:PSS/P3HT:PC ₆₀ BM/Al with 200 nm square pillar and optical absorption enhancement	629	13.3	57.6	4.82
[348]	P3HT:PC ₆₁ BM/ITO	580	7.3	61	2.6
[348]	P3HT:PC ₆₁ BM/nanomesh	590	5.7	58	2
[348]	PTB7:PC ₇₁ BM/ITO	710	12.9	65	6
[348]	PTB7:PC ₇₁ BM/nanomesh	700	10.2	65	4.6
[353]	ZnO nanowire-P3HT hybrid solar cell	370	2.71	54	0.57
[350]	PBDTTT-EFT-EHIDTBR	1030	18.5	63	12
[350]	PBDTTT-EFT:PC ₇₁ BM	780	15.9	66	8.5
[351]	PNOz4T:PC ₆₁ BM	970	14.6	62	8.8
[351]	PNOz4T:PC ₇₁ BM	960	14.5	64	8.9
[355]	hPDI3/PTB7	760	13	62	6.3
[355]	hPDI3/PTB7-Th	800	14.3	67	7.7
[355]	hPDI4/PTB7	780	12.7	63	6.4
[355]	hPDI4/PTB7-Th	800	15	68	8.1
[356]	p-SWNT/n-Si	570	27.9	69	11.1
[356]	MoO _x -coated SWNT/Si	590	36.6	78	17
[357]	O-IDTBR:P3HT	720	13.9	60	6.3
[357]	EH-IDTBR:P3HT	760	12.1	62	6
[380]	Ternary PTB7:PID2:PC ₇₁ BM	720	16.8	68.7	8.22
[381]	Glass/ITO/PEDOT:PSS/P3HT:PCBM	630	12.6	63	4.2
[358]	Glass/ITO/PEDOT:PSS/PCDTBT:PC ₇₀ BM	880	10.6	66	6
[359]	PBDTTT-CT: P(NDI2OD-T2)	810	8.20	66.2	4.16
[364]	P3HT:PCBM:NCS-EHT	520	6.34	48	1.60
[367]	PTB7-Th:PID2: PC ₇₁ BM	780	16.68	70.8	9.20
[368]	Ag NPs-P3HT:PCBM	600	8.98	57	3.10
[371]	ITO coated glass/PEDOT:PSS/P3HT:PCBM	600	6.12	56.63	2.05
[373]	PTB7: PC ₇₁ BM	770	19.88	65.3	8.76
[373]	PTB7: PC ₆₁ BM	740	16.30	66.1	7.88
[374]	PTB7: PTB7: PC ₇₁ BM with ITO TCE	690	8.80	60	3.65
[374]	PTB7: PTB7: PC ₇₁ BM with Ag NW TCE	690	14.40	61	5.96
[374]	PTB7: PTB7: PC ₇₁ BM with Ag NW-Graphene TCE	690	15.83	60	6.47
[375]	PTB7-Th:BAF-4CN	898	15.8	68.1	9.7
[375]	PTB7-Th:BAF-2HDT/DIO	902	15.4	71.5	9.9
[376]	DOC6-IC/PBDB-T	910	19.21	60.11	10.52
[376]	DOC8-IC/PBDB-T	920	17.74	57.65	9.41
[376]	DOC2C6-IC/PBDB-T	930	18.85	63.33	11.1
[376]	DC6-IC/PBDB-T	990	11.19	62.21	6.87
[376]	DOC2C6-2F/PBDB-T	850	21.35	73.15	13.24
[377]	ITO/PEDOT:PSS/PTB7: PC ₇₁ BM w/o CIL	620	15.96	59.48	5.53
[377]	ITO/PEDOT:PSS/PTB7: PC ₇₁ BM/PFN CIL	720	16.37	63.61	7.45
[377]	ITO/PEDOT:PSS/PTB7: PC ₇₁ BM/FN-FN	760	15.40	71.39	8.36
[377]	ITO/PEDOT:PSS/PTB7: PC ₇₁ BM with (FN-E) ₂	760	16.39	71.52	8.91
[382]	ITO/MoO ₃ /DIP:MoO ₃ /DIP:Cs ₂ CO ₃ /BCP/Al	720	0.169	40	0.049
[378]	IPA treated ITO/PEDOT:PSS/PCDTBT:PC ₆₀ BM/Al	733	8	56	3.3
[383]	Cu-Ce ₆ Me ₃ :C ₇₀ planar-heterojunction	330	4.45	58	0.85
[383]	Ce ₆ Me ₃ :C ₇₀ planar heterojunction solar cell	490	3.88	50	0.93

Therefore, selection of solar materials is also very important in the design of solar cells to achieve a desired PV performance.

11. Conclusion

According to the current economic growth figures, the world needs energy of over 30 TW in 2050 and over 50 TW in the end of this 21st centenary. A major part of this energy should be generated by environment friendly renewable energy sources. At this moment, solar cells are the largest source of renewable energy. For future sustainable and renewable energy technologies, it is essential to develop innovative and environmental friendly materials for harvesting solar energy. III-V solar cells, DSSCs, PSCs and organic solar cells have been considered as the most promising solutions to meet the global energy demands. To date, the highest conversion

Table-10

An overview of bandgap comparison of some of the popular solar materials.

Ref.	Solar Materials	Bandgap (eV)
[97]	Bulk Silicon	1.1
[97]	Silicon Nanowire (5 nm) Diameter	1.4
[88]	Silicon Quantum Dot (2 nm)	1.7
[77]	c-Si	1.12
[22]	a-Si:H	1.77
[77]	GaAs	1.42
[77]	GaInP	1.80
[77]	CdTe	1.45
[77]	CdZnTe	1.80
[77]	CZTS	1.45
[30]	GaP	2.26
[68]	ZnO	3.37
[68]	FTO	3.44
[183]	TiO ₂	3.2
[9]	CH ₃ NH ₃ SnI ₃	1.3
[231]	CH ₃ NH ₃ PbI _{3-x} Cl _x	1.5
[231]	Zn ₂ SnO ₄	3.8
[240]	CZTSSe ₃ -S	1.12
[240]	CZTSSe ₇ -S	1.117
[224]	InGaN	0.7–3.4
[221]	InGaAs	0.74–1
[212]	InN	0.7
[207]	(Al _{0.7} Ga _{0.3}) _{0.53} In _{0.47} P	2.3
[203]	GaN	3.42
[202]	GaAsSbN	1.25
[21]	ZrO _{2-x}	1.5
[22]	CIGS	1.12
[22]	InP	1.38
[22]	CdTe _{1-x} Se _x	1.42
[342]	P3HT	1.9
[375]	PTB7-Th	1.58
[364]	CuInS ₂	1.5
[152]	CH ₃ NH ₃ SnI ₃	3.6
[152]	CH ₃ NH ₃ SnI ₃	1.23
[152]	CH ₃ NH ₃ SnIBr ₂	1.75
[152]	MA ₂ SnBr ₃	2.3
[152]	FASnI ₃	1.4
[152]	(FA) _{0.75} (MA) _{0.25} SnI ₃	1.33
[152]	CsSnI ₃	1.3
[152]	CsSnI ₂ Br	1.37
[152]	CsSnBr ₃	1.75
[152]	CsSnBr ₂	1.63
[152]	CsGeI ₃	1.63
[152]	MAGEI ₃	2
[152]	MA ₂ CuCl ₂ Br ₂	2.12
[152]	MAPbI ₃	1.55
[145]	CH ₃ NH ₃ PbBr ₃	2.2
[169]	CH ₃ NH ₃ PbCl _{3-x} I _x	1.55
[132]	PTB7	1.81
[169]	PDPP3T	1.56
[131]	FA _{0.83} Cs _{0.17} Pb(I _{0.6} Br _{0.4}) ₃	1.72
[131]	BA _{0.05} (FA _{0.83} Cs _{0.17}) _{0.95} Pb(I _{0.8} Br _{0.2}) ₃	1.61
[158]	MA _{0.5} Pb _{0.5} I ₃	1.17
[158]	FA _{0.83} Cs _{0.17} Pb(I _{0.5} Br _{0.5}) ₃	1.8
[158]	FA _{0.75} Cs _{0.25} Sn _{0.5} Pb _{0.5} I ₃	1.22
[124]	CsPbI ₃	1.73
[119]	CsPbBr ₃ Quantum Dots	2.40
[116]	MAPbBr _{3-x} Cl _x	2.3
[110]	CdS	2.25
[110]	CdSe	1.70
[110]	Sb ₂ S ₃	1.65
[110]	Sb ₂ Se ₃	1.13
[295]	CuIn _x Ga _(1-x) Se ₂	1.3
[285]	Al _{0.3} Ga _{0.7} As	1.80

efficiency attained by silicon, perovskite, DSSCs, III-V SCs, flexible SCs, quantum dot cell and organic solar cells are 27.6%, 25.2%, 12.3%, 53.8%, 15.38%, 18.05% and 13.76% respectively. Among all leading PV technologies, III-V materials based multi-junction solar cells are the most efficient PV technology with over 50% PCE. To further enhance the PCE, it is essential to improve the carrier collection, light absorption and also to reduce the thermalization energy loss. Even though the PCE of perovskite PV cells have exceeded 25%, the operational stability, reliability and large area device efficiency should be further improved before commercialization. Compared with all perovskite tandem solar cells, perovskite/silicon hybrid tandem solar cells are found to be effective in improving the PCE due to the effective utilization of solar spectrum. The organic solar materials suffer from poor carrier mobility which limits its PCE of organic PV cells. Tandem cell technology can be used for effectively enhancing the PCE of organic PV cells. In the future, the stability, reliability, flexibility and optical transparency of the organic solar cells needs to be addressed before enter into the photovoltaic market. Solar cells have emerged as an attractive source of electric energy for future power generating windows, power saving display systems, self-powered wearable electronic devices, building integrated photovoltaics and electric vehicles.

Appendix A. Supplementary data

Supplementary data to this article can be found online at <https://doi.org/10.1016/j.spmi.2020.106549>.

Conflict of interest form

The authors declare that there is no conflict of interest reported in this paper.

References

- [1] I. Ramiro, A. Martí, E. Antolin, A. Luque, Review of experimental results related to the operation of intermediate band solar cells, *IEEE Journal of Photovoltaics* 4 (2014) 736–748.
- [2] U. Römer, R. Peibst, T. Ohrdes, B. Lim, J. Krügener, T. Wietler, R. Brendel, Ion implantation for poly-Si passivated back-junction back-contacted solar cells, *IEEE Journal of Photovoltaics* 5 (2015) 507–514.
- [3] B. Min, M. Müller, H. Wagner, G. Fischer, R. Brendel, P.P. Altermatt, H. Neuhaus, A roadmap toward 24% efficient PERC solar cells in industrial mass production, *IEEE Journal of Photovoltaics* 7 (2017) 1541–1550.
- [4] C. Kranz, B. Wolpensinger, R. Brendel, T. Dullweber, Analysis of local aluminum rear contacts of bifacial PERC+ solar cells, *IEEE Journal of Photovoltaics* 6 (2016) 830–836.
- [5] A. Blakers, Development of the PERC solar cell, *IEEE Journal of Photovoltaics* 9 (2019) 629–635.
- [6] V.L. Dalal, J. Zhu, M. Welsh, M. Noack, Microcrystalline Si: H solar cells fabricated using ECR plasma deposition, *IEE Proc. Circ. Dev. Syst.* 150 (2003) 316–321.
- [7] R. Núñez, M. Victoria, S. Askins, I. Antón, C. Domínguez, R. Herrero, G. Sala, Spectral impact on multijunction solar cells obtained by means of component cells of a different technology, *IEEE Journal of Photovoltaics* 8 (2018) 646–653.
- [8] R. Österbacka, A. Pivrikas, G. Juška, A. Poškus, H. Aarnio, G. Sliažys, K. Genevičius, K. Arlauskas, N.S. Sariciftci, Effect of 2-d delocalization on charge transport and recombination in bulk-heterojunction solar cells, *IEEE J. Sel. Top. Quant. Electron.* 16 (2010) 1738–1745.
- [9] E.F. Fernández, F.A. Cruz, T.K. Mallick, S. Sundaram, Effect of spectral irradiance variations on the performance of highly efficient environment-friendly solar cells, *IEEE Journal of Photovoltaics* 5 (2015) 1150–1157.
- [10] J.-H. Guo, J.E. Cotter, Laser-grooved backside contact solar cells with 680-mV open-circuit voltage, *IEEE Trans. Electron. Dev.* 51 (2004) 2186–2192.
- [11] F. Schindler, B. Michl, J. Schön, W. Kwapił, W. Warta, M.C. Schubert, Solar cell efficiency losses due to impurities from the crucible in multicrystalline silicon, *IEEE Journal of Photovoltaics* 4 (2013) 122–129.
- [12] D. Millstein, R. Wiser, M. Bolinger, G. Barbose, The climate and air-quality benefits of wind and solar power in the United States, *Nature Energy* 2 (2017) 17134.
- [13] A. Martí, A. Luque, Three-terminal heterojunction bipolar transistor solar cell for high-efficiency photovoltaic conversion, *Nat. Commun.* 6 (2015) 6902.
- [14] B. Endres, M. Ciorga, M. Schmid, M. Utz, D. Bougeard, D. Weiss, G. Bayreuther, C. Back, Demonstration of the spin solar cell and spin photodiode effect, *Nat. Commun.* 4 (2013) 2068.
- [15] F. Guo, N. Li, F.W. Fecher, N. Gasparini, C.O.R. Quiroz, C. Bronnbauer, Y. Hou, V.V. Radmilović, V.R. Radmilović, E. Specker, A generic concept to overcome bandgap limitations for designing highly efficient multi-junction photovoltaic cells, *Nat. Commun.* 6 (2015) 7730.
- [16] Y. Xu, T. Gong, J.N. Munday, The generalized Shockley-Queisser limit for nanostructured solar cells, *Sci. Rep.* 5 (2015) 13536.
- [17] J.-H. Yun, E. Lee, H.-H. Park, D.-W. Kim, W.A. Anderson, J. Kim, N.M. Litchinitser, J. Zeng, J. Yi, M.M.D. Kumar, Incident light adjustable solar cell by periodic nanolens architecture, *Sci. Rep.* 4 (2014) 6879.
- [18] Y. Kim, N.D. Lam, K. Kim, W.-K. Park, J. Lee, Ge nanopillar solar cells epitaxially grown by metalorganic chemical vapor deposition, *Sci. Rep.* 7 (2017) 42693.
- [19] L. Cojocaru, S. Uchida, K. Tamaki, P.V. Jayaweera, S. Kaneko, J. Nakazaki, T. Kubo, H. Segawa, Determination of unique power conversion efficiency of solar cell showing hysteresis in the IV curve under various light intensities, *Sci. Rep.* 7 (2017) 11790.
- [20] Y. Zhang, S. Chen, D. Hu, Y. Xu, S. Wang, F. Qin, Y. Cao, B.-O. Guan, A. Miroshnichenko, M. Gu, Coloring solar cells with simultaneously high efficiency by low-index dielectric nanoparticles, *Nanomater. Energy* 62 (2019) 682–690.
- [21] A. Sinhamahapatra, J.-P. Jeon, J. Kang, B. Han, J.-S. Yu, Oxygen-deficient zirconia (ZrO_{2-x}): a new material for solar light absorption, *Sci. Rep.* 6 (2016) 27218.
- [22] P.K. Nayak, S. Mahesh, H.J. Snaith, D. Cahen, Photovoltaic solar cell technologies: analysing the state of the art, *Nature Reviews Materials* 4 (2019) 269.
- [23] R. Varache, O.N. Aguila, A. Valla, N. Nguyen, D. Munoz, Role of the front electron collector in rear emitter silicon heterojunction solar cells, *IEEE Journal of Photovoltaics* 5 (2015) 711–717.
- [24] J. Müller, D. Hinken, S. Blankemeyer, H. Kohlenberg, U. Sonntag, K. Bothe, T. Dullweber, M. Kontges, R. Brendel, Resistive power loss analysis of PV modules made from halved 15.6×15.6 cm² silicon PERC solar cells with efficiencies up to 20.0%, *IEEE Journal of Photovoltaics* 1 (2015) 189–194.
- [25] F. Kiefer, C. Ulzhofer, T. Brendemuhl, N.-P. Harder, R. Brendel, V. Mertens, S. Bordihn, C. Peters, J.W. Müller, High efficiency n-type emitter-wrap-through silicon solar cells, *IEEE Journal of Photovoltaics* 1 (2011) 49–53.
- [26] M. Taguchi, A. Yano, S. Tohoda, K. Matsuyama, Y. Nakamura, T. Nishiwaki, K. Fujita, E. Maruyama, 24.7% record efficiency HIT solar cell on thin silicon wafer, *IEEE Journal of Photovoltaics* 4 (2013) 96–99.
- [27] N. Wehmeier, B. Lim, A. Merkle, A. Tempez, S. Legendre, H. Wagner, A. Nowack, T. Dullweber, P.P. Altermatt, PECVD BSG diffusion sources for simplified high-efficiency n-PERT BJ and BJBC solar cells, *IEEE Journal of Photovoltaics* 6 (2015) 119–125.

- [28] P. Saint-Cast, J. Benick, D. Kania, L. Weiss, M. Hofmann, J. Rentsch, R. Preu, S.W. Glunz, High-efficiency c-Si solar cells passivated with ALD and PECVD aluminum oxide, *IEEE Electron. Device Lett.* 31 (2010) 695–697.
- [29] A. Ebong, I.B. Cooper, B.C. Rounsville, A. Rohatgi, M. Dovrat, E. Kritchman, D. Brusilovsky, A. Benichou, Capitalizing on the glass-etching effect of silver plating chemistry to contact Si solar cells with homogeneous 100–110\$ Ω emitters, *IEEE Electron. Device Lett.* 32 (2011) 779–781.
- [30] M. Feifel, T. Rachow, J. Benick, J. Ohlmann, S. Janz, M. Hermle, F. Dimroth, D. Lackner, Gallium phosphide window layer for silicon solar cells, *IEEE Journal of Photovoltaics* 6 (2015) 384–390.
- [31] A. Ebong, I.B. Cooper, B. Rounsville, A. Rohatgi, M. Dovrat, E. Kritchman, D. Brusilovsky, A. Benichou, On the ink jetting of full front Ag gridlines for cost-effective metallization of Si solar cells, *IEEE Electron. Device Lett.* 33 (2012) 637–639.
- [32] W. Yin, X. Wang, F. Zhang, L. Zhang, 19.6% cast mono-MWT solar cells and 268 W modules, *IEEE Journal of Photovoltaics* 3 (2013) 697–701.
- [33] J. Wu, Y. Liu, X. Wang, L. Zhang, Application of ion implantation emitter in PERC solar cells, *IEEE Journal of Photovoltaics* 4 (2013) 52–57.
- [34] M. Glatthaar, R. Rohit, A. Rodofili, Y.J. Snow, J. Nekarda, J. Bartsch, Novel plating processes for silicon heterojunction solar cell metallization using a structured seed layer, *IEEE Journal of Photovoltaics* 7 (2017) 1569–1573.
- [35] V. Shanmugam, J. Wong, I.M. Peters, J. Cunnusamy, M. Zahn, A. Zhou, R. Yang, X. Chen, A.G. Aberle, T. Mueller, Analysis of fine-line screen and stencil-printed metal contacts for silicon wafer solar cells, *IEEE Journal of Photovoltaics* 5 (2015) 525–533.
- [36] T.-Y. Chang, C.-L. Chang, H.-Y. Lee, P.-T. Lee, A metal-insulator-semiconductor solar cell with high open-circuit voltage using a stacking structure, *IEEE Electron. Device Lett.* 31 (2010) 1419–1421.
- [37] J. Bullock, C. Samundsett, A. Cuevas, D. Yan, Y. Wan, T. Allen, Proof-of-concept p-type silicon solar cells with molybdenum oxide local rear contacts, *IEEE Journal of Photovoltaics* 5 (2015) 1591–1594.
- [38] E. Lohmuller, B. Thaidigsmann, M. Pospischil, U. Jager, S. Mack, J. Specht, J. Nekarda, M. Retzlaff, A. Krieg, F. Clement, 20% efficient passivated large-area metal wrap through solar cells on boron-doped Cz silicon, *IEEE Electron. Device Lett.* 32 (2011) 1719–1721.
- [39] G. Galbati, V.D. Mihaileti, R. Roescu, A. Halm, L.J. Koduvvelukalathu, R. Kopecek, K. Peter, J. Libal, Large-area back-contact back-junction solar cell with efficiency exceeding 21%, in: *IEEE 38th Photovoltaic Specialists Conference (PVSC) PART 2*, IEEE, 2012, pp. 1–6, 2012.
- [40] T. Böscke, D. Kania, A. Helbig, C. Schöllhorn, M. Dupke, P. Sadler, M. Braun, T. Roth, D. Stichtenoth, T. Wütherich, Bifacial n-type cells with > 20% front-side efficiency for industrial production, *IEEE Journal of Photovoltaics* 3 (2013) 674–677.
- [41] A. Ebong, N. Chen, V. Unsur, A. Chowdhury, B. Damiani, Innovative front grid design, four-streets and five-busbars (4S-5BB), for high efficiency industrial Al-BSF silicon solar cell, *IEEE Electron. Device Lett.* 37 (2016) 459–462.
- [42] K. Masuko, M. Shigematsu, T. Hashiguchi, D. Fujishima, M. Kai, N. Yoshimura, T. Yamaguchi, Y. Ichihashi, T. Mishima, N. Matsubara, Achievement of more than 25% conversion efficiency with crystalline silicon heterojunction solar cell, *IEEE Journal of Photovoltaics* 4 (2014) 1433–1435.
- [43] Y. Gassenbauer, K. Ramspeck, B. Bethmann, K. Dressler, J. Moschner, M. Fiedler, E. Brouwer, R. Drößler, N. Lenck, F. Heyer, Rear-surface passivation technology for crystalline silicon solar cells: a versatile process for mass production, *IEEE Journal of Photovoltaics* 3 (2012) 125–130.
- [44] J. Benick, A. Richter, R. Müller, H. Hauser, F. Feldmann, P. Krenckel, S. Riepe, F. Schindler, M. Hermle, High-efficiency n-type HP mc silicon solar cells, *IEEE journal of photovoltaics* 7 (2017) 1171–1175.
- [45] A.-K. Volk, N. Tucher, J. Seiffe, H. Hauser, M. Zimmer, B. Bläsi, M. Hofmann, J. Rentsch, Honeycomb structure on multi-crystalline silicon Al-BSF solar cell with 17.8% efficiency, *IEEE Journal of Photovoltaics* 5 (2015) 1027–1033.
- [46] W. Wang, J. Sheng, S. Yuan, Y. Sheng, W. Cai, Y. Chen, C. Zhang, Z. Feng, P.J. Verlinden, Industrial screen-printed n-type rear-junction solar cells with 20.6% efficiency, *IEEE Journal of Photovoltaics* 5 (2015) 1245–1249.
- [47] U. Jäger, S. Mack, C. Wufka, A. Wolf, D. Biro, R. Preu, Benefit of selective emitters for p-type silicon solar cells with passivated surfaces, *IEEE Journal of Photovoltaics* 3 (2012) 621–627.
- [48] P. Feng, G. Liu, W. Wu, Y. Shi, Q. Wan, Improving the blue response and efficiency of multicrystalline silicon solar cells by surface nanotexturing, *IEEE Electron. Device Lett.* 37 (2016) 306–309.
- [49] R.L. Hoye, K.A. Bush, F. Oviedo, S.E. Sofia, M. Thway, X. Li, Z. Liu, J. Jean, J.P. Mailoa, A. Osherov, Developing a robust recombination contact to realize monolithic perovskite tandems with industrially common P-type silicon solar cells, *IEEE Journal of Photovoltaics* 8 (2018) 1023–1028.
- [50] T. Böscke, D. Kania, C. Schöllhorn, D. Stichtenoth, A. Helbig, P. Sadler, M. Braun, M. Dupke, M. Weiß, A. Grohe, Fully ion implanted and coactivated industrial n-type cells with 20.5% efficiency, *IEEE Journal of Photovoltaics* 4 (2013) 48–51.
- [51] A. Ingenito, S.L. Luxembourg, P. Spinelli, J. Liu, J.C.O. Lizcano, A.W. Weeber, O. Isabella, M. Zeman, Optimized metal-free back reflectors for high-efficiency open rear c-Si solar cells, *IEEE Journal of Photovoltaics* 6 (2015) 34–40.
- [52] R. Gogolin, M. Turcu, R. Ferré, J. Clemens, N.-P. Harder, R. Brendel, J. Schmidt, Analysis of series resistance losses in a-Si: H/c-Si heterojunction solar cells, *IEEE Journal of Photovoltaics* 4 (2014) 1169–1176.
- [53] G. Coletti, Y. Wu, G. Janssen, J. Loffler, B. Van Aken, F. Li, Y. Shen, W. Yang, J. Shi, G. Li, 3% MWT Silicon heterojunction solar cell—a novel heterojunction integrated concept embedding low ag consumption and high module efficiency, *IEEE Journal of Photovoltaics* 5 (2014) 55–60, 2014.
- [54] J. Dong, L. Tao, Y. Zhu, Z. Yang, Z. Xia, R. Sidhu, G. Xing, High-efficiency full back contacted cells using industrial processes, *IEEE Journal of Photovoltaics* 4 (2013) 130–133.
- [55] C. Gong, E. Van Kerschaver, J. Robbelein, T. Janssens, N. Posthuma, J. Poortmans, R. Mertens, Screen-printed aluminum-alloyed \$ Ω emitter on high-efficiency N-type interdigitated back-contact silicon solar cells, *IEEE Electron. Device Lett.* 31 (2010) 576–578.
- [56] L. Sivec, B. Yan, G. Yue, J. Owens-Mawson, J. Yang, S. Guha, Advances in light trapping for hydrogenated nanocrystalline silicon solar cells, *IEEE Journal of Photovoltaics* 3 (2012) 27–34.
- [57] S. Jeong, M.D. McGeehee, Y. Cui, All-back-contact ultra-thin silicon nanocone solar cells with 13.7% power conversion efficiency, *Nat. Commun.* 4 (2013) 2950.
- [58] G.K. Dalapati, S. Masudyan-Panah, A. Kumar, C.C. Tan, H.R. Tan, D. Chi, Aluminium alloyed iron-silicide/silicon solar cells: a simple approach for low cost environmental-friendly photovoltaic technology, *Sci. Rep.* 5 (2015) 17810.
- [59] A.B. Morales-Vilches, A. Cruz, S. Pingel, S. Neubert, L. Mazzarella, D. Meza, L. Korte, R. Schlatmann, B. Stannowski, ITO-free silicon heterojunction solar cells with ZnO: Al/SiO₂ front electrodes reaching a conversion efficiency of 23%, *IEEE Journal of Photovoltaics* 9 (2018) 34–39.
- [60] A. Ingenito, G. Nogay, J. Stuckelberger, P. Wyss, L. Gnocchi, C. Allebé, J. Horzel, M. Despeisse, F.-J. Haug, P. Löper, Phosphorous-doped silicon carbide as front-side full-area passivating contact for double-side contacted c-Si solar cells, *IEEE Journal of Photovoltaics* 9 (2018) 346–354.
- [61] R. Lopez-Delgado, M. Tostado-Plascencia, M.E. Álvarez-Ramos, A. Ayón, Silicon solar cell efficiency improvement employing photoluminescent properties of chlorophyll-A, *Microelectron. Eng.* (2019) 111047.
- [62] C. Geisler, S. Kluska, S. Hopman, J. Giesecke, M. Glatthaar, Passivation-induced cavity defects in laser-doped selective emitter Si solar cells—formation model and recombination analysis, *IEEE Journal of Photovoltaics* 5 (2015) 792–798.
- [63] Z. Qiu, C. Ke, A.G. Aberle, R. Stangl, Efficiency potential of rear heterojunction stripe contacts applied in hybrid silicon wafer solar cells, *IEEE Journal of Photovoltaics* 5 (2015) 1053–1061.
- [64] J. Greulich, T. Fellmeth, M. Glatthaar, D. Biro, S. Rein, Comparison of analytical and numerical models for the optimization of c-si solar cells' front metallization, *IEEE Journal of Photovoltaics* 2 (2012) 588–591.
- [65] S. Fischer, A. Ivaturi, B. Fröhlich, M. Rüdiger, A. Richter, K.W. Krämer, B.S. Richards, J.C. Goldschmidt, Upconverter silicon solar cell devices for efficient utilization of sub-band-gap photons under concentrated solar radiation, *IEEE journal of photovoltaics* 4 (2013) 183–189.
- [66] W. Deng, D. Chen, Z. Xiong, P.J. Verlinden, J. Dong, F. Ye, H. Li, H. Zhu, M. Zhong, Y. Yang, 20.8% PERC solar cell on 156 mm × 156 mm P-type multicrystalline silicon substrate, *IEEE Journal of Photovoltaics* 6 (2015) 3–9.
- [67] A. Pivrikas, H. Neugebauer, N.S. Sariciftci, Charge carrier lifetime and recombination in bulk heterojunction solar cells, *IEEE J. Sel. Top. Quant. Electron.* 16 (2010) 1746–1758.
- [68] M. Padilla, B. Michl, N. Hagedorn, C. Reichel, S. Kluska, A. Fell, M. Kasemann, W. Warta, M.C. Schubert, Local series resistance imaging of silicon solar cells with complex current paths, *IEEE Journal of Photovoltaics* 5 (2015) 752–758.

- [69] Z. Liu, N. Sahraei, B. Hoex, A.G. Aberle, I.M. Peters, Optical modeling of alkaline saw-damage-etched rear surfaces of monocrystalline silicon solar cells, *IEEE Journal of Photovoltaics* 4 (2014) 1436–1444.
- [70] J. Yang, J. Goguen, R. Kleiman, Silicon solar cell with integrated tunnel junction for multijunction photovoltaic applications, *IEEE Electron. Device Lett.* 33 (2012) 1732–1734.
- [71] Y.-W. Ok, A.D. Upadhyaya, Y. Tao, F. Zimbardi, K. Ryu, M.-H. Kang, A. Rohatgi, Ion-implanted and screen-printed large area 20% efficient N-type front junction Si solar cells, *Sol. Energy Mater. Sol. Cell.* 123 (2014) 92–96.
- [72] D. Suwito, U. Jager, J. Benick, S. Janz, M. Hermle, S.W. Glunz, Industrially feasible rear passivation and contacting scheme for high-efficiency n-type solar cells yielding a $\$ V_{oc}$ of 700 mV, *IEEE Trans. Electron. Dev.* 57 (2010) 2032–2036.
- [73] A.W. Blakers, A. Wang, A.M. Milne, J. Zhao, M.A. Green, 22.8% efficient silicon solar cell, *Appl. Phys. Lett.* 55 (1989) 1363–1365.
- [74] R. Preu, S. Glunz, S. Schäfer, R. Lüdemann, W. Wetling, W. Pfleging, Laser ablation—a low-cost approach for passivated rear contact formation in crystalline silicon solar cell technology, in: Proceedings of the 16th European Photovoltaic Solar Energy Conference, 2000, pp. 1181–1184.
- [75] T. Dullweber, J. Schmidt, Industrial silicon solar cells applying the passivated emitter and rear cell (PERC) concept—a review, *IEEE journal of photovoltaics* 6 (2016) 1366–1381.
- [76] G. Du, B. Chen, N. Chen, R. Hu, Efficient boron doping in the back surface field of crystalline silicon solar cells via alloyed-aluminum–boron paste, *IEEE Electron. Device Lett.* 33 (2012) 573–575.
- [77] I. Almansouri, A. Ho-Baillie, S.P. Bremner, M.A. Green, Supercharging silicon solar cell performance by means of multijunction concept, *IEEE Journal of Photovoltaics* 5 (2015) 968–976.
- [78] H. Schulze-Huxel, S. Blankemeyer, R. Bock, A. Merkle, S. Kajari-Schröder, R. Brendel, Al-Foil on encapsulant for the interconnection of Al-metallized silicon solar cells, *IEEE Journal of Photovoltaics* 3 (2012) 77–82.
- [79] M. Rüdiger, H. Steinkeimper, M. Hermle, S.W. Glunz, Numerical current density loss analysis of industrially relevant crystalline silicon solar cell concepts, *IEEE Journal of Photovoltaics* 4 (2014) 533–539.
- [80] S. Kluska, A. Büchler, J. Bartsch, B. Grüberl, A.A. Brand, S. Gutscher, G. Cimotti, J. Nekarda, M. Glatthaar, Easy plating—a simple approach to suppress parasitically metallized areas in front side Ni/Cu plated crystalline Si solar cells, *IEEE Journal of Photovoltaics* 7 (2017) 1270–1277.
- [81] M.D. Lammert, R.J. Schwartz, The interdigitated back contact solar cell: a silicon solar cell for use in concentrated sunlight, *IEEE Trans. Electron. Dev.* 24 (1977) 337–342.
- [82] R.M. Swanson, S.K. Beckwith, R.A. Crane, W. Eades, Y.H. Kwark, R. Sinton, S. Swirhun, Point-contact silicon solar cells, *IEEE Trans. Electron. Dev.* 31 (1984) 661–664.
- [83] Y. Chen, Y. Yang, J.K. Marmon, X. Zhang, Z. Feng, P.J. Verlinden, H. Shen, Independent Al₂O₃/SiNx: H and SiO₂/SiN x: H passivation of p+ and n+ silicon surfaces for high-performance interdigitated back contact solar cells, *IEEE Journal of Photovoltaics* 7 (2016) 51–57.
- [84] D. Hinken, A. Milsted, R. Bock, B. Fischer, K. Bothe, M. Schutze, J. Isenberg, A. Schulze, M. Wagner, Determination of the base-dopant concentration of large-area crystalline silicon solar cells, *IEEE Trans. Electron. Dev.* 57 (2010) 2831–2837.
- [85] J. Wong, S. Duttagupta, R. Stangl, B. Hoex, A.G. Aberle, A systematic loss analysis method for rear-passivated silicon solar cells, *IEEE Journal of Photovoltaics* 5 (2015) 619–626.
- [86] M. Rauer, C. Schmiga, R. Woehl, K. Ruhle, M. Hermle, M. Horteis, D. Biro, S.W. Glunz, Investigation of aluminum-alloyed local contacts for rear surface-passivated silicon solar cells, *IEEE Journal of Photovoltaics* 1 (2011) 22–28.
- [87] R. Lopez-Delgado, Y. Zhou, A. Zazueta-Raynaud, H. Zhao, J. Pelayo, A. Vomiero, M. Álvarez-Ramos, F. Rosei, A. Ayon, Enhanced conversion efficiency in Si solar cells employing photoluminescent down-shifting CdSe/CdS core/shell quantum dots, *Sci. Rep.* 7 (2017) 14104.
- [88] T. Saga, Advances in crystalline silicon solar cell technology for industrial mass production, *NPG Asia Mater.* 2 (2010) 96–102.
- [89] M.M. Furchi, F. Höller, L. Dobusch, D.K. Polyushkin, S. Schuler, T. Mueller, Device physics of van der Waals heterojunction solar cells, *npj 2D Materials and Applications* 2 (2018) 3.
- [90] W. Shockley, The theory of p-n junctions in semiconductors and p-n junction transistors, *Bell System Technical Journal* 28 (1949) 435–489.
- [91] J. Boroumand, S. Das, A. Vázquez-Guardado, D. Franklin, D. Chanda, Unified electromagnetic-electronic design of light trapping silicon solar cells, *Sci. Rep.* 6 (2016) 31013.
- [92] A. Tyagi, K. Ghosh, A. Kottantharayil, S. Lodha, An analytical model for the electrical characteristics of passivated carrier-selective contact (CSC) solar cell, *IEEE Trans. Electron. Dev.* 66 (2019) 1377–1385.
- [93] S. Dhar, C. Banerjee, H. Saha, K. Ghosh, Modeling and analysis of lifetime curve of amorphous silicon/crystalline silicon heterostructure solar cell, *IEEE Trans. Electron. Dev.* 63 (2016) 3996–4002.
- [94] W.-C. Lee, M.-L. Tsai, Y.-L. Chen, W.-C. Tu, Fabrication and analysis of chemically-derived graphene/pyramidal si heterojunction solar cells, *Sci. Rep.* 7 (2017) 46478.
- [95] A. Nandi, S. Mandal, S. Ghosh, S. Dhar, S. Majumdar, H. Saha, S.M. Hossain, Application of hybrid rGO-ITO bilayer TCO on a-Si solar cell for performance enhancement, *IEEE Journal of Photovoltaics* 9 (2018) 12–17.
- [96] X. Lu, Y. Li, S. Lun, X. Wang, J. Gao, Y. Wang, Y. Zhang, High efficiency light trapping scheme used for ultrathin c-Si solar cells, *Sol. Energy Mater. Sol. Cell.* 196 (2019) 57–64.
- [97] M.K. Sahoo, P. Kale, Integration of silicon nanowires in solar cell structure for efficiency enhancement: a review, *Journal of Materomics* 5 (1) (2018) 34–48.
- [98] K. Krauß, A.A. Brand, F. Fertig, S. Rein, J. Nekarda, Fast regeneration processes to avoid light-induced degradation in multicrystalline silicon solar cells, *IEEE Journal of Photovoltaics* 6 (2016) 1427–1431.
- [99] A. Tomasi, B. Paviet-Salomon, Q. Jeangros, J. Haschke, G. Christmann, L. Barraud, A. Descoeuilles, J.P. Seif, S. Nicolay, M. Despeisse, Simple processing of back-contacted silicon heterojunction solar cells using selective-area crystalline growth, *Nature Energy* 2 (2017) 17062.
- [100] H.-J. Syu, S.-C. Shiu, C.-F. Lin, Effect of nanowire length to silicon nanowire/PEDOT: PSS solar cells, in: 2011 37th IEEE Photovoltaic Specialists Conference, IEEE, 2011, 002490-002491.
- [101] M. Dutta, H.T. Bui, N. Fukata, Effect of nanowire length on the performance of silicon nanowires based solar cell, *Adv. Nat. Sci. Nanosci. Nanotechnol.* 5 (2014), 045014.
- [102] L. He, C. Jiang, H. Wang, D. Lai, Simple approach of fabricating high efficiency Si nanowire/conductive polymer hybrid solar cells, *IEEE Electron. Device Lett.* 32 (2011) 1406–1408.
- [103] Z. Ge, L. Xu, Y. Cao, T. Wu, H. Song, Z. Ma, J. Xu, K. Chen, Substantial improvement of short wavelength response in n-SiNW/PEDOT: PSS solar cell, *Nanoscale research letters* 10 (2015) 1–8.
- [104] M. Kulakci, F. Es, B. Ozdemir, H.E. Unalan, R. Turan, Application of Si nanowires fabricated by metal-assisted etching to crystalline Si solar cells, *IEEE Journal of Photovoltaics* 3 (2012) 548–553.
- [105] K.-T. Lee, J.-Y. Jang, J. Zhang, S.-M. Yang, S. Park, H.J. Park, Highly efficient colored perovskite solar cells integrated with ultrathin subwavelength plasmonic nanoresonators, *Sci. Rep.* 7 (2017) 10640.
- [106] H.J. Snaith, Present status and future prospects of perovskite photovoltaics, *Nat. Mater.* 17 (2018) 372.
- [107] M. Stolterfoht, C.M. Wolff, J.A. Márquez, S. Zhang, C.J. Hages, D. Rothhardt, S. Albrecht, P.L. Burn, P. Meredith, T. Unold, Visualization and suppression of interfacial recombination for high-efficiency large-area pin perovskite solar cells, *Nature Energy* 3 (2018) 847.
- [108] M.I. Saidaminov, J. Kim, A. Jain, R. Quintero-Bermudez, H. Tan, G. Long, F. Tan, A. Johnston, Y. Zhao, O. Voznyy, Suppression of atomic vacancies via incorporation of isovalent small ions to increase the stability of halide perovskite solar cells in ambient air, *Nature Energy* 3 (2018) 648.
- [109] M. Kaltenbrunner, G. Adam, E.D. Głowacki, M. Drack, R. Schwödauer, L. Leonat, D.H. Apaydin, H. Groiss, M.C. Scharber, M.S. White, Flexible high power-weight perovskite solar cells with chromium oxide–metal contacts for improved stability in air, *Nat. Mater.* 14 (2015) 1032.
- [110] J.H. Rhee, C.-C. Chung, E.W.-G. Diau, A perspective of mesoscopic solar cells based on metal chalcogenide quantum dots and organometal-halide perovskites, *NPG Asia Mater.* 5 (2013) e68.

- [111] J. Huang, Y. Yuan, Y. Shao, Y. Yan, Understanding the physical properties of hybrid perovskites for photovoltaic applications, *Nature Reviews Materials* 2 (2017) 17042.
- [112] J. Lin, M. Lai, L. Dou, C.S. Kley, H. Chen, F. Peng, J. Sun, D. Lu, S.A. Hawks, C. Xie, Thermochromic halide perovskite solar cells, *Nat. Mater.* 17 (2018) 261.
- [113] Z. Li, T.R. Klein, D.H. Kim, M. Yang, J.J. Berry, M.F. van Hest, K. Zhu, Scalable fabrication of perovskite solar cells, *Nature Reviews Materials* 3 (2018) 18017.
- [114] M. Alsari, A.J. Pearson, J.T.-W. Wang, Z. Wang, A. Montisci, N.C. Greenham, H.J. Snaith, S. Lilliu, R.H. Friend, Degradation kinetics of inverted perovskite solar cells, *Sci. Rep.* 8 (2018) 5977.
- [115] J.M. Ball, A. Petrozzi, Defects in perovskite-halides and their effects in solar cells, *Nature Energy* 1 (2016) 16149.
- [116] S.D. Stranks, H.J. Snaith, Metal-halide perovskites for photovoltaic and light-emitting devices, *Nat. Nanotechnol.* 10 (2015) 391.
- [117] Y. Zhang, Y. Xuan, Comprehensive design of omnidirectional high-performance perovskite solar cells, *Sci. Rep.* 6 (2016) 29705.
- [118] W. Nie, J.-C. Blancon, A.J. Neukirch, K. Appavoo, H. Tsai, M. Chhowalla, M.A. Alam, M.Y. Sfeir, C. Katan, J. Even, Light-activated photocurrent degradation and self-healing in perovskite solar cells, *Nat. Commun.* 7 (2016) 11574.
- [119] C. Liu, M. Hu, X. Zhou, J. Wu, L. Zhang, W. Kong, X. Li, X. Zhao, S. Dai, B. Xu, Efficiency and stability enhancement of perovskite solar cells by introducing CsPbI₃ quantum dots as an interface engineering layer, *NPG Asia Mater.* 10 (2018) 552.
- [120] N. Aristidou, C. Eames, I. Sanchez-Molina, X. Bu, J. Kosco, M.S. Islam, S.A. Haque, Fast oxygen diffusion and iodide defects mediate oxygen-induced degradation of perovskite solar cells, *Nat. Commun.* 8 (2017) 15218.
- [121] N.-G. Park, M. Grätzel, T. Miyasaka, K. Zhu, K. Emery, Towards stable and commercially available perovskite solar cells, *Nature Energy* 1 (2016) 16152.
- [122] K. Li, J. Xiao, X. Yu, T. Li, D. Xiao, J. He, P. Zhou, Y. Zhang, W. Li, Z. Ku, An efficient, flexible perovskite solar module exceeding 8% prepared with an ultrafast PbI₂ deposition rate, *Sci. Rep.* 8 (2018) 442.
- [123] T. Leijtens, G.E. Eperon, S. Pathak, A. Abate, M.M. Lee, H.J. Snaith, Overcoming ultraviolet light instability of sensitized TiO₂ with meso-superstructured organometal tri-halide perovskite solar cells, *Nat. Commun.* 4 (2013) 2885.
- [124] B. Li, Y. Zhang, L. Fu, T. Yu, S. Zhou, L. Zhang, L. Yin, Surface passivation engineering strategy to fully-inorganic cubic CsPbI₃ perovskites for high-performance solar cells, *Nat. Commun.* 9 (2018) 1076.
- [125] S.-W. Lee, S. Kim, S. Bae, K. Cho, T. Chung, L.E. Mundt, S. Lee, S. Park, H. Park, M.C. Schubert, UV degradation and recovery of perovskite solar cells, *Sci. Rep.* 6 (2016) 38150.
- [126] W. Zhang, S. Pathak, N. Sakai, T. Stergiopoulos, P.K. Nayak, N.K. Noel, A.A. Haghighirad, V.M. Burlakov, D.W. DeQuilettes, A. Sadhanala, Enhanced optoelectronic quality of perovskite thin films with hypophosphorous acid for planar heterojunction solar cells, *Nat. Commun.* 6 (2015) 10030.
- [127] Q. Zhao, G. Li, J. Song, Y. Zhao, Y. Qiang, X. Gao, Improving the photovoltaic performance of perovskite solar cells with acetate, *Sci. Rep.* 6 (2016) 38670.
- [128] J.C. Yu, J.A. Hong, E.D. Jung, D.B. Kim, S.-M. Baek, S. Lee, S. Cho, S.S. Park, K.J. Choi, M.H. Song, Highly efficient and stable inverted perovskite solar cell employing PEDOT: GO composite layer as a hole transport layer, *Sci. Rep.* 8 (2018) 1070.
- [129] J. Li, B. Huang, E.N. Esfahani, L. Wei, J. Yao, J. Zhao, W. Chen, Touching is believing: interrogating halide perovskite solar cells at the nanoscale via scanning probe microscopy, *npj Quantum Materials* 2 (2017) 1–7.
- [130] J. Schlipf, A.M. Askar, F. Pantle, B.D. Wiltshire, A. Sura, P. Schneider, L. Huber, K. Shankar, P. Müller-Buschbaum, Top-down approaches towards single crystal perovskite solar cells, *Sci. Rep.* 8 (2018) 4906.
- [131] Z. Wang, Q. Lin, F.P. Chmiel, N. Sakai, L.M. Herz, H.J. Snaith, Efficient ambient-air-stable solar cells with 2D–3D heterostructured butylammonium-caesium-formamidinium lead halide perovskites, *Nature Energy* 2 (2017) 17135.
- [132] H. Wang, Y. Rahaq, V. Kumar, A composite light-harvesting layer from photoactive polymer and halide perovskite for planar heterojunction solar cells, *Sci. Rep.* 6 (2016) 29567.
- [133] H.-W. Chen, T.-Y. Huang, T.-H. Chang, Y. Sanehira, C.-W. Kung, C.-W. Chu, M. Ikegami, T. Miyasaka, K.-C. Ho, Efficiency enhancement of hybrid perovskite solar cells with MEH-PPV hole-transporting layers, *Sci. Rep.* 6 (2016) 34319.
- [134] S.S. Mali, C.S. Shim, C.K. Hong, Highly porous Zinc Stannate (Zn 2 SnO 4) nanofibers scaffold photoelectrodes for efficient methyl ammonium halide perovskite solar cells, *Sci. Rep.* 5 (2015) 11424.
- [135] S. Albrecht, B. Rech, Perovskite solar cells: on top of commercial photovoltaics, *Nature Energy* 2 (2017) 16196.
- [136] K. Tvingstedt, O. Malinkiewicz, A. Baumann, C. Deibel, H.J. Snaith, V. Dyakonov, H.J. Bolink, Radiative efficiency of lead iodide based perovskite solar cells, *Sci. Rep.* 4 (2014) 6071.
- [137] G. Zhao, Q. Cai, X. Liu, P. Li, Y. Zhang, G. Shao, C. Liang, PbS QDs as electron blocking layer toward efficient and stable perovskite solar cells, *IEEE Journal of Photovoltaics* 9 (2018) 194–199.
- [138] S. Sanders, D. Stümmel, P. Pfeiffer, N. Ackermann, G. Simkus, M. Heukens, P. Baumann, A. Vescan, H. Kalisch, Chemical vapor deposition of organic-inorganic bismuth-based Perovskite films for solar cell application, *Sci. Rep.* 9 (2019) 1–8.
- [139] W. Tress, K. Domanski, B. Carlsen, A. Agarwalla, E.A. Alharbi, M. Graetzel, A. Hagfeldt, Performance of perovskite solar cells under simulated temperature-illumination real-world operating conditions, *Nature Energy* (2019) 1.
- [140] C. Cai, K. Zhou, H. Guo, Y. Pei, Z. Hu, J. Zhang, Y. Zhu, Enhanced hole extraction by NiO nanoparticles in carbon-based perovskite solar cells, *Electrochim. Acta* 312 (2019) 100–108.
- [141] K. Wang, L. Zheng, T. Zhu, X. Yao, C. Yi, X. Zhang, Y. Cao, L. Liu, W. Hu, X. Gong, Efficient perovskite solar cells by hybrid perovskites incorporated with heterovalent neodymium cations, *Nanomater. Energy* 61 (2019) 352–360.
- [142] A. Solanki, P. Yadav, S.-H. Turren-Cruz, S.S. Lim, M. Saliba, T.C. Sum, Cation influence on carrier dynamics in perovskite solar cells, *Nanomater. Energy* 58 (2019) 604–611.
- [143] G. Niu, X. Guo, L. Wang, Review of recent progress in chemical stability of perovskite solar cells, *J. Mater. Chem. 3* (2015) 8970–8980.
- [144] C.-C. Chueh, C.-Z. Li, A.K.-Y. Jen, Recent progress and perspective in solution-processed interfacial materials for efficient and stable polymer and organometal perovskite solar cells, *Energy Environ. Sci.* 8 (2015) 1160–1189.
- [145] J. Cui, H. Yuan, J. Li, X. Xu, Y. Shen, H. Lin, M. Wang, Recent progress in efficient hybrid lead halide perovskite solar cells, *Sci. Technol. Adv. Mater.* 16 (2015), 036004.
- [146] A. Chilvery, S. Das, P. Guggilla, C. Brantley, A. Sunda-Meya, A perspective on the recent progress in solution-processed methods for highly efficient perovskite solar cells, *Sci. Technol. Adv. Mater.* 17 (2016) 650–658.
- [147] X. Qin, Z. Zhao, Y. Wang, J. Wu, Q. Jiang, J. You, Recent progress in stability of perovskite solar cells, *J. Semiconduct.* 38 (2017), 011002.
- [148] M.K. Assadi, S. Bakhoda, R. Saidur, H. Hanafi, Recent progress in perovskite solar cells, *Renew. Sustain. Energy Rev.* 81 (2018) 2812–2822.
- [149] W.-Q. Wu, D. Chen, R.A. Caruso, Y.-B. Cheng, Recent progress in hybrid perovskite solar cells based on n-type materials, *J. Mater. Chem. 5* (2017) 10092–10109.
- [150] S. Yun, X. Zhou, J. Even, A. Hagfeldt, Recent Progress of First Principles Calculations in CH₃NH₃PbI₃ Perovskite Solar Cells, 2017.
- [151] U. Mehmood, A. Al-Ahmed, M. Afzaal, F.A. Al-Sulaiman, M. Daud, Recent progress and remaining challenges in organometallic halides based perovskite solar cells, *Renew. Sustain. Energy Rev.* 78 (2017) 1–14.
- [152] Q. Zhang, H. Ting, S. Wei, D. Huang, C. Wu, W. Sun, B. Qu, S. Wang, Z. Chen, L. Xiao, Recent progress in lead-free perovskite (-like) solar cells, *Materials today energy* 8 (2018) 157–165.
- [153] M. Becker, M. Wark, Recent progress in the solution-based sequential deposition of planar perovskite solar cells, *Cryst. Growth Des.* 18 (2018) 4790–4806.
- [154] A.A. Said, J. Xie, Q. Zhang, Recent progress in organic electron transport materials in inverted perovskite solar cells, *Small* (2019) 1900854.
- [155] Y. Zhao, Q. Ye, Z. Chu, F. Gao, X. Zhang, J. You, Recent progress in high-efficiency planar-structure perovskite solar cells, *Energy & Environmental Materials* 2 (2019) 93–106.
- [156] B. Gil, A.J. Yun, Y. Lee, J. Kim, B. Lee, B. Park, Recent progress in inorganic hole transport materials for efficient and stable perovskite solar cells, *Electronic Materials Letters* (2019) 1–20.

- [157] W. Deng, Z. Yuan, S. Liu, Z. Yang, J. Li, E. Wang, X. Wang, J. Li, Plasmonic enhancement for high-efficiency planar heterojunction perovskite solar cells, *J. Power Sources* 432 (2019) 112–118.
- [158] D. Zhao, Y. Yu, C. Wang, W. Liao, N. Shrestha, C.R. Grice, A.J. Cimaroni, L. Guan, R.J. Ellingson, K. Zhu, Low-bandgap mixed tin-lead iodide perovskite absorbers with long carrier lifetimes for all-perovskite tandem solar cells, *Nature Energy* 2 (2017) 17018.
- [159] P. Docampo, J.M. Ball, M. Darwich, G.E. Eperon, H.J. Snaith, Efficient organometal trihalide perovskite planar-heterojunction solar cells on flexible polymer substrates, *Nat. Commun.* 4 (2013) 2761.
- [160] Q. Lin, A. Armin, R.C.R. Nagiri, P.L. Burn, P. Meredith, Electro-optics of perovskite solar cells, *Nat. Photon.* 9 (2015) 106.
- [161] M. Liu, M.B. Johnston, H.J. Snaith, Efficient planar heterojunction perovskite solar cells by vapour deposition, *Nature* 501 (2013) 395.
- [162] V.W. Bergmann, S.A. Weber, F.J. Ramos, M.K. Nazeeruddin, M. Grätzel, D. Li, A.L. Domanski, I. Lieberwirth, S. Ahmad, R. Berger, Real-space observation of unbalanced charge distribution inside a perovskite-sensitized solar cell, *Nat. Commun.* 5 (2014) 5001.
- [163] J.H. Heo, S.H. Im, J.H. Noh, T.N. Mandal, C.-S. Lim, J.A. Chang, Y.H. Lee, H.-j. Kim, A. Sarkar, M.K. Nazeeruddin, Efficient inorganic–organic hybrid heterojunction solar cells containing perovskite compound and polymeric hole conductors, *Nat. Photon.* 7 (2013) 486.
- [164] Y. Li, J.K. Cooper, W. Liu, C.M. Sutter-Fella, M. Amani, J.W. Beeman, A. Javey, J.W. Ager, Y. Liu, F.M. Toma, Defective TiO₂ with high photoconductive gain for efficient and stable planar heterojunction perovskite solar cells, *Nat. Commun.* 7 (2016) 12446.
- [165] C.-S. Jiang, M. Yang, Y. Zhou, B. To, S.U. Nanayakkara, J.M. Luther, W. Zhou, J.J. Berry, J. Van De Lagemaat, N.P. Padture, Carrier separation and transport in perovskite solar cells studied by nanometre-scale profiling of electrical potential, *Nat. Commun.* 6 (2015) 8397.
- [166] L.E. Mundt, W. Kwapisil, M.A. Yakoob, J.P. Herterich, M. Kohlstädt, U. Würfel, M.C. Schubert, S.W. Glunz, Quantitative local loss analysis of blade-coated perovskite solar cells, *IEEE Journal of Photovoltaics* 9 (2019) 452–459.
- [167] S. Bai, P. Da, C. Li, Z. Wang, Z. Yuan, F. Fu, M. Kawecki, X. Liu, N. Sakai, J.T.-W. Wang, Planar perovskite solar cells with long-term stability using ionic liquid additives, *Nature* 571 (2019) 245–250.
- [168] K. Yang, K. Huang, X. Li, S. Zheng, P. Hou, J. Wang, H. Guo, H. Song, B. Li, H. Li, Radiation tolerance of perovskite solar cells under gamma ray, *Org. Electron.* 71 (2019) 79–84.
- [169] S. Luo, W.A. Daoud, Recent progress in organic–inorganic halide perovskite solar cells: mechanisms and material design, *J. Mater. Chem. 3* (2015) 8992–9010.
- [170] A. Gagliardi, S. Mastrianni, D. Gentilini, F. Giordano, A. Reale, T.M. Brown, A. Di Carlo, Multiscale modeling of dye solar cells and comparison with experimental data, *IEEE J. Sel. Top. Quant. Electron.* 16 (2010) 1611–1618.
- [171] A.L. Cost, High-efficiency solar cell based on dye-sensitized colloidal TiO₂ film, brian O'Reagan and michael Grätzel, *Nature* 353 (1991) 737–746.
- [172] J.-C. Chou, C.-M. Chu, Y.-H. Liao, C.-H. Huang, Y.-J. Lin, H. Wu, Y.-H. Nien, Fabrication and photovoltaic properties of dye-sensitized solar cells modified by graphene oxide and magnetic bead, *IEEE Electron. Device Lett.* 36 (2015) 711–713.
- [173] I.K. Popoola, M.A. Gondal, J.M. AlGhamdi, T.F. Qahtan, Photofabrication of highly transparent platinum counter electrodes at ambient temperature for bifacial dye sensitized solar cells, *Sci. Rep.* 8 (2018) 12864.
- [174] M. Freitag, J. Teuscher, Y. Saygili, X. Zhang, F. Giordano, P. Liska, J. Hua, S.M. Zakeeruddin, J.-E. Moser, M. Grätzel, Dye-sensitized solar cells for efficient power generation under ambient lighting, *Nat. Photon.* 11 (2017) 372.
- [175] T. Hosseini, I. Flores-Vivian, K. Sobolev, N. Kouklin, Concrete embedded dye-synthesized photovoltaic solar cell, *Sci. Rep.* 3 (2013) 2727.
- [176] B.E. Hardin, H.J. Snaith, M.D. McGehee, The renaissance of dye-sensitized solar cells, *Nat. Photon.* 6 (2012) 162.
- [177] M.J. Yun, Y.H. Sim, S.I. Cha, S.H. Seo, D.Y. Lee, High energy conversion efficiency with 3-D micro-patterned photoanode for enhancement diffusivity and modification of photon distribution in dye-sensitized solar cells, *Sci. Rep.* 7 (2017) 15027.
- [178] M.J. Yun, S.I. Cha, H.S. Kim, S.H. Seo, D.Y. Lee, Monolithic-structured single-layered textile-based dye-sensitized solar cells, *Sci. Rep.* 6 (2016) 34249.
- [179] S. Kar, J.K. Roy, J. Leszczynski, In silico designing of power conversion efficient organic lead dyes for solar cells using todays innovative approaches to assure renewable energy for future, *NPJ Computational Materials* 3 (2017) 22.
- [180] M. Klein, R. Pankiewicz, M. Zalas, W. Stampor, Magnetic field effects in dye-sensitized solar cells controlled by different cell architecture, *Sci. Rep.* 6 (2016) 30077.
- [181] S. Ito, S.M. Zakeeruddin, P. Comte, P. Liska, D. Kuang, M. Grätzel, Bifacial dye-sensitized solar cells based on an ionic liquid electrolyte, *Nat. Photon.* 2 (2008) 693.
- [182] Y. Cao, Y. Saygili, A. Ummadisingu, J. Teuscher, J. Luo, N. Pellet, F. Giordano, S.M. Zakeeruddin, J.-E. Moser, M. Freitag, 11% efficiency solid-state dye-sensitized solar cells with copper (II/I) hole transport materials, *Nat. Commun.* 8 (2017) 15390.
- [183] W. Ghann, H. Kang, T. Sheikh, S. Yadav, T. Chavez-Gil, F. Nesbitt, J. Uddin, Fabrication, optimization and characterization of natural dye sensitized solar cell, *Sci. Rep.* 7 (2017) 41470.
- [184] J. Dutta, V.K. Rai, M.M. Durai, R. Thangavel, Development of Y2O3: Ho³⁺/Yb³⁺ upconverting nanophosphors for enhancing solar cell efficiency of dye-sensitized solar cells, *IEEE Journal of Photovoltaics* 9 (4) (2019) 1040–1045.
- [185] J.-C. Chou, C.-C. Ko, P.-Y. Kuo, C.-H. Lai, Y.-H. Nien, J.-X. Chang, Fabrication of dye-sensitized solar cells using Zinc oxide nanorod-modified titanium dioxide photoanode, *IEEE Trans. Nanotechnol.* 18 (2019) 553–561.
- [186] J.-C. Chou, C.-C. Lu, Y.-H. Liao, C.-H. Lai, Y.-H. Nien, C.-H. Kuo, C.-C. Ko, Fabrication and electrochemical impedance analysis of dye-sensitized solar cells with titanium dioxide compact layer and graphene oxide dye absorption layer, *IEEE Trans. Nanotechnol.* 18 (2019) 461–466.
- [187] V.A.E.B. Nehme, M.A.E.B. Nehme, T.H. Ghaddar, New pyridyl-based dyes for co-sensitization in dye sensitized solar cells, *Sol. Energy* 187 (2019) 108–114.
- [188] M. Motlak, N.A. Barakat, M.S. Akhtar, A.G. El-Deen, M. Obaid, C.S. Kim, K.A. Khalil, A.A. Almajid, High-efficiency dye-sensitized solar cells based on nitrogen and graphene oxide co-incorporated TiO₂ nanofibers photoelectrode, *Chem. Eng. J.* 268 (2015) 153–161.
- [189] X. Luan, L. Chen, J. Zhang, G. Qu, J.C. Flake, Y. Wang, Electrophoretic deposition of reduced graphene oxide nanosheets on TiO₂ nanotube arrays for dye-sensitized solar cells, *Electrochim. Acta* 111 (2013) 216–222.
- [190] F.A.S. Lima, I.F. Vasconcelos, M. Lira-Cantú, Electrochemically synthesized mesoporous thin films of ZnO for highly efficient dye sensitized solar cells, *Ceram. Int.* 41 (2015) 9314–9320.
- [191] W. Liu, S. He, T. Yang, Y. Feng, G. Qian, J. Xu, S. Miao, TEOS-assisted synthesis of porous MoS₂ with ultra-small exfoliated sheets and applications in dye-sensitized solar cells, *Appl. Surf. Sci.* 313 (2014) 498–503.
- [192] C.-Y. Chen, M. Wang, J.-Y. Li, N. Pootrakulchote, L. Alibabaei, C.-h. Ngoc-le, J.-D. Decoppet, J.-H. Tsai, C. Grätzel, C.-G. Wu, Highly efficient light-harvesting ruthenium sensitizer for thin-film dye-sensitized solar cells, *ACS Nano* 3 (2009) 3103–3109.
- [193] A. Yella, H.-W. Lee, H.N. Tsao, C. Yi, A.K. Chandiran, M.K. Nazeeruddin, E.W.-G. Diau, C.-Y. Yeh, S.M. Zakeeruddin, M. Grätzel, Porphyrin-sensitized solar cells with cobalt (II/III)-based redox electrolyte exceed 12 percent efficiency, *Science* 334 (2011) 629–634.
- [194] J. Burschka, A. Dualeh, F. Kessler, E. Baranoff, N.-L. Cevey-Ha, C. Yi, M.K. Nazeeruddin, M. Grätzel, Tris (2-(1-H-pyrazol-1-yl) pyridine) cobalt (III) as p-type dopant for organic semiconductors and its application in highly efficient solid-state dye-sensitized solar cells, *J. Am. Chem. Soc.* 133 (2011) 18042–18045.
- [195] S. Mathew, A. Yella, P. Gao, R. Humphry-Baker, B.F. Curchod, N. Ashari-Astani, I. Tavernelli, U. Rothlisberger, M.K. Nazeeruddin, M. Grätzel, Dye-sensitized solar cells with 13% efficiency achieved through the molecular engineering of porphyrin sensitizers, *Nat. Chem.* 6 (2014) 242–247.
- [196] V. Lojpur, I.L. Validžić, Influence of different light sources, light intensities, and water flow lens (WFL) system on dye-sensitized solar cell performances, *IEEE Journal of Photovoltaics* 9 (2018) 492–498.
- [197] D. Bari, A. Cester, N. Wrachien, L. Ciamparuchi, T.M. Brown, A. Reale, A. Di Carlo, G. Meneghesso, Reliability study of ruthenium-based dye-sensitized solar cells (DSCs), *IEEE Journal of Photovoltaics* 2 (2012) 27–34.
- [198] J.R. González, I. Rey-Stolle, C. Algorta, B. Galiana, Microplasma breakdown in high-concentration III-V solar cells, *IEEE Electron. Device Lett.* 26 (2005) 867–869.
- [199] P. Iles, Y.-C. Yeh, F. Ho, C.-L. Chu, C. Cheng, High-efficiency (> 20% AM0) GaAs solar cells grown on inactive-Ge substrates, *IEEE Electron. Device Lett.* 11 (1990) 140–142.

- [200] F. Dimroth, T.N. Tibbits, M. Niemeyer, F. Predan, P. Beutel, C. Karcher, E. Oliva, G. Siefer, D. Lackner, P. Fuß-Kailuweit, Four-junction wafer-bonded concentrator solar cells, *IEEE Journal of Photovoltaics* 6 (2015) 343–349.
- [201] J.-L. Hou, C.-H. Wu, S.-J. Chang, Electrochromic device integrated with gainp/gaas/ge triple-junction solar cell, *IEEE Electron. Device Lett.* 36 (2014) 207–209.
- [202] T.W. Kim, Y. Kim, K. Kim, J.J. Lee, T. Kuech, L.J. Mawst, 1.25-eV GaAsSbN/Ge double-junction solar cell grown by metalorganic vapor phase epitaxy for high efficiency multijunction solar cell application, *IEEE Journal of Photovoltaics* 4 (2014) 981–985.
- [203] J.-P. Shim, S.-R. Jeon, Y.-K. Jeong, D.-S. Lee, Improved efficiency by using transparent contact layers in InGaN-based pin solar cells, *IEEE Electron. Device Lett.* 31 (2010) 1140–1142.
- [204] K. Derendorf, S. Essig, E. Oliva, V. Klinger, T. Roesener, S.P. Philipps, J. Benick, M. Hermle, M. Schachtner, G. Siefer, Fabrication of GaInP/GaAs//Si solar cells by surface activated direct wafer bonding, *IEEE Journal of Photovoltaics* 3 (2013) 1423–1428.
- [205] Z. Bi, J. Zhang, L. Lv, Y. Hao, The effect of 3-MeV proton irradiation on the performance of InGaN/GaN MQWs solar cells, *IEEE Photon. Technol. Lett.* 26 (2014) 1492–1494.
- [206] S.-w. Zeng, X.-m. Cai, B.-p. Zhang, Demonstration and study of photovoltaic performances of InGaN pin homojunction solar cells, *IEEE J. Quant. Electron.* 46 (2010) 783–787.
- [207] M. Lueck, C. Andre, A. Pitera, M.L. Lee, E. Fitzgerald, S. Ringel, Dual junction GaInP/GaAs solar cells grown on metamorphic SiGe/Si substrates with high open circuit voltage, *IEEE Electron. Device Lett.* 27 (2006) 142–144.
- [208] D. Shahjerdi, B. Hekmatshoar, D.K. Sadana, Low-temperature a-Si: H/GaAs heterojunction solar cells, *IEEE Journal of Photovoltaics* 1 (2011) 104–107.
- [209] F. Dimroth, T. Roesener, S. Essig, C. Weuffen, A. Wekkeli, E. Oliva, G. Siefer, K. Volz, T. Hannappel, D. Häussler, Comparison of direct growth and wafer bonding for the fabrication of GaInP/GaAs dual-junction solar cells on silicon, *IEEE Journal of Photovoltaics* 4 (2014) 620–625.
- [210] W.-C. Yang, C. Lo, C.-Y. Wei, W.-S. Lou, Cell-temperature determination in InGaP-(In) GaAs–Ge triple-junction solar cells, *IEEE Electron. Device Lett.* 32 (2011) 1412–1414.
- [211] B.W. Liou, In $_x$ \$ Ga $_{1-x}$ \$ N–GaN-Based solar cells with a multiple-quantum-well structure on SiCN–Si (111) substrates, *IEEE Photon. Technol. Lett.* 22 (2010) 215–217.
- [212] J.-K. Sheu, C.-C. Yang, S.-J. Tu, K.-H. Chang, M.-L. Lee, W.-C. Lai, L.-C. Peng, Demonstration of GaN-based solar cells with GaN/InGaN superlattice absorption layers, *IEEE Electron. Device Lett.* 30 (2009) 225–227.
- [213] B.R. Jampana, A.G. Melton, M. Jamil, N.N. Faleev, R.L. Opila, I.T. Ferguson, C.B. Honsberg, Design and realization of wide-band-gap (\$ \sim \$2.67 eV) InGaN pn junction solar cell, *IEEE Electron. Device Lett.* 31 (2009) 32–34.
- [214] M.-C. Tseng, R.-H. Horng, Y.-L. Tsai, D.-S. Wuu, H.-H. Yu, Fabrication and characterization of GaAs solar cells on copper substrates, *IEEE Electron. Device Lett.* 30 (2009) 940–942.
- [215] R. Cariou, J. Benick, P. Beutel, N. Razek, C. Flötgen, M. Hermle, D. Lackner, S.W. Glunz, A.W. Bett, M. Wimplinger, Monolithic two-terminal III–V//Si triple-junction solar cells with 30.2% efficiency under 1-Sun AM1.5G, *IEEE Journal of Photovoltaics* 7 (2016) 367–373.
- [216] I. Garcia, R.M. France, J.F. Geisz, W.E. McMahon, M.A. Steiner, S. Johnston, D.J. Friedman, Metamorphic III–V solar cells: recent progress and potential, *IEEE Journal of Photovoltaics* 6 (2015) 366–373.
- [217] M. Feifel, J. Ohlmann, J. Benick, T. Rachow, S. Janz, M. Hermle, F. Dimroth, J. Belz, A. Beyer, K. Volz, MOVPE grown gallium phosphide–silicon heterojunction solar cells, *IEEE Journal of Photovoltaics* 7 (2017) 502–507.
- [218] D.J. Farrell, H. Sodabani, Y. Wang, M. Sugiyama, Y. Okada, A hot-electron thermophotonic solar cell demonstrated by thermal up-conversion of sub-bandgap photons, *Nat. Commun.* 6 (2015) 8685.
- [219] D.-T. Nguyen, L. Lombez, F. Gibelli, S. Boyer-Richard, A. Le Corre, O. Durand, J.-F. Guillemoles, Quantitative experimental assessment of hot carrier-enhanced solar cells at room temperature, *Nature Energy* 3 (2018) 236.
- [220] S. Essig, C. Allebé, T. Remo, J.F. Geisz, M.A. Steiner, K. Horowitz, L. Barraud, J.S. Ward, M. Schnabel, A. Descoeuadres, Raising the one-sun conversion efficiency of III–V//Si solar cells to 32.8% for two junctions and 35.9% for three junctions, *Nature Energy* 2 (2017) 17144.
- [221] Y.-C. Kao, H.-M. Chou, S.-C. Hsu, A. Lin, C.-C. Lin, Z.-H. Shih, C.-L. Chang, H.-F. Hong, R.-H. Horng, Performance comparison of III–V//Si and III–V//InGaAs multi-junction solar cells fabricated by the combination of mechanical stacking and wire bonding, *Sci. Rep.* 9 (2019) 4308.
- [222] P. Krogsstrup, H.I. Jørgensen, M. Heiss, O. Demichel, J.V. Holm, M. Aagesen, J. Nygård, A.F. i Morral, Single-nanowire solar cells beyond the Shockley–Queisser limit, *Nat. Photon.* 7 (2013) 306.
- [223] T.-N. Lin, S.R.M.S. Santiago, J.-A. Zheng, Y.-C. Chao, C.-T. Yuan, J.-L. Shen, C.-H. Wu, C.-A.J. Lin, W.-R. Liu, M.-C. Cheng, Enhanced conversion efficiency of III–V triple-junction solar cells with graphene quantum dots, *Sci. Rep.* 6 (2016) 39163.
- [224] G. Siddharth, V. Garg, B.S. Sengar, R. Bhardwaj, P. Kumar, S. Mukherjee, Analytical study of performance parameters of InGaN/GaN multiple quantum well solar cell, *IEEE Trans. Electron. Dev.* 66 (2019) 3399–3404.
- [225] S. Eyderman, S. John, Light-trapping and recycling for extraordinary power conversion in ultra-thin gallium-arsenide solar cells, *Sci. Rep.* 6 (2016) 28303.
- [226] C.-H. Hsu, E.Y. Chang, H.-J. Chang, H.-W. Yu, H.Q. Nguyen, C.-C. Chung, J.-S. Maa, K. Pande, Gold-free fully Cu-metallized InGaP/InGaAs/Ge triple-junction solar cells, *IEEE Electron. Device Lett.* 35 (2014) 1275–1277.
- [227] D. Martín-Martín, E. García-Tarabés, I. Rey-Stolle, Assessment of rear-surface processing strategies for III–V on Si multijunction solar cells based on numerical simulations, *IEEE Trans. Electron. Dev.* 63 (2015) 252–258.
- [228] L.-K. Yeh, W.-C. Tian, K.-Y. Lai, J.-H. He, Exceptionally omnidirectional broadband light harvesting scheme for multi-junction concentrator solar cells achieved via ZnO nanoneedles, *Sci. Rep.* 6 (2016) 39134.
- [229] I. Sayed, S. Bedair, Quantum well solar cells: principles, recent progress, and potential, *IEEE Journal of Photovoltaics* 9 (2019) 402–423.
- [230] N. Miyashita, Y. He, T. Agui, H. Juso, T. Takamoto, Y. Okada, Inverted lattice-matched triple junction solar cells with 1.0 eV GaInNAsSb subcell by MOCVD/MBE hybrid growth, *IEEE Journal of Photovoltaics* 9 (2019) 666–672.
- [231] I.K. Popoola, M.A. Gondal, T.F. Qahtan, Recent progress in flexible perovskite solar cells: materials, mechanical tolerance and stability, *Renew. Sustain. Energy Rev.* 82 (2018) 3127–3151.
- [232] H.-G. Im, S. Jeong, J. Jin, J. Lee, D.-Y. Youn, W.-T. Koo, S.-B. Kang, H.-J. Kim, J. Jang, D. Lee, Hybrid crystalline-ITO/metal nanowire mesh transparent electrodes and their application for highly flexible perovskite solar cells, *NPG Asia Mater.* 8 (2016) e282.
- [233] T. Akama, W. Okita, R. Nagai, C. Li, T. Kaneko, T. Kato, Schottky solar cell using few-layered transition metal dichalcogenides toward large-scale fabrication of semitransparent and flexible power generator, *Sci. Rep.* 7 (2017) 11967.
- [234] G. Dennler, N.S. Sariciftci, Flexible conjugated polymer-based plastic solar cells: from basics to applications, *Proc. IEEE* 93 (2005) 1429–1439.
- [235] H. Kim, D. Xu, C. John, Y. Wu, Modeling thermo-mechanical stress of flexible CIGS solar cells, *IEEE Journal of Photovoltaics* 9 (2019) 499–505.
- [236] B. Louis, Investigation and Development of CIGS Solar Cells on Flexible Substrates and with Alternative Electrical Back Contacts Presented by, ETH Zurich (Doctor of Sciences Thesis), 2009.
- [237] S.-Y. Park, E.-W. Lee, S.-H. Lee, S.-W. Park, W.K. Kim, S.H. Lee, W.-G. Lee, B.J. Lee, H.K. Bae, J.H. Yoo, Investigation of ZnO/CdS/CuInxGa1 – xSe2 interface reaction by using hot-stage TEM, *Curr. Appl. Phys.* 10 (2010) S399–S401.
- [238] C.R. Brown, V.R. Whiteside, D. Poplavskyy, K. Hossain, M.S. Dhoubhadel, I.R. Sellers, Flexible Cu (in, Ga) Se $_{2}$ \$ solar cells for outer planetary missions: investigation under low-intensity low-temperature conditions, *IEEE Journal of Photovoltaics* 9 (2019) 552–558.
- [239] H. Lu, J. Luo, Y. Liu, Y. Zhong, J. Wang, Y. Zhang, Highly performance flexible polymer solar cells by flipping the bilayer film of Ag nanowires and polyvinyl alcohol on polyethylene terephthalate as transparent conductive electrodes, *IEEE Journal of Photovoltaics* 9 (2019) 710–714.
- [240] K.-J. Yang, S. Kim, S.-Y. Kim, K. Ahn, D.-H. Son, S.-H. Kim, S.-J. Lee, Y.-I. Kim, S.-N. Park, S.-J. Sung, Flexible Cu 2 ZnSn (S, Se) 4 solar cells with over 10% efficiency and methods of enlarging the cell area, *Nat. Commun.* 10 (2019) 2959.
- [241] L.E. Mundt, F.D. Heinz, S. Albrecht, M. Mundus, M. Saliba, J.P. Correa-Baena, E.H. Anaraki, L. Korte, M. Grätzel, A. Hagfeldt, Nondestructive probing of perovskite silicon tandem solar cells using multiwavelength photoluminescence mapping, *IEEE Journal of Photovoltaics* 7 (2017) 1081–1086.

- [242] J.Y. Zhengshan, K.C. Fisher, B.M. Wheelwright, R.P. Angel, Z.C. Holman, PVMirror: a new concept for tandem solar cells and hybrid solar converters, *IEEE Journal of Photovoltaics* 5 (2015) 1791–1799.
- [243] T.P. White, N.N. Lal, K.R. Catchpole, Tandem solar cells based on high-efficiency c-Si bottom cells: top cell requirements for > 30% efficiency, *IEEE Journal of Photovoltaics* 4 (2013) 208–214.
- [244] L. Wang, M. Diaz, B. Conrad, X. Zhao, D. Li, A. Soeriyadi, A. Gerger, A. Lochtefeld, C. Ebert, I. Perez-Wurfl, Material and device improvement of GaAsP top solar cells for GaAsP/SiGe tandem solar cells grown on Si substrates, *IEEE Journal of Photovoltaics* 5 (2015) 1800–1804.
- [245] S. Pattnaiak, T. Xiao, R. Shinar, J. Shinar, V. Dalal, Novel hybrid amorphous/organic tandem junction solar cell, *IEEE Journal of Photovoltaics* 3 (2012) 295–299.
- [246] T. Kim, J.H. Jeon, S. Han, D.-K. Lee, H. Kim, W. Lee, K. Kim, Organic-inorganic hybrid tandem multijunction photovoltaics with extended spectral response, *Appl. Phys. Lett.* 98 (2011) 183503.
- [247] A. Singh, A. Gagliardi, Efficiency of all-perovskite two-terminal tandem solar cells: a drift-diffusion study, *Sol. Energy* 187 (2019) 39–46.
- [248] K.L. Schulthe, M.A. Steiner, M.R. Young, J.F. Geisz, Internal resistive barriers related to Zinc diffusion during the growth of inverted metamorphic multijunction solar cells, *IEEE Journal of Photovoltaics* 9 (2018) 167–173.
- [249] D.M. Tex, T. Nakamura, M. Imaizumi, T. Ohshima, Y. Kanemitsu, Direct evaluation of influence of electron damage on the subcell performance in triple-junction solar cells using photoluminescence decays, *Sci. Rep.* 7 (2017) 1985.
- [250] J. You, L. Dou, K. Yoshimura, T. Kato, K. Ohya, T. Moriarty, K. Emery, C.-C. Chen, J. Gao, G. Li, A polymer tandem solar cell with 10.6% power conversion efficiency, *Nat. Commun.* 4 (2013) 1446.
- [251] T. Kim, H. Kim, J. Park, H. Kim, Y. Yoon, S.-M. Kim, C. Shin, H. Jung, I. Kim, D.S. Jeong, Triple-junction hybrid tandem solar cells with amorphous silicon and polymer-fullerene blends, *Sci. Rep.* 4 (2014) 7154.
- [252] W.J. Da Silva, F.K. Schneider, A.R. bin Mohd Yusoff, J. Jang, High performance polymer tandem solar cell, *Sci. Rep.* 5 (2015) 18090.
- [253] M. Trahms, M. Jošt, C.T. Trinh, N. Preissler, S. Albrecht, R. Schlättermann, B. Rech, D. Amkreutz, All-thin-film tandem cells based on liquid phase crystallized silicon and perovskites, *IEEE Journal of Photovoltaics* 9 (2019) 621–628.
- [254] N. Valdes, J. Lee, W. Shafarman, Comparison of Ag and Ga alloying in low bandgap CuInSe₂-based solar cells, *Sol. Energy Mater. Sol. Cell.* 195 (2019) 155–159.
- [255] S. Chen, L. Zhu, M. Yoshita, T. Mochizuki, C. Kim, H. Akiyama, M. Imaizumi, Y. Kanemitsu, Thorough subcells diagnosis in a multi-junction solar cell via absolute electroluminescence-efficiency measurements, *Sci. Rep.* 5 (2015) 7836.
- [256] A. Hadipour, B. de Boer, J. Wildeman, F.B. Kooistra, J.C. Hummelen, M.G. Turbiez, M.M. Wienk, R.A. Janssen, P.W. Blom, Solution-processed organic tandem solar cells, *Adv. Funct. Mater.* 16 (2006) 1897–1903.
- [257] J.Y. Kim, K. Lee, N.E. Coates, D. Moses, T.-Q. Nguyen, M. Dante, A.J. Heeger, Efficient tandem polymer solar cells fabricated by all-solution processing, *Science* 317 (2007) 222–225.
- [258] J. Yang, R. Zhu, Z. Hong, Y. He, A. Kumar, Y. Li, Y. Yang, A robust inter-connecting layer for achieving high performance tandem polymer solar cells, *Adv. Mater.* 23 (2011) 3465–3470.
- [259] W. Li, A. Furlan, K.H. Hendriks, M.M. Wienk, R.A. Janssen, Efficient tandem and triple-junction polymer solar cells, *J. Am. Chem. Soc.* 135 (2013) 5529–5532.
- [260] C.H. Chou, W.L. Kwan, Z. Hong, L.M. Chen, Y. Yang, A metal-oxide interconnection layer for polymer tandem solar cells with an inverted architecture, *Adv. Mater.* 23 (2011) 1282–1286.
- [261] W. Liu, S. Li, J. Huang, S. Yang, J. Chen, L. Zuo, M. Shi, X. Zhan, C.Z. Li, H. Chen, Nonfullerene tandem organic solar cells with high open-circuit voltage of 1.97 V, *Adv. Mater.* 28 (2016) 9729–9734.
- [262] T. Duong, Y. Wu, H. Shen, J. Peng, X. Fu, D. Jacobs, E.C. Wang, T.C. Kho, K.C. Fong, M. Stocks, Rubidium multication perovskite with optimized bandgap for perovskite-silicon tandem with over 26% efficiency, *Advanced Energy Materials* 7 (2017) 1700228.
- [263] J.r.m. Werner, L. Barraud, A. Walter, M. Bräuninger, F. Sahli, D. Sacchetto, N. Tétreault, B. Paviet-Salomon, S.-J. Moon, C. Allebé, Efficient near-infrared-transparent perovskite solar cells enabling direct comparison of 4-terminal and monolithic perovskite/silicon tandem cells, *ACS Energy Letters* 1 (2016) 474–480.
- [264] D.P. McMeekin, G. Sadoughi, W. Rehman, G.E. Eperon, M. Saliba, M.T. Hörrantner, A. Haghighirad, N. Sakai, L. Korte, B. Rech, A mixed-cation lead mixed-halide perovskite absorber for tandem solar cells, *Science* 351 (2016) 151–155.
- [265] C.D. Bailie, M.G. Christoforo, J.P. Mailoa, A.R. Bowring, E.L. Unger, W.H. Nguyen, J. Burschka, N. Pellet, J.Z. Lee, M. Grätzel, Semi-transparent perovskite solar cells for tandems with silicon and CIGS, *Energy Environ. Sci.* 8 (2015) 956–963.
- [266] K.A. Bush, A.F. Palmstrom, J.Y. Zhengshan, M. Boccard, R. Cheacharoen, J.P. Mailoa, D.P. McMeekin, R.L. Hoye, C.D. Bailie, T. Leijtens, 23.6%-efficient monolithic perovskite/silicon tandem solar cells with improved stability, *Nature Energy* 2 (2017) 1–7.
- [267] Y. Wu, D. Yan, J. Peng, Y. Wan, S.P. Phang, H. Shen, N. Wu, C. Barugkin, X. Fu, S. Surve, Monolithic perovskite/silicon-homojunction tandem solar cell with over 22% efficiency, *Energy Environ. Sci.* 10 (2017) 2472–2479.
- [268] F. Sahli, B.A. Kamino, J. Werner, M. Bräuninger, B. Paviet-Salomon, L. Barraud, R. Monnard, J.P. Seif, A. Tomasi, Q. Jeangros, Improved optics in monolithic perovskite/silicon tandem solar cells with a nanocrystalline silicon recombination junction, *Advanced Energy Materials* 8 (2018) 1701609.
- [269] J. Werner, C.-H. Weng, A. Walter, L. Fesquet, J.P. Seif, S. De Wolf, B. Niesen, C. Ballif, Efficient monolithic perovskite/silicon tandem solar cell with cell area > 1 cm², *J. Phys. Chem. Lett.* 7 (2016) 161–166.
- [270] S. Albrecht, M. Saliba, J.P.C. Baena, F. Lang, L. Kegelmann, M. Mews, L. Steier, A. Abate, J. Rappich, L. Korte, Monolithic perovskite/silicon-heterojunction tandem solar cells processed at low temperature, *Energy Environ. Sci.* 9 (2016) 81–88.
- [271] J.P. Mailoa, C.D. Bailie, E.C. Johlin, E.T. Hoke, A.J. Akey, W.H. Nguyen, M.D. McGehee, T. Buonassisi, A 2-terminal perovskite/silicon multijunction solar cell enabled by a silicon tunnel junction, *Appl. Phys. Lett.* 106 (2015) 121105.
- [272] D. Zhao, C. Wang, Z. Song, Y. Yu, C. Chen, X. Zhao, K. Zhu, Y. Yan, Four-terminal all-perovskite tandem solar cells achieving power conversion efficiencies exceeding 23%, *ACS Energy Letters* 3 (2018) 305–306.
- [273] G.E. Eperon, T. Leijtens, K.A. Bush, R. Prasanna, T. Green, J.T.-W. Wang, D.P. McMeekin, G. Volonakis, R.L. Milot, R. May, Perovskite-perovskite tandem photovoltaics with optimized band gaps, *Science* 354 (2016) 861–865.
- [274] A. Rajagopal, Z. Yang, S.B. Jo, I.L. Braly, P.W. Liang, H.W. Hillhouse, A.K.Y. Jen, Highly efficient perovskite–perovskite tandem solar cells reaching 80% of the theoretical limit in photovoltage, *Adv. Mater.* 29 (2017) 1702140.
- [275] D. Forgács, L. Gil-Escríg, D. Pérez-Del-Rey, C. Momblona, J. Werner, B. Niesen, C. Ballif, M. Sessolo, H.J. Bolink, Efficient monolithic perovskite/perovskite tandem solar cells, *Advanced Energy Materials* 7 (2017) 1602121.
- [276] F. Jiang, T. Liu, B. Luo, J. Tong, F. Qin, S. Xiong, Z. Li, Y. Zhou, A two-terminal perovskite/perovskite tandem solar cell, *J. Mater. Chem. 4* (2016) 1208–1213.
- [277] L.M. Fraas, J.E. Avery, V.S. Sundaram, V.T. Dinh, T.M. Davenport, M.J. O'Neill, Tandem solar cells with 31%(AM0) and 37%(AM1. 5D) energy conversion efficiencies, *IEEE Aero. Electron. Syst. Mag.* 4 (1989) 3–9.
- [278] I. Celik, A.B. Philips, Z. Song, Y. Yan, R.J. Ellingson, M.J. Heben, D. Apul, Energy payback time (EPBT) and energy return on energy invested (eroi) of perovskite tandem photovoltaic solar cells, *IEEE Journal of Photovoltaics* 8 (2017) 305–309.
- [279] T. Leijtens, K.A. Bush, R. Prasanna, M.D. McGehee, Opportunities and challenges for tandem solar cells using metal halide perovskite semiconductors, *Nature Energy* 3 (2018) 828.
- [280] G. Li, W.-H. Chang, Y. Yang, Low-bandgap conjugated polymers enabling solution-processable tandem solar cells, *Nature Reviews Materials* 2 (2017) 17043.
- [281] A. Pusch, P. Pearce, N.J. Ekins-Daukes, Analytical expressions for the efficiency limits of radiatively coupled tandem solar cells, *IEEE Journal of Photovoltaics* 9 (2019) 679–687.
- [282] L. Yan, C. Han, B. Shi, Y. Zhao, X. Zhang, A review on c-Si bottom cell for monolithic perovskite/silicon tandem solar cells, *Materials Today Nano* (2019) 100045.

- [283] I. Ramiro, J. Villa, P. Lam, S. Hatch, J. Wu, E. López, E. Antolin, H. Liu, A. Martí, A. Luque, Wide-bandgap InAs/InGaP quantum-dot intermediate band solar cells, *IEEE journal of photovoltaics* 5 (2015) 840–845.
- [284] D.M. Tex, I. Kamiya, Y. Kanemitsu, Control of hot-carrier relaxation for realizing ideal quantum-dot intermediate-band solar cells, *Sci. Rep.* 4 (2014) 4125.
- [285] S. Asahi, H. Teranishi, K. Kusaki, T. Kaizu, T. Kita, Two-step photon up-conversion solar cells, *Nat. Commun.* 8 (2017) 14962.
- [286] Z. Sun, G. Sitbon, T. Pons, A.A. Bakulin, Z. Chen, Reduced carrier recombination in PbS-CuInS₂ quantum dot solar cells, *Sci. Rep.* 5 (2015) 10626.
- [287] T.K. Das, P. Ilaiyaraaja, C. Sudakar, Whispering gallery mode enabled efficiency enhancement: defect and size controlled CdSe quantum dot sensitized whisisperic solar cells, *Sci. Rep.* 8 (2018) 9709.
- [288] H.-V. Han, C.-C. Lin, Y.-L. Tsai, H.-C. Chen, K.-J. Chen, Y.-L. Yeh, W.-Y. Lin, H.-C. Kuo, P. Yu, A highly efficient hybrid GaAs solar cell based on colloidal-quantum-dot-sensitization, *Sci. Rep.* 4 (2014) 5734.
- [289] Y. Cao, A. Stavrinadis, T. Lasanta, D. So, G. Konstantatos, The role of surface passivation for efficient and photostable PbS quantum dot solar cells, *Nature Energy* 1 (2016) 16035.
- [290] N.J. Davis, M.L. Böhm, M. Tabachnyk, F. Wisnivesky-Rocca-Rivarola, T.C. Jellico, C. Ducati, B. Ehrler, N.C. Greenham, Multiple-exciton generation in lead selenide nanorod solar cells with external quantum efficiencies exceeding 120%, *Nat. Commun.* 6 (2015) 8259.
- [291] Z. Yang, J.Z. Fan, A.H. Proppe, F.P.G. de Arquer, D. Rossouw, O. Voznyy, X. Lan, M. Liu, G. Walters, R. Quintero-Bermudez, Mixed-quantum-dot solar cells, *Nat. Commun.* 8 (2017) 1325.
- [292] T. Kada, S. Asahi, T. Kaizu, Y. Harada, R. Tamaki, Y. Okada, T. Kita, Efficient two-step photocarrier generation in bias-controlled InAs/GaAs quantum dot superlattice intermediate-band solar cells, *Sci. Rep.* 7 (2017) 5865.
- [293] A.K. Rath, M. Bernechea, L. Martinez, F.P.G. De Arquer, J. Osmond, G. Konstantatos, Solution-processed inorganic bulk nano-heterojunctions and their application to solar cells, *Nat. Photon.* 6 (2012) 529.
- [294] J. Tian, T. Shen, X. Liu, C. Fei, L. Lv, G. Cao, Enhanced performance of PbS-quantum-dot-sensitized solar cells via optimizing precursor solution and electrolytes, *Sci. Rep.* 6 (2016) 23094.
- [295] M. Bernechea, N.C. Miller, G. Xercavins, D. So, A. Stavrinadis, G. Konstantatos, Solution-processed solar cells based on environmentally friendly AgBiS₂ nanocrystals, *Nat. Photon.* 10 (2016) 521.
- [296] D.H. Phuc, H.T. Tung, Quantum dot sensitized solar cell based on the different photoelectrodes for the enhanced performance, *Sol. Energy Mater. Sol. Cell.* 196 (2019) 78–83.
- [297] S.S. Mali, C.S. Shim, C.K. Hong, Highly stable and efficient solid-state solar cells based on methylammonium lead bromide (CH₃NH₃PbBr₃) perovskite quantum dots, *NGP Asia Mater.* 7 (2015), e208.
- [298] J. Hou, H. Zhao, F. Huang, Q. Jing, H. Cao, Q. Wu, S. Peng, G. Cao, High performance of Mn-doped CdSe quantum dot sensitized solar cells based on the vertical ZnO nanorod arrays, *J. Power Sources* 325 (2016) 438–445.
- [299] B. Vermang, Y. Ren, O. Donzel-Gargand, C. Frisk, J. Joel, P. Salomé, J. Borme, S. Sadewasser, C. Platzer-Björkman, M. Edoff, Rear surface optimization of CZTS solar cells by use of a passivation layer with nanosized point openings, *IEEE Journal of Photovoltaics* 6 (2015) 332–336.
- [300] C. Ornaghi, M. Stöger, G. Beaucarne, J. Poortmans, P. Schatzschneider, Thin film polycrystalline silicon solar cell on ceramics with a seeding layer formed via aluminium-induced crystallisation of amorphous silicon, *IEE Proc. Circ. Dev. Syst.* 150 (2003) 287–292.
- [301] P.M. Salomé, A. Hultqvist, V. Fjällström, M. Edoff, B. Aitken, K. Vaidyanathan, K. Zhang, K. Fuller, C.K. Williams, Cu (in, Ga) Se _{1-x} bf ₂ solar cells with varying Na content prepared on nominally alkali-free glass substrates, *IEEE Journal of Photovoltaics* 3 (2013) 852–858.
- [302] B. Vermang, J.T. Wätjen, C. Frisk, V. Fjällström, F. Rostvall, M. Edoff, P. Salomé, J. Borme, N. Nicoara, S. Sadewasser, Introduction of Si PERC rear contacting design to boost efficiency of Cu (in, Ga) Se _{1-x} bf ₂ solar cells, *IEEE Journal of Photovoltaics* 4 (2014) 1644–1649.
- [303] C. Ke, S. Chakraborty, A. Kumar, P. Widenborg, A.G. Aberle, I.M. Peters, Investigation of interdigitated metallization patterns for polycrystalline silicon thin-film solar cells on glass, *IEEE Journal of Photovoltaics* 5 (2014) 137–144.
- [304] R.-H. Horng, S.-T. Lin, Y.-L. Tsai, M.-T. Chu, W.-Y. Liao, M.-H. Wu, R.-M. Lin, Y.-C. Lu, Improved conversion efficiency of GaN/InGaN thin-film solar cells, *IEEE Electron. Device Lett.* 30 (2009) 724–726.
- [305] J.G. Mutitu, U. Obahigbon, S. Shi, W. Shafarman, D.W. Prather, Light trapping in thin-film Cu (InGa) Se _{1-x} bf ₂ solar cells, *IEEE Journal of Photovoltaics* 4 (2014) 948–953.
- [306] B. Vermang, V. Fjällström, X. Gao, M. Edoff, Improved rear surface passivation of Cu (in, Ga) Se _{1-x} bf ₂ solar cells: a combination of an Al _{1-x} bf ₂ O _x bf ₃ rear surface passivation layer and nanosized local rear point contacts, *IEEE Journal of Photovoltaics* 4 (2013) 486–492.
- [307] M. Liao, C. Chen, The investigation of optimal Si-SiGe hetero-structure thin-film solar cell with theoretical calculation and quantitative analysis, *IEEE Trans. Nanotechnol.* 10 (2010) 770–773.
- [308] S. Venkatraj, J. Wang, P. Vayalakkara, A.G. Aberle, Light scattering enhancement by double scattering technique for multijunction thin-film silicon solar cells, *IEEE Journal of Photovoltaics* 3 (2013) 605–612.
- [309] U. Das, S. Morrison, E. Centurioni, A. Madan, Thin film silicon materials and solar cells grown by pulsed PECVD technique, *IEE Proc. Circ. Dev. Syst.* 150 (2003) 282–286.
- [310] J.S. Park, S. Kim, Z. Xie, A. Walsh, Point defect engineering in thin-film solar cells, *Nature Reviews Materials* 3 (2018) 194–210.
- [311] C. Yan, J. Huang, K. Sun, S. Johnston, Y. Zhang, H. Sun, A. Pu, M. He, F. Liu, K. Eder, Cu₂ZnSnS₄ solar cells with over 10% power conversion efficiency enabled by heterojunction heat treatment, *Nature Energy* 3 (2018) 764.
- [312] L. Kranz, C. Gretener, J. Perrenoud, R. Schmitt, F. Pianezzi, F. La Mattina, P. Blösch, E. Cheah, A. Chirilă, C.M. Fella, Doping of polycrystalline CdTe for high-efficiency solar cells on flexible metal foil, *Nat. Commun.* 4 (2013) 2306.
- [313] H. Dang, V.P. Singh, Nanowire CdS-CdTe solar cells with molybdenum oxide as contact, *Sci. Rep.* 5 (2015) 14859.
- [314] Y. Zhao, M. Boccard, S. Liu, J. Becker, X.-H. Zhao, C.M. Campbell, E. Suarez, M.B. Lassise, Z. Holman, Y.-H. Zhang, Monocrystalline CdTe solar cells with open-circuit voltage over 1 V and efficiency of 17%, *Nature Energy* 1 (2016) 16067.
- [315] J.D. Poplawsky, W. Guo, N. Paudel, A. Ng, K. More, D. Leonard, Y. Yan, Structural and compositional dependence of the CdTe x Se 1 – x alloy layer photoactivity in CdTe-based solar cells, *Nat. Commun.* 7 (2016) 12537.
- [316] D. Domíne, P. Buehlmann, J. Bailat, A. Billet, A. Feltrin, C. Ballif, Optical management in high-efficiency thin-film silicon micromorph solar cells with a silicon oxide based intermediate reflector, *Phys. Status Solidi Rapid Res. Lett.* 2 (2008) 163–165.
- [317] D. Wang, G. Su, New strategy to promote conversion efficiency using high-index nanostructures in thin-film solar cells, *Sci. Rep.* 4 (2014) 7165.
- [318] H.-H. Fang, F. Wang, S. Adjokatse, N. Zhao, J. Even, M.A. Loi, Photoexcitation dynamics in solution-processed formamidinium lead iodide perovskite thin films for solar cell applications, *Light Sci. Appl.* 5 (2016), e16056.
- [319] A. Tamang, A. Hongsingthong, V. Jovanov, P. Sichanugrist, B.A. Khan, R. Dewan, M. Konagai, D. Knipp, Enhanced photon management in silicon thin film solar cells with different front and back interface texture, *Sci. Rep.* 6 (2016) 29639.
- [320] S. Chander, M.S. Dhaka, Exploration of CdMnTe thin film solar cells, *Sol. Energy* 183 (2019) 544–550.
- [321] T. Kato, J.-L. Wu, Y. Hirai, H. Sugimoto, V. Bermudez, Record efficiency for thin-film polycrystalline solar cells up to 22.9% achieved by Cs-treated Cu (In, Ga) (Se, S) ₂, *IEEE Journal of Photovoltaics* 9 (2018) 325–330.
- [322] N.H. Valdes, J. Lee, W.N. Shafarman, Ag alloying and KF treatment effects on low bandgap CuInSe₂ solar cells, *IEEE Journal of Photovoltaics* 9 (2019) 906–911.
- [323] T.S. Lopes, J.M. Cunha, S. Bose, J.R. Barbosa, J. Borme, O. Donzel-Gargand, C. Rocha, R. Silva, A. Hultqvist, W.-C. Chen, Rear optical reflection and passivation using a nanopatterned metal/dielectric structure in thin-film solar cells, *IEEE Journal of Photovoltaics* 9 (2019) 1421–1427.
- [324] C.B. Mo, S.J. Park, S. Bae, M.-h. Lim, J. Nam, D. Kim, J. Yang, D. Suh, B.K. Min, D. Kim, Impact of buffer layer process and Na on shunt paths of monolithic series-connected CIGSSe thin film solar cells, *Sci. Rep.* 9 (2019) 3666.
- [325] Y. Wu, M. Zhao, D. Zhuang, N. Zhang, X. Yu, Y. Wei, X. Lyu, G. Ren, C. Wang, L. Hu, The effect of Rb doping on CZTSSe solar cells, *Sol. Energy* 187 (2019) 269–273.

- [326] M. Franckevičius, V. Pakštas, G. Grincienė, E. Kamaraukas, R. Giraitis, J. Nekrasovas, A. Selskis, R. Juškėnas, G. Niaura, Efficiency improvement of superstrate CZTSSe solar cells processed by spray pyrolysis approach, *Sol. Energy* 185 (2019) 283–289.
- [327] J. Huang, D. Yang, W. Li, J. Zhang, L. Wu, W. Wang, Copassivation of polycrystalline CdTe absorber by CuCl thin films for CdTe solar cells, *Appl. Surf. Sci.* 484 (2019) 1214–1222.
- [328] J. Gong, Y. Kong, J. Li, K. Wang, X. Wang, Z. Zhang, Z. Ding, X. Xiao, Enhancing photocurrent of Cu (In, Ga) Se₂ solar cells with actively controlled Ga grading in the absorber layer, *Nanomater. Energy* 62 (2019) 205–211.
- [329] Y. Cao, X. Zhu, H. Chen, X. Zhang, J. Zhou, Z. Hu, J. Pang, Towards high efficiency inverted Sb₂Se₃ thin film solar cells, *Sol. Energy Mater. Sol. Cell.* 200 (2019) 109945.
- [330] M. Gloeckler, I. Sankin, Z. Zhao, CdTe solar cells at the threshold to 20% efficiency, *IEEE Journal of Photovoltaics* 3 (2013) 1389–1393.
- [331] A. Banerjee, T. Su, D. Beglau, G. Pietka, F.S. Liu, S. Almutawalli, J. Yang, S. Guha, High-efficiency, multijunction nc-Si: H-based solar cells at high deposition rate, *IEEE Journal of Photovoltaics* 2 (2012) 99–103.
- [332] D. Caputo, G. De Cesare, M. Tucci, Built-in enhancement in a-Si: H solar cell by chromium silicide layer, *IEEE Electron. Device Lett.* 31 (2010) 689–691.
- [333] D. Batibay, Y.S. Ocak, M.F. Genisel, R. Turan, Co-sputtered Cu₂ZnTi (S: Se) 4 absorbers for thin film solar cells, *Renew. Energy* 145 (2020) 1672–1676.
- [334] L. Guo, C. Grice, B. Zhang, S. Xing, L. Li, X. Qian, F. Yan, Improved stability and efficiency of CdSe/Sb₂Se₃ thin-film solar cells, *Sol. Energy* 188 (2019) 586–592.
- [335] A.H. Fallahpour, D. Gentilini, A. Gagliardi, M.A. der Maur, P. Lugli, A. Di Carlo, Systematic study of the PCE and device operation of organic tandem solar cells, *IEEE Journal of Photovoltaics* 6 (2015) 202–210.
- [336] K.Q. Le, Broadband and polarization-insensitive solar absorption enhancement in thin-film organic solar cells using metallic nanopillars, *IEEE Journal of Photovoltaics* 4 (2014) 1566–1569.
- [337] D. Liu, Y. Zhang, X. Fang, F. Zhang, T. Song, B. Sun, An 11%-power-conversion-efficiency organic-inorganic hybrid solar cell achieved by facile organic passivation, *IEEE Electron. Device Lett.* 34 (2013) 345–347.
- [338] Z. Zhou, S. Xu, J. Song, Y. Jin, Q. Yue, Y. Qian, F. Liu, F. Zhang, X. Zhu, High-efficiency small-molecule ternary solar cells with a hierarchical morphology enabled by synergizing fullerene and non-fullerene acceptors, *Nature Energy* 3 (2018) 952.
- [339] M. List, T. Sarkar, P. Perkhun, J. Ackermann, C. Luo, U. Würfel, Correct determination of charge transfer state energy from luminescence spectra in organic solar cells, *Nat. Commun.* 9 (2018) 3631.
- [340] N.C. Davy, M. Sezen-Edmonds, J. Gao, X. Lin, A. Liu, N. Yao, A. Kahn, Y.-L. Loo, Pairing of near-ultraviolet solar cells with electrochromic windows for smart management of the solar spectrum, *Nature Energy* 2 (2017) 17104.
- [341] H. Lee, D. Lee, D.H. Sin, S.W. Kim, M.S. Jeong, K. Cho, Effect of donor–acceptor molecular orientation on charge photogeneration in organic solar cells, *NPG Asia Mater.* 10 (2018) 469.
- [342] P. Cheng, G. Li, X. Zhan, Y. Yang, Next-generation organic photovoltaics based on non-fullerene acceptors, *Nat. Photon.* 12 (2018) 131–142.
- [343] S. Bi, Z. Ouyang, S. Shaik, D. Li, Effect of donor-acceptor vertical composition profile on performance of organic bulk heterojunction solar cells, *Sci. Rep.* 8 (2018) 9574.
- [344] V.A. Trukhanov, V.V. Bruevich, D.Y. Paraschuk, Fill factor in organic solar cells can exceed the Shockley-Queisser limit, *Sci. Rep.* 5 (2015) 11478.
- [345] D. Qian, Z. Zheng, H. Yao, W. Tress, T.R. Hopper, S. Chen, S. Li, J. Liu, S. Chen, J. Zhang, Design rules for minimizing voltage losses in high-efficiency organic solar cells, *Nat. Mater.* 17 (2018) 703.
- [346] L. Krückemeier, P. Kaienburg, J. Flohre, K. Bittkau, I. Zonno, B. Krogmeier, T. Kirchartz, Developing design criteria for organic solar cells using well-absorbing non-fullerene acceptors, *Commun. Phys.* 1 (2018) 27.
- [347] M. Mirsaefai, A.H. Fallahpour, P. Lugli, H.-G. Rubahn, J. Adam, M. Madsen, The influence of electrical effects on device performance of organic solar cells with nano-structured electrodes, *Sci. Rep.* 7 (2017) 5300.
- [348] C. Stelling, C.R. Singh, M. Karg, T.A. König, M. Thelakkat, M. Retsch, Plasmonic nanomeshes: their ambivalent role as transparent electrodes in organic solar cells, *Sci. Rep.* 7 (2017) 42530.
- [349] J. Kurpiers, T. Ferron, S. Roland, M. Jakoby, T. Thiede, F. Jaiser, S. Albrecht, S. Janietz, B.A. Collins, I.A. Howard, Probing the pathways of free charge generation in organic bulk heterojunction solar cells, *Nat. Commun.* 9 (2018) 2038.
- [350] D. Baran, N. Gasparini, A. Wadsworth, C.H. Tan, N. Wehbe, X. Song, Z. Hamid, W. Zhang, M. Neophytou, T. Kirchartz, Robust nonfullerene solar cells approaching unity external quantum efficiency enabled by suppression of geminate recombination, *Nat. Commun.* 9 (2018) 2059.
- [351] K. Kawashima, Y. Tamai, H. Ohkita, I. Osaka, K. Takimiya, High-efficiency polymer solar cells with small photon energy loss, *Nat. Commun.* 6 (2015) 10085.
- [352] U. Würfel, D. Neher, A. Spies, S. Albrecht, Impact of charge transport on current–voltage characteristics and power-conversion efficiency of organic solar cells, *Nat. Commun.* 6 (2015) 6951.
- [353] C. Thu, P. Ehrenreich, K.K. Wong, E. Zimmermann, J. Dorman, W. Wang, A. Fakharuddin, M. Putnik, C. Drivas, A. Koutsoubelitis, Role of the metal-oxide work function on photocurrent generation in hybrid solar cells, *Sci. Rep.* 8 (2018) 3559.
- [354] D. Bartesaghi, I. del Carmen Pérez, J. Kniepert, S. Roland, M. Turbiez, D. Neher, L.J.A. Koster, Competition between recombination and extraction of free charges determines the fill factor of organic solar cells, *Nat. Commun.* 6 (2015) 7083.
- [355] Y. Zhong, M.T. Trinh, R. Chen, G.E. Purdum, P.P. Khlyabich, M. Sezen, S. Oh, H. Zhu, B. Fowler, B. Zhang, Molecular helices as electron acceptors in high-performance bulk heterojunction solar cells, *Nat. Commun.* 6 (2015) 8242.
- [356] F. Wang, D. Kozawa, Y. Miyuchi, K. Hiraoka, S. Mouri, Y. Ohno, K. Matsuda, Considerably improved photovoltaic performance of carbon nanotube-based solar cells using metal oxide layers, *Nat. Commun.* 6 (2015) 6305.
- [357] S. Holliday, R.S. Ashraf, A. Wadsworth, D. Baran, S.A. Yousaf, C.B. Nielsen, C.-H. Tan, S.D. Dimitrov, Z. Shang, N. Gasparini, High-efficiency and air-stable P3HT-based polymer solar cells with a new non-fullerene acceptor, *Nat. Commun.* 7 (2016) 11585.
- [358] S.H. Park, A. Roy, S. Beaupré, S. Cho, N. Coates, J.S. Moon, D. Moses, M. Leclerc, K. Lee, A.J. Heeger, Bulk heterojunction solar cells with internal quantum efficiency approaching 100%, *Nat. Photon.* 3 (2009) 297.
- [359] Y.J. Kim, S. Ahn, D.H. Wang, C.E. Park, A mechanistic understanding of a binary additive system to synergistically boost efficiency in all-polymer solar cells, *Sci. Rep.* 5 (2015) 18024.
- [360] J. Hou, O. Inganäs, R.H. Friend, F. Gao, Organic solar cells based on non-fullerene acceptors, *Nat. Mater.* 17 (2018) 119–128.
- [361] S.D. Oosterhout, M.M. Wienk, S.S. Van Bavel, R. Thiedmann, L.J.A. Koster, J. Gilot, J. Loos, V. Schmidt, R.A. Janssen, The effect of three-dimensional morphology on the efficiency of hybrid polymer solar cells, *Nat. Mater.* 8 (2009) 818.
- [362] D. Neher, J. Kniepert, A. Elimelech, L.J.A. Koster, A new figure of merit for organic solar cells with transport-limited photocurrents, *Sci. Rep.* 6 (2016) 24861.
- [363] C. Yan, S. Barlow, Z. Wang, H. Yan, A.K.-Y. Jen, S.R. Marder, X. Zhan, Non-fullerene acceptors for organic solar cells, *Nature Reviews Materials* 3 (2018) 18003.
- [364] A. Lefrançois, B. Luszczynska, B. Pepin-Donat, C. Lombard, B. Bouthinon, J.-M. Verilhac, M. Gromova, J. Faure-Vincent, S. Pouget, F. Chandezon, Enhanced charge separation in ternary P3HT/PCBM/CuInS₂ nanocrystals hybrid solar cells, *Sci. Rep.* 5 (2015) 7768.
- [365] N. Li, J.D. Perea, T. Kassar, M. Richter, T. Heumueller, G.J. Matt, Y. Hou, N.S. Guldal, H. Chen, S. Chen, Abnormal strong burn-in degradation of highly efficient polymer solar cells caused by spinodal donor-acceptor demixing, *Nat. Commun.* 8 (2017) 14541.
- [366] G.F. Dibb, M.-A. Muth, T. Kirchartz, S. Engmann, H. Hoppe, G. Gobsch, M. Thelakkat, N. Blouin, S. Tierney, M. Carrasco-Orozco, Influence of doping on charge carrier collection in normal and inverted geometry polymer: fullerene solar cells, *Sci. Rep.* 3 (2013) 3335.
- [367] L. Lu, W. Chen, T. Xu, L. Yu, High-performance ternary blend polymer solar cells involving both energy transfer and hole relay processes, *Nat. Commun.* 6 (2015) 7327.
- [368] B. Wu, X. Wu, C. Guan, K.F. Tai, E.K.L. Yeow, H.J. Fan, N. Mathews, T.C. Sum, Uncovering loss mechanisms in silver nanoparticle-blended plasmonic organic solar cells, *Nat. Commun.* 4 (2013) 2004.

- [369] E. Vella, H. Li, P. Grégoire, S.M. Tuladhar, M.S. Vezie, S. Few, C.M. Bazán, J. Nelson, C. Silva-Acuña, E.R. Bittner, Ultrafast decoherence dynamics govern photocarrier generation efficiencies in polymer solar cells, *Sci. Rep.* 6 (2016) 29437.
- [370] G. Li, R. Zhu, Y. Yang, Polymer solar cells, *Nat. Photon.* 6 (2012) 153.
- [371] I.C. Ghosekar, G.C. Patil, Improving organic solar cell efficiency using solution processed poly (3-hexylthiophene) buffer layer, *Micro & Nano Lett.* 14 (2019) 74–77.
- [372] A. Agresti, S. Pescetelli, Y. Busby, T. Aernouts, Thermally induced fullerene domain coarsening process in organic solar cells, *IEEE Trans. Electron. Dev.* 66 (2018) 678–688.
- [373] N. Chander, E. Jayaraman, M. Rawat, A. Bagui, S.S.K. Iyer, Stability and reliability of PTB7: PC71BM and PTB7: PC61BM inverted organic solar cells: a comparative study, *IEEE Journal of Photovoltaics* 9 (2018) 183–193.
- [374] N. Ye, T. Liang, L. Zhan, Y. Kong, S. Xie, X. Ma, H. Chen, H. Su, M. Xu, High-performance bendable organic solar cells with silver nanowire-graphene hybrid electrode, *IEEE Journal of Photovoltaics* 9 (2018) 214–219.
- [375] R. Datt, A. Bagui, A. Siddiqui, R. Sharma, V. Gupta, S. Yoo, S. Kumar, S.P. Singh, Effectiveness of solvent vapor annealing over thermal annealing on the photovoltaic performance of non-fullerene acceptor based BHJ solar cells, *Sci. Rep.* 9 (2019) 8529.
- [376] H. Huang, Q. Guo, S. Feng, Z. Bi, W. Xue, J. Yang, J. Song, C. Li, X. Xu, Z. Tang, Noncovalently fused-ring electron acceptors with near-infrared absorption for high-performance organic solar cells, *Nat. Commun.* 10 (2019) 1–10.
- [377] X. Zhang, X. Chen, S. Huang, X. Peng, Fluorene dimers as the cathode interlayers in organic solar cells, *Synth. Met.* 253 (2019) 110–115.
- [378] A. Aghassi, C.D. Fay, Effects of IPA treatment on the photovoltaic performance of bulk heterojunction organic solar cells, *J. Phys. Chem. Solid.* 130 (2019) 136–143.
- [379] M.-U. Halbich, D. Zielke, R. Gogolin, R. Sauer-Stiegitz, W. Lövenich, J. Schmidt, Improved surface passivation and reduced parasitic absorption in PEDOT: PSS/c-Si heterojunction solar cells through the admixture of sorbitol, *Sci. Rep.* 9 (2019) 1–8.
- [380] L. Lu, T. Xu, W. Chen, E.S. Landry, L. Yu, Ternary blend polymer solar cells with enhanced power conversion efficiency, *Nat. Photon.* 8 (2014) 716.
- [381] B. Liu, R.-Q. Png, L.-H. Zhao, L.-L. Chua, R.H. Friend, P.K. Ho, High internal quantum efficiency in fullerene solar cells based on crosslinked polymer donor networks, *Nat. Commun.* 3 (2012) 1321.
- [382] S. Izawa, A. Perrot, J.-H. Lee, M. Hiramoto, Organic pi homojunction solar cell, *Org. Electron.* 71 (2019) 45–49.
- [383] S. Wang, S. Duan, Y. Wang, C. Sun, X.-F. Wang, S.-i. Sasaki, Chlorophyll-based organic solar cells with improved power conversion efficiency, *Journal of Energy Chemistry* 38 (2019) 88–93.
- [384] Lingxian Meng, Yamin Zhang, Xiangjian Wan, Organic and solution-processed tandem solar cells with 17.3% efficiency, *Science* 361 (2018) 1094–1098.